Development of Models for the Sodium
Version of the Two-Phase Three Dimensional
Thermal Hydraulics Code THERMIT
by
Gregory J. Wilson
Mujid S. Kazimi

Energy Laboratory Report No. MIT-EL 80-010

May 1980

DEVELOPMENT OF MODELS FOR THE SODIUM

VERSION OF THE TWO-PHASE THREE DIMENSIONAL

THERMAL HYDRAULICS CODE THERMIT

by

Gregory J. Wilson
Mujid S. Kazimi

Energy Laboratory and
Department of Nuclear Engineering

Massachusetts Institute of Technology
Cambridge, Massachusetts   02139

Topical Report of the
MIT Sodium Boiling Project

REPORTS IN REACTOR THERMAL HYDARULICS RELATED TO THE
MIT ENERGY LABORATORY ELECTRIC POWER PROGRAM

A. Topical Reports   (For availability check Energy Laboratory
                        Headquarters, Room E19-439, MIT, Cambridge,
                        Massachusetts, 02139)

A.1 General Applications
A.2 PWR Applications
A.3 BWR Applications
A.4 LMFBR Applications

A.1 M. Massoud, "A Condensed Review of Nuclear Reactor Thermal-
     Hydraulic Computer Codes for Two-Phase Flow Analysis," MIT
     Energy Laboratory Report MIT-EL-79-018, February 1979.

     J.E. Kelly and M.S. Kazimi, "Development and Testing of the
     Three Dimensional, Two-Fluid Code THERMIT for LWR Core and
     Subchannel Applications," MIT Energy Laboratory Report
     MIT-EL-79-046, December 1979.

A.2 P. Moreno, C. Chiu, R. Bowring, E. Khan, J. Liu, N. Todreas,
     "Methods for Steady-State Thermal/Hydraulic Analysis of PWR
     Cores," MIT Energy Laboratory Report MIT-EL-76-006, Rev. 1,
     July 1977 (Orig. 3/77).

     J.E. Kelly, J. Loomis, L. Wolf, "LWR Core Thermal-Hydraulic
     Analysis--Assessment and Comparison of the Range of Applica-
     bility of the Codes COBRA-IIIC/MIT and COBRA IV-1," MIT
     Energy Laboratory Report MIT-EL-78-026, September 1978.

     J. Liu, N. Todreas, "Transient Thermal Analysis of PWR's by
     a Single Pass Procedure Using a Simplified Model Layout," MIT
     Energy Laboratory Report MIT-EL-77-008, Final, February 1979,
     (Draft, June 1977).

     J. Liu, N. Todreas, "The Comparison of Available Data on PWR
     Assembly Thermal Behavior with Analytic Predictions," MIT
     Energy Laboratory Report MIT-EL-77-009, Final, February 1979,
     (Draft, June 1977).

A.3 L. Guillebaud, A. Levin, W. Boyd, A. Faya, L. Wolf, "WOSUB-
     A Subchannel Code for Steady-State and Transient Thermal-
     Hydraulic Analysis of Boiling Water Reactor Fuel Bundles,"
     Vol. II, Users Manual, MIT-EL-78-024. July 1977.

L. Wolf, A Faya, A. Levin, W. Boyd, L. Guillebaud, "WOSUB-A Subchannel Code for Steady-State and Transient Thermal-Hydraulic Analysis of Boiling Water Reactor Fuel Pin Bundles," Vol. III, Assessment and Comparison, MIT-EL-78-025, October 1977.

L. Wolf, A. Faya, A. Levin, L. Guillebaud, "WOSUB-A Subchannel Code for Steady-State Reactor Fuel Pin Bundles," Vol. I, Model Description, MIT-EL-78-023, September 1978.

A. Faya, L. Wolf and N. Todreas, "Development of a Method for BWR Subchannel Analysis," MIT-EL-79-027, November 1979.

A. Faya, L. Wolf and N. Todreas, "CANAL User's Manual," MIT-EL-79-028, November 1979.

A.4   W.D. Hinkle, "Water Tests for Determining Post-Voiding Behavior in the LMFBR," MIT Energy Laboratory Report MIT-EL-76-005, June 1976.

W.D. Hinkle, Ed., "LMFBR Safety and Sodium Boiling - A State of the Art Reprot," Draft DOE Report, June 1978.

M.R. Granziera, P. Griffith, W.D. Hinkle, M.S. Kazimi, A. Levin, M. Manahan, A. Schor, N. Todreas, G. Wilson, "Development of Computer Code for Multi-dimensional Analysis of Sodium Voiding in the LMFBR," Preliminary Draft Report, July 1979.

M. Granziera, P. Griffith, W. Hinkle (ed.), M. Kazimi, A. Levin, M. Manahan, A. Schor, N. Todreas, R. Vilim, G. Wilson, "Development of Computer Code Models for Analysis of Subassembly Voiding in the LMFBR," Interim Report of the MIT Sodium Boiling Project Covering Work Through September 30, 1979, MIT-EL-80-005.

A. Levin and P. Griffith, "Development of a Model to Predict Flow Oscillations in Low-Flow Sodium Boiling," MIT-EL-80-006, April 1980.

M.R. Granziera and M. Kazimi, "A Two Dimensional, Two Fluid Model for Sodium Boiling in LMFBR Assemblies," MIT-EL-80-011, May 1980.

G. Wilson and M. Kazimi, "Development of Models for the Sodium Version of the Two-Phase Three Dimensional Thermal Hydraulics Code THERMIT," MIT-EL-80-010, May 1980.

B. Papers

B.1 General Applications
B.2 PWR Applications
B.3 BWR Applications
B.4 LMFBR Applications

B.1 J.E. Kelly and M.S. Kazimi, "Development of the Two-Fluid Multi-Dimensional Code THERMIT for LWR Analysis," accepted for presentation 19th National Heat Transfer Conference, Orlando, Florida, August 1980.

J.E. Kelly and M.S. Kazimi, "THERMIT, A Three-Dimensional, Two-Fluid Code for LWR Transient Analysis," accepted for presentation at Summer Annual American Nuclear Society Meeting, Las Vegas, Nevada, June 1980.

B.2 P. Moreno, J. Kiu, E. Khan, N. Todreas, "Steady State Thermal Analysis of PWR's by a Single Pass Procedure Using a Simplified Method," American Nuclear Society Transactions, Vol. 26

P. Moreno, J. Liu, E. Khan, N. Todreas, "Steady-State Thermal Analysis of PWR's by a Single Pass Procedure Using a Simplified Nodal Layout," Nuclear Engineering and Design, Vol. 47, 1978, pp. 35-48.

C. Chiu, P. Moreno, R. Bowring, N. Todreas, "Enthalpy Transfer Between PWR Fuel Assemblies in Analysis by the Lumped Sub-channel Model," Nuclear Engineering and Design, Vol. 53, 1979, 165-186.

B.3 L. Wolf and A. Faya, "A BWR Subchannel Code with Drift Flux and Vapor Diffusion Transport," American Nuclear Society Transactions, Vol. 28, 1978, p. 553.

B.4 W.D. Hinkle, (MIT), P.M Tschamper (GE), M.H. Fontana, (ORNL), R.E. Henry (ANL), and A. Padilla, (HEDL), for U.S. Department of Energy, "LMFBR Safety & Sodium Boiling," paper presented at the ENS/ANS International Topical Meeting on Nuclear Reactor Safety, October 16-19, 1978, Brussels, Belgium.

M.I. Autruffe, G.J. Wilson, B. Stewart and M. Kazimi, "A Proposed Momentum Exchange Coefficient for Two-Phase Modeling of Sodium Boiling," Proc. Int. Meeting Fast Reactor Safety Technology, Vol. 4, 2512-2521, Seattle, Washington, August 1979.

M.R. Granziera and M.S. Kazimi, "NATOF-2D: A Two Dimensional Two-Fluid Model for Sodium Flow Transient Analysis," Trans. ANS, 33, 515, November 1979.

NOTICE

ABSTRACT

Several different models and correlations were developed and incorporated in the sodium version of THERMIT, a thermal-hydraulics code written at MIT for the purpose of analyzing transients under LMFBR conditions. This includes: a mechanism for the inclusion of radial heat conduction in the sodium coolant as well as radial heat loss to the structure surrounding the test section. The fuel rod conduction scheme was modified to allow for more flexibility in modelling the gas plenum regions and fuel restructuring. The formulas for mass and momentum exchange between the liquid and vapor phases were improved. The single phase and two phase friction factors were replaced by correlations more appropriate to LMFBR assembly geometry.

The models incorporated in THERMIT were tested by running the code to simulate the results of the THORS Bundle 6A experiments performed at Oak Ridge National Laboratory. The results demonstrate the increased accuracy provided by the inclusion of these effects.

ACKNOWLEDGEMENT

TABLE OF CONTENTS

LIST OF FIGURES

List of Figures (continued)

List of Figures (continued)

LIST OF TABLES

NOMENCLATURE

Letter	Definition	Units (SI)
A	Flow area	m^2
A	Interfacial area of mass exchange	m^{-1}
cf	Contact fraction	–
c_p	Specific heat	J/kg°K
D	Diameter	m
De	Equivalent diameter	m
D_h	Hydraulic diameter	m
D_v	Volumetrically defined hydraulic diameter	m
f	Friction factor	–
F	Force per unit volume	N/m^3
g	Gravitational acceleration	m/sec^2
G	Mass flux	$kg/m^2 sec$
h	Heat transfer coefficient	$W/m^2°K$
$h_{interfacial}$	Two-fluid heat exchange coefficient	$W/m^3°K$
H	Wire wrap lead length	m
k	Thermal conductivity	W/m°K
K	Momentum exchange coefficient	$kg/m^3 sec$
L	Length	m
N	Bubble density	m^{-3}
Nu	Nusselt number	–
p	Pressure	N/m^2
P	Pitch	m
P_h	Heated perimeter	m
Pe	Peclet number	–
Pr	Prandtl number	–
q	Heat flow	W
q"	Heat flux	W/m^2
q'''	Heat generation	W/m^3

Nomenclature (continued)

Letter	Definition	Units (SI)
r	Radius	m
Re	Reynolds number	-
R_g	Gas constant for sodium	J/kg°K
t	Time	sec
T	Temperature	°K
u	Velocity	m/sec
v	Velocity	m/sec
V	Volume	m^3
x	Quality	-
X	Flow split parameter	-
X_{tt}	Two phase Martinelli parameter	-
x,y,z	Spatial coordinates	m

Greek

α	Thermal diffusivity	m^2/sec
α	Void fraction	-
Γ	Mass exchange coefficient	$kg/m^3 sec$
λ	Constant in interfacial mass exchange coefficient	-
μ	Viscosity	kg/m sec
ρ	Density	kg/m^3
$\phi_{\ell,0}^2$	Two phase friction multiplier	-

Superscripts

n	Old time level	
n+1	New time level	

Subscripts

b	Bubble	

Nomenclature (continued)

Subscripts	Definition
c	Condensation
e	Evaporation
i	Interface
i	Node number
ℓ	Liquid
N	Total number of nodes
s	Saturation
T	Total
TP	Two phase
v	Vapor
w	Wall

Chapter 1:   INTRODUCTION

1.1 Description of THERMIT for Sodium

The computer code THERMIT was developed at MIT in order to model transient situations in light water reactor cores. The work described in this thesis was part of a project undertaken at MIT to modify THERMIT to be able to analyze sodium-cooled reactor cores. For the sake of clarity, it is necessary to provide a brief description of the code before describing the modifications made to it. This section will describe the characteristics, solution technique, and some of the restrictions of THERMIT. For more details the reader should refer to Reference [1]. Several people have been involved in the adaptation of THERMIT to sodium. This section will review their work, also. The next section will introduce the models I have developed, which constitute the bulk of this thesis.

THERMIT is a three dimensional transient, two phase, thermal-hydraulics code that simulates conditions in a reactor core. It uses a rectangular (x,y,z) coordinate system. Only the thermal-hydraulic aspects of the reactor are considered (neutronic effects are ignored). This assumes that the reactor power is a known function of

space and time. THERMIT uses the two-fluid model for two phase (i.e. vapor and liquid) flow. This models the liquid and vapor as separate fluids coupled by exchange coefficients. Thus, six fluid dynamics equations must be solved (conservation of mass, momentum, and energy for both phases). In order to simulate a transient, THERMIT is run until a steady state is achieved, and then the necessary parameters are altered, producing the transient results. In addition to the fluid dynamics calculations, THERMIT solves the radial heat conduction problem in the fuel rods (neglecting axial and azimuthal conduction).

The method of solution of the fluid dynamics equations is what distinguishes THERMIT most from other fluid dynamics codes. THERMIT uses a partially implicit scheme in solving the first order finite difference form of the equations. The terms involving sonic velocity and inter-facial exchange have been treated implicitly. Only the liquid and vapor convection terms are treated explicitly, and this introduces a time step limitation. The equations are solved by a two-level iteration procedure. Each time step advancement is reduced to a Newton iteration problem. Each Newton iteration is in turn reduced to a set of linear equations in pressure alone, which is solved by a block Gauss-Seidel iteration procedure. The heat conduction

equations are solved implicitly, and are coupled to the fluid with a fully implicit boundary condition (see Appendix E of Ref. [1]).

THERMIT does have some restrictions, other than the time step limit just mentioned. The partial differential equations are not well-posed in the mathematical sense. This means that the size of the fluid mesh cells cannot be exceedingly small, or the solution will not be well-behaved.

THERMIT allows considerable flexibility in the boundary conditions at the inlet and the outlet. The user may specify either pressure or velocity boundary conditions. In the case of a transient these values may vary with time according to a user-supplied table. The capability of varying power with time exists also.

Many changes were made in the water version of THERMIT in order to convert it to sodium. The remainder of this section will briefly describe the changes made by M. Manahan, A. Schor, R. Vilim, and A. Cheng (see Reference [18]).

As previously mentioned, THERMIT uses rectangular coordinates. In analyzing LWR square array rod bundles only one axial hydraulic diameter was required as user input. The hexagonal arrays encountered in LMFBR analysis

necessitated the modification of THERMIT to accept radially variable heated and wetted equivalent diameters.

The bulk of the work done on THERMIT involved replacing all the equations and correlations developed for water with the appropriate ones pertaining to sodium. Correlations for the following physical properties were employed: saturation temperature, surface tension, and liquid and vapor internal energies, densities, conductivities, and viscosities. A new correlation for the heat transfer coefficient at the fuel-sodium interface was developed and implemented.

Work is currently underway to implement an improved model for calculating the geometry and material properties of the fuel rod. This model will be more applicable to an LMFBR fuel rod than the previous one. It will be able to handle such phenomena as restructuring of fuel and dynamic gap conductance.

The final changes to be described in this section were designed to accelerate convergence. First of all, the code was converted to double precision. This reduced the round-off error. The second change was to allow the suppression of transverse velocities. This significantly reduced the time necessary to reach a steady state, and therefore resulted in considerable savings in computer time.

1.2 - Models Developed

1.2.1 - Fluid Conduction Model

In the water version of THERMIT the only mechanism by which heat may be transferred between two adjacent fluid mesh cells is through transverse velocities. Thus, if the transverse velocities are low, the rate of heat transfer is low also. Clearly there will be heat transfer between cells due to conduction, even if the transverse velocities are zero. In the case of water, which does not have an exceptionally high thermal conductivity, the loss of accuracy may not be that great, but for liquid sodium, where the thermal conductivity is two orders of magnitude greater than water, conduction effects cannot be ignored.

Therefore, a radial heat conduction capability has been incorporated in THERMIT for sodium. This model is described in detail in Chapter 2. The model only applies in the single phase liquid region, because upon boiling the thermal conductivity of sodium drops so drastically as to make conduction effects negligible. Axial conduction is not included, because convection is far more important, except in cases of extremely low flow.

1.2.2 - Structure Conduction Model

In the water version of THERMIT the outer boundary of the test section (in the radial direction) is considered

to be adiabatic. In other words, no heat is allowed to leave the system in the radial direction. When modeling large systems (for example, an entire reactor core) this is not a bad assumption, but for smaller systems (like a single rod bundle) radial heat losses to the structure surrounding the system may be significant. Once again, the effect is more pronounced with liquid sodium than with water, due to the large thermal conductivity of the former. As with the fluid conduction model, no heat is lost from fluid cells in which vapor is present.

Chapter 3 describes the structure conduction model in detail. The model employed is similar in many respects to the fuel rod conduction model in the water version of THERMIT. The structure is represented by a user-specified number of concentric radial regions, each of which may contain a different material. Therefore, composite structures may be represented. All calculations (except the coupling term with the fluid dynamics) are performed implicitly. This model may be bypassed, if so desired, thus simulating the adiabatic condition previously in THERMIT.

1.2.3 - Fuel Rod Conduction Model

A new and much more general fuel rod model has been incorporated in the sodium version of THERMIT. The

previous version allowed only three radial zones in the
fuel rod (representing the fuel, clad, and gap). This
model is inadequate for representing such phenomena as
fuel redistribution and central voiding. The new fuel
rod conduction model (described in detail in Chapter 4)
permits the user to specify the number of radial zones
desired and the thermal properties of each. The second
major modification is that the structure of the fuel rod
may be varied axially as well. The water version of
THERMIT required the structure of the fuel rod to remain
constant in the axial direction. In order to model the
gas plenum region of the LMFBR fuel rod, axially variable
fuel rod properties must be permitted. This is done
by allowing the user to specify the number of axial
regions desired and the geometry and materials in each
region.

The solution scheme for the fuel rod conduction has
not been altered. Only the arrays containing the geomet-
rical parameters and thermal properties were changed.
This involved altering many input parameters. These
changes are described in detail in Section 4.2 and are
summarized in the input description of THERMIT for sodium
(Appendix A).

1.2.4 - Interfacial Exchange Coefficients

The most uncertain aspect of the two fluid equations is the form of the interfacial exchange coefficients, which represent the mass, momentum and energy transfer between the liquid and vapor phases. The values of these coefficients are very uncertain even for water, but for sodium this is even more true.

Chapter 5 describes the correlations adopted for the mass and momentum exchange coefficients in the sodium version of THERMIT. In the case of the energy exchange coefficient a large constant ($h_{interfacial} = 1.0 \times 10^{10}$ W/m^3 °K) is assumed. This forces near thermal equilibrium between phases.

For the mass exchange coefficient a modified version of the Nigmatulin Model [7] is used. The original model assumes bubbly flow, with a constant bubble density. In sodium boiling at low pressures the annular flow regime dominates, for large void fractions. The revised model takes this into account in developing a mass exchange coefficient that is dependent on the flow regime encountered.

The momentum exchange coefficient is taken from M.A. Autruffe [9]. This correlation was derived from single tube sodium boiling data. In addition, the momentum exchange between phases due to mass transfer is

included. This effect was neglected in the water version of THERMIT. Section 5.2 shows that at large void fractions this phenomena can be important, however.

It should be noted that these correlations have not been tested very extensively, especially in triangular rod bundle geometries, so their applicability is not beyond question. They do represent the best information available, however. The modular construction of THERMIT permits the user to incorporate new correlations quite easily, as they become available.

1.2.5 - Friction Factor Correlations

In the two-fluid formulation of two phase, three dimensional flow it is necessary to supply liquid and vapor friction factors for both the axial and the transverse directions. Because of the complex geometry involved in LMFBR reactor cores, no one correlation can be applied directly for either direction. Chapter 6 describes the combinations of correlations incorporated in the sodium version of THERMIT.

For the liquid friction factor in the axial direction, the flow is divided into three categories: laminar ($Re < 400$), turbulent ($Re > 2,600$), and transition ($400 \leq Re \leq 2,600$). Separate correlations are used for laminar and turbulent flow, while a combination of the two is taken for transition flow.

The vapor friction factor in the axial direction is much less refined, due to lack of data. A turbulent formula developed for flow in a pipe is employed over the full Reynolds Number range. Because the sodium version of THERMIT assumes dryout occurs for void fractions above 0.957, the vapor does not come in contact with the fuel rod below this value. Therefore, the vapor friction factor is zero in this range.

The friction factors in the transverse direction are basically the same as those described in the THERMIT description (Reference [1]), with the exception that because of the assumption that no vapor comes in contact with the wall for void fractions below 0.957 the vapor friction factor is zero in this region. Some modifications have also been made in the form of the laminar friction factors in two phase flow. See Section 6.3 for details.

1.3 Results

Chapter 7 discusses the results obtained from six runs made with THERMIT. Cases A, B, and C were simulations of the THORS Bundle 6A experiments done at Oak Ridge [6]. These simulations show the value of the structure conduction and fuel rod models in improving the predictions of THERMIT for this 19 pin bundle. Cases D, E, and F extend this analysis to a 217 pin bundle, typical of the Clinch

River Breeder Reactor. These final three cases evaluate the relative importance of the inclusion of radial heat losses when modeling loss-of-flow transients in LMFBR's.

Finally, Chapter 8 summarizes the findings of this thesis, and makes recommendations for future work in improving the capability of THERMIT to model transients in LMFBR analysis.

Chapter 2: FLUID CONDUCTION MODEL

2.1 Basic Assumptions

Two options have been developed in THERMIT for the inclusion of heat conduction between adjacent fluid channels. The first option is a fully explicit formulation, while the second is partially implicit, and will be described in Section 2.3. Both models contain certain basic assumptions.

The first assumption made is that the conduction effects become negligible when boiling occurs in at least one of the two adjacent channels. This is justified under normal reactor conditions, because the thermal conductivity of sodium vapor is significantly less than that of liquid sodium (i.e. at 800°k, k_{ℓ} = 66.98 W/m°k and k_v = 5.42 x 10^{-2} W/m°k, so $k_{\ell}/k_v \approx 1236$). This radical change in thermal conductivity, coupled with the extremely high void fractions encountered in sodium boiling at low pressures, ensures that liquid-to-vapor and vapor-to-vapor conduction effects are completely negligible. Therefore, when boiling occurs in a channel conduction heat transfer through its faces is neglected.

Only radial conduction is incorporated in THERMIT now, although the model permits the inclusion of axial conduction if desired. In normal situations convection

dominates the heat transfer, due to the large axial velocity
of the liquid sodium. Only in cases of extremely low flow
will axial conduction become significant. For example,
it has been shown that for the Clinch River Breeder Reactor
core the velocity could be reduced by at least three orders
of magnitude before axial conduction effects become as
large as 2% (Reference [2]).

The third major assumption is that the effective
Nusselt Number for conduction (defined below) is a constant,
independent of fluid conditions. This assumption is neces-
sitated by the lack of data available for sodium flow in
the geometry modeled in THERMIT. The current fluid con-
duction model allows the user to input a value for the
Nusselt Number, which remains constant throughout the cal-
culation. If in the future a Nusselt Number correlation
is developed for this type of geometry it could be incor-
porated with a minimum amount of work.

It should be noted that this model only considers
heat transfer between _fluid_ channels. The heat flow through
all external faces is taken into account in the model des-
cribed in Chapter 3.

2.2 Fully Explicit Formulation

The net rate of flow of heat into a given fluid cell
is expressed as the sum of the heat fluxes from each of

the four sides (ignoring the two sides perpendicular to the axial direction). The heat flow term for each side is calculated by multiplying the temperature difference by an effective conduction heat transfer coefficient. For the configuration of Figure 2.1,

$$q_{1-0}^{(n+1)} = A_{1-0} h_{1-0}^{(n)} (T_{\ell,1}^{(n)} - T_{\ell,0}^{(n)}), \text{ and} \qquad (2-1)$$

$$q_T^{(n+1)} = q_{1-0}^{(n+1)} + q_{2-0}^{(n+1)} + q_{3-0}^{(n+1)} + q_{4-0}^{(n+1)} \qquad (2-2)$$

where

q_{1-0} = heat flow from channel 1 to channel 0 (W),

q_T = total heat flow into channel 0 (W),

A_{1-0} = heat flow area between channels 1 and 0 (m^2),

h_{1-0} = effective conduction heat transfer coefficient between channels 1 and 0 (W/m^2°k),

$T_{\ell,0}$ and $T_{\ell,1}$ are the liquid temperatures in channels 0 and 1, respectively. The superscripts refer to the time step at which the quantities are measured. Note that in Equation (2-1) the heat flow, q_{1-0}^{n+1}, is calculated entirely from quantities evaluated at time step n. This is what makes the method explicit.

Referring to Equation (2-1), the quantity A_{1-0} is known from geometry, and $T_{\ell,1}^{(n)}$ and $T_{\ell,0}^{(n)}$ are known from the solution of the problem at time step n, so only $h_{1-0}^{(n)}$ remains to be calculated. This is done by considering the problem as
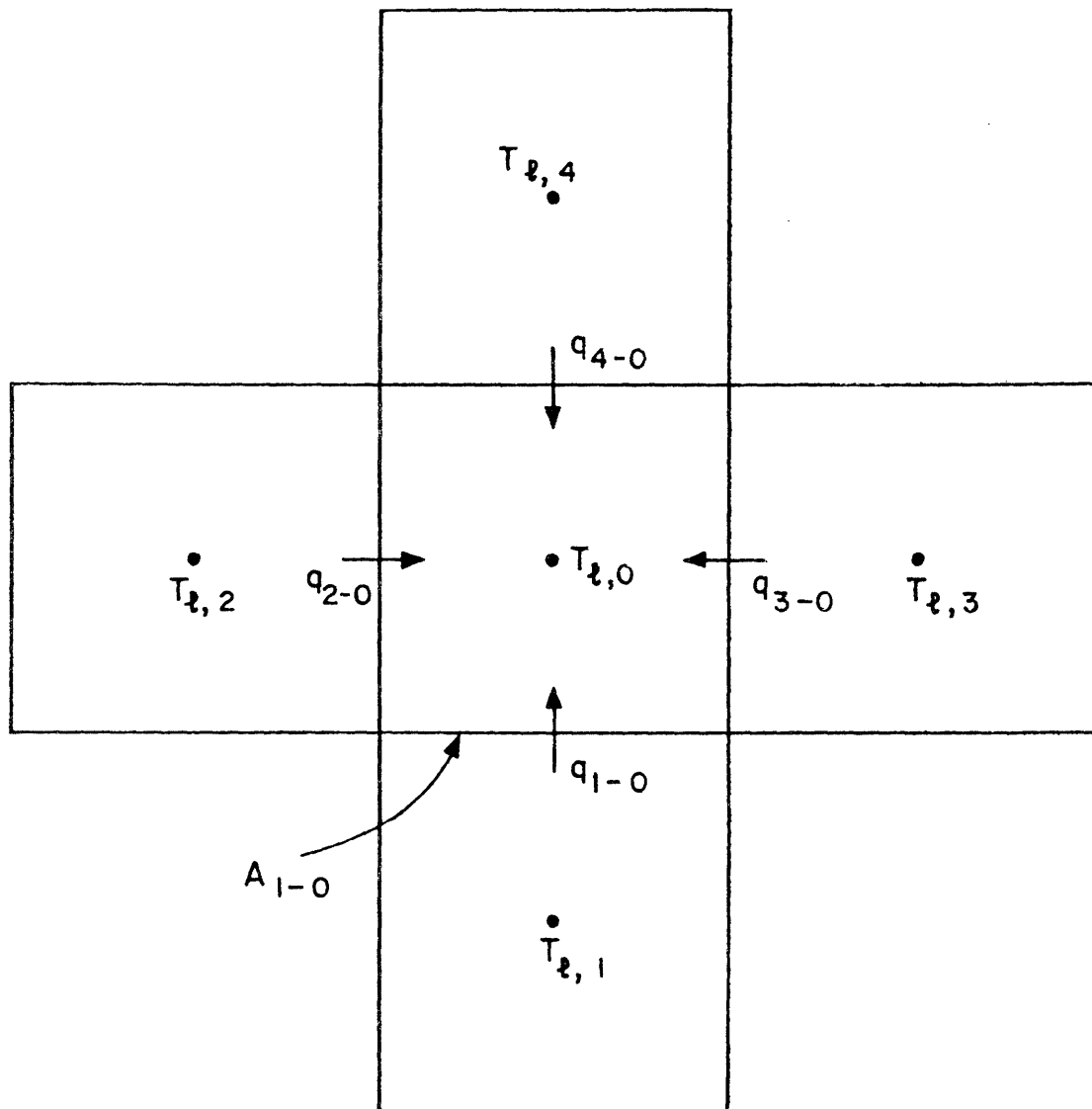
Figure 2.1 Top View of Fluid Channels

two resistances in series (see Figure 2.2). An interface
temperature, T_i, is defined at the boundary between the
two channels, and the heat transfer coefficients within
each channel, h_1 and h_0, are defined as:

$$q''_{1-0} = h_0(T_i - T_{\ell,0}) = h_1(T_{\ell,1} - T_i) \qquad (2-3)$$

To calculate h_0 and h_1 the constant Nusselt Number
approximation described above is used:

$$h_0 = Nu\frac{k_0}{De_0} \quad , \qquad h_1 = Nu\frac{k_1}{De_1} \quad , \qquad (2-4)$$

where

k = thermal conductivity of sodium (W/m°k),

De = equivalent diameter = $\dfrac{4 \times A_f}{P_h}$ (m),

P_h = heated perimeter of channel (m),

A_f = cross-sectional flow area of channel (m^2)

Solving Equation (2-3) for T_i,

$$T_i = \frac{h_1 T_{\ell,1} + h_0 T_{\ell,0}}{h_1 + h_0} \qquad (2-5)$$

Rearranging Equation (2-1), and substituting Equation
(2-3),

$$h_{1-0} = \frac{q''_{1-0}}{T_{\ell,1} - T_{\ell,0}} = \frac{h_0(T_i - T_{\ell,0})}{T_{\ell,1} - T_{\ell,0}} \qquad (2-6)$$
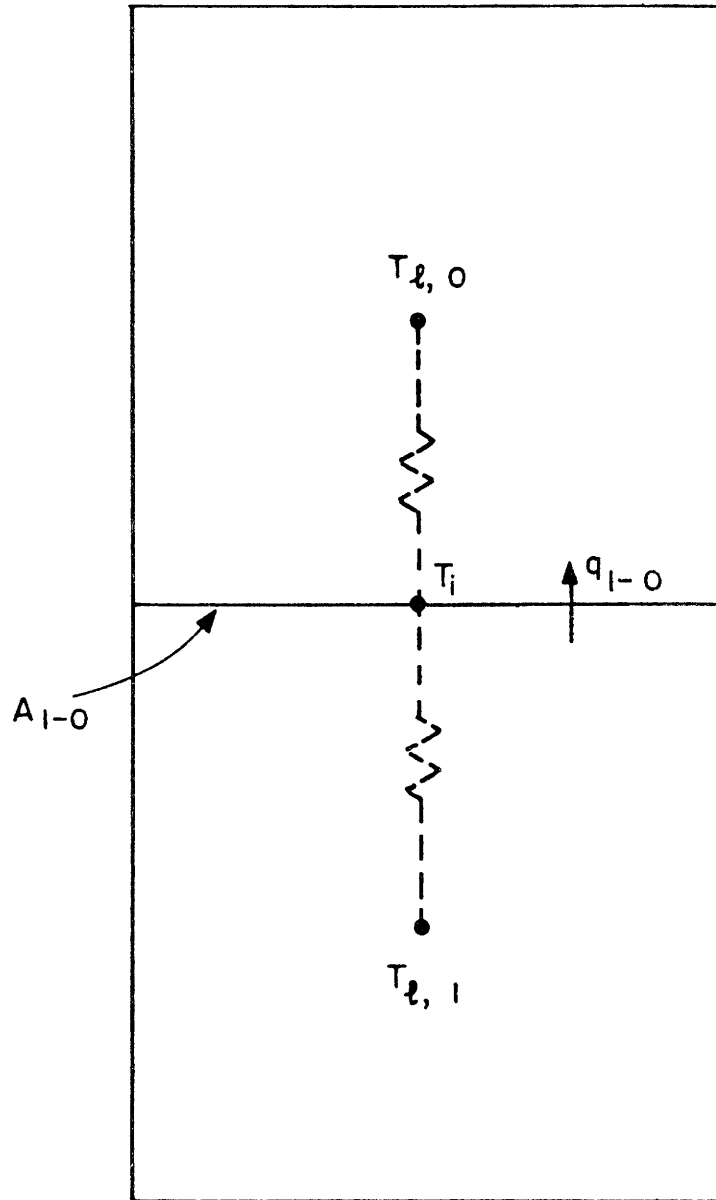
Figure 2.2   Closeup of Two Fluid Channels, Showing the Heat
Transfer Between Them

Finally, introducing Equation (2-5) into (2-6),

$$h_{1-0} = \frac{h_1 h_0}{h_1 + h_0} \tag{2-7}$$

Therefore, the solution technique for the fully explicit model is as follows: given the geometry of the problem, solve Equations (2-4) for h_0 and h_1, use Equation (2-7) to obtain h_{1-0}, and plug the results into (2-1) to get $q_{1-0}^{(n+1)}$. These steps are repeated for each face of the channel.

The major advantage of the explicit method is that it uses very little computer time, and is therefore inexpensive. In addition, it ensures strict conservation of energy (i.e. $q_{1-0}^{(n+1)} = -q_{0-1}^{(n+1)}$). The disadvantage of the explicit method is that it introduces a stability limit on the time step size that may be more restrictive than the convective limit currently used in the code. The time step limitation for conduction in two dimensions [3] is:

$$\Delta t < \frac{(\Delta \chi)^2}{4\alpha} \tag{2-8}$$

where α = thermal diffusivity = $\frac{k}{\rho c_p}$.

When using a very fine mesh the explicit method can introduce unreasonable limitations on the time step size. In most cases, however, the convective limit will be more restrictive than the conduction limit.

2.3 Partially Implicit Formulation

The partially implicit formulation currently in THERMIT was developed at M.I.T. by Andrei Schor for the purpose of circumventing the stability problem introduced by the explicit model. Equations (2-1) and (2-2) are modified so as to be implicit in one temperature:

$$q_{1-0}^{(n+1)} = A_{1-0} h_{1-0}^{(n)} (T_{\ell,1}^{(n)} - T_{\ell,0}^{(n+1)}) \tag{2-9}$$

$$q_T^{(n+1)} = A_{1-0} h_{1-0}^{(n)} (T_{\ell,1}^{(n)} - T_{\ell,0}^{(n+1)}) + A_{2-0} h_{2-0}^{(n)} (T_{\ell,2}^{(n)} - T_{\ell,0}^{(n+1)})$$

$$+ A_{3-0} h_{3-0}^{(n)} (T_{\ell,3}^{(n)} - T_{\ell,0}^{(n+1)}) + A_{4-0} h_{4-0}^{(n)} (T_{\ell,4}^{(n)} - T_{\ell,0}^{(n+1)}) \tag{2-10}$$

This formulation avoids the time step limitation of the explicit method, but it introduces another problem: lack of energy conservation. The heat flow from channel 1 to channel 0, q_{1-0}, should have the same magnitude (but opposite sign) as the heat flow from channel 0 to channel 1, q_{0-1}. This is certainly the case in the explicit formulation, where both $T_{\ell,0}$ and $T_{\ell,1}$ are evaluated at the old time step, but in the partially implicit method this condition is only satisfied if $T_{\ell,1}^{(n)} - T_{\ell,0}^{(n+1)} = T_{\ell,1}^{(n+1)} - T_{\ell,0}^{(n)}$, which is not true in general.

Thus the choice between the fully explicit and partially implicit formulations involves a trade-off. The explicit method strictly conserves energy, but may introduce a greater

limitation on the time step size, while the partially implicit method avoids the time step limitation, but fails to strictly conserve energy.

2.4 Programming Information

This section is designed to supplement the THERMIT Users' Manual [1], in explaining the implementation of the models discussed in the previous two sections.

The fluid conduction model requires only one additional input variable above those described in Reference [1] (see Appendix A for the complete input description for the sodium version of THERMIT). The user specifies the conduction Nusselt Number, "rnuss", which is used in Equation (2-4). If a positive real number is entered, the partially implicit method is used, with Nu = "rnuss", while a negative real number specifies the explicit option, with Nu = -"rnuss". (The number 7.0 is recommended for |"rnuss"|, because it represents a typical value for the Nusselt Number in liquid sodium.) A value of 0.0 allows the user to bypass the conduction model completely.

The inclusion of the fluid conduction model required the addition of two subroutines to THERMIT. The first one, QCOND, is called from subroutine NEWTON, and performs the bulk of the calculations. It calls another new subroutine, HTRAN, which solves Equations (2-4) and (2-7). The result of these calculations is an array which stores the net heat

flow into each fluid cell (see Equation (2-2)). This array is passed into subroutine JACOB, which solves the mass and energy equations. If the partially implicit option is chosen, an additional derivative term is included in the Jacobian matrix.

2.5 Sample Cases

The explicit version of the fluid conduction model in THERMIT has been tested for two cases. The first was a four channel (2x2) steady-state run in which two diagonally opposite channels were heated by fuel pins, while the other two were unheated. All transverse velocities were set equal to zero. This insured that any heat transfer between adjacent channels was due to conduction alone. Temperatures were calculated at sixteen axial positions, of which only the second, third and fourth were heated. Appendix B.1 contains the THERMIT input file for this run.

The results of the simulation are shown in Figure 2.3. The heated channels increased in temperature up to the top of the heated section (node four), and then cooled off as they lost heat to the cooler, unheated channels. The temperature in the unheated channels increased steadily as they received heat from the heated channels, until the temperatures became nearly equal at the top of the channels.

The second test case was of an entirely different nature (see Appendix B.2). It was a nine channel (3x3) transient in
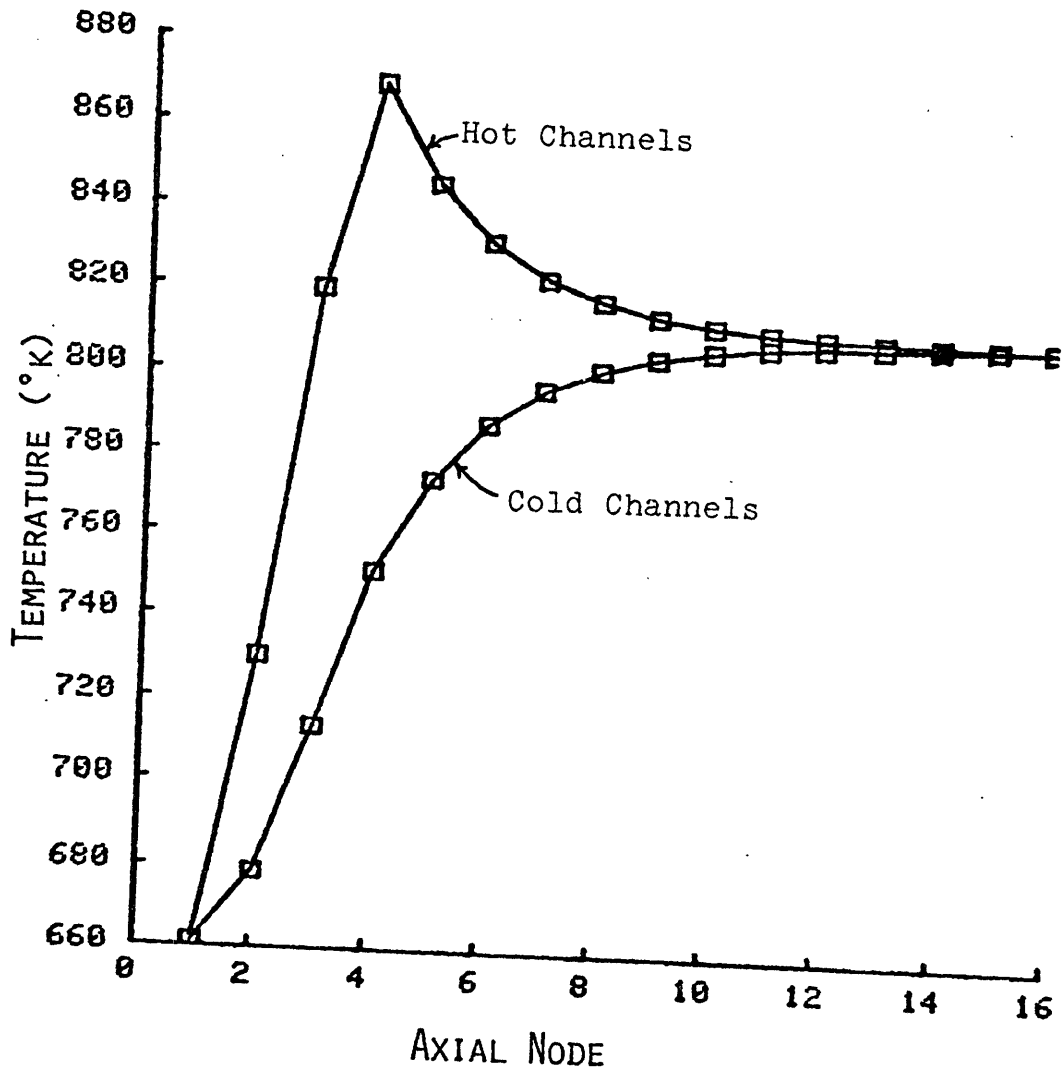
Figure 2.3   Fluid Conduction Test Case - 4 Channel

which the axial and transverse velocities were initially

set at zero, with the latter being held constant at zero

throughout the transient, for the reason described above.

The fluid was unheated, but a temperature variation between

channels was introduced (see Figure 2.4). Slight axial

velocities were induced, due to the thermal expansion and

contraction in each channel. Because of these small axial

velocities some heat was carried out of the system, so the

final equilibrium temperature was about 832.91°k, instead

of the predicted 833.33°k. The temperature vs. time history

is plotted in Figure 2.5 for the center, corner, and side

channels. A time step of 5.0 seconds was used (significantly

below the 35 second conduction limit imposed by Equation (2-8)).

As shown, all channels approached a single equilibrium temp-

erature as time progressed.

In order to test the partially implicit fluid conduction

model in THERMIT the nine channel case described above was

run again, using the same time step size (see Appendix B.3).

The results are shown in Figure 2.6. In this case the final

equilibrium temperature was only 828.65°k, 4.26 degrees less

than the final temperature of the explicit case. This dif-

ference can be attributed to the lack of strict conservation

of energy discussed in Section 2.3. As larger time steps

become necessary, however, the desirability of the partially

implicit method will increase.
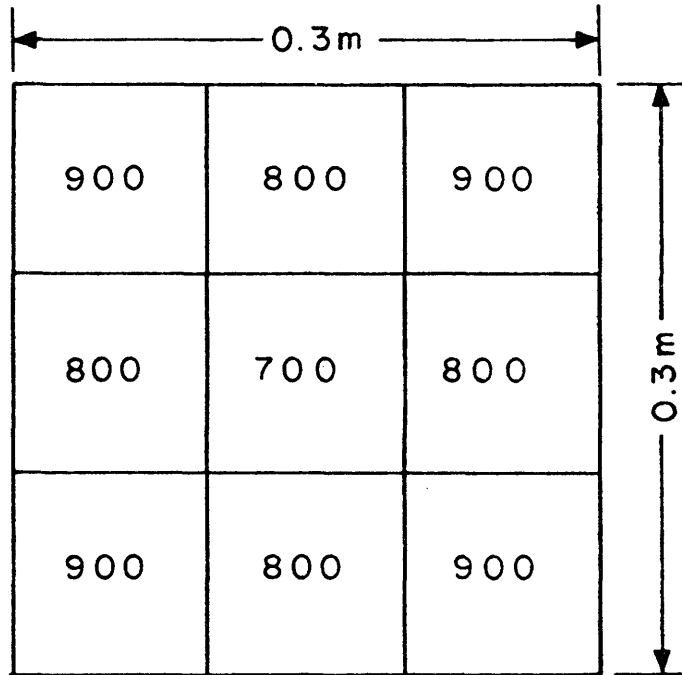
(Numbers indicate initial temperatures in channels in °K)

Figure 2.4   Geometry for 9 Channel Fluid Conduction
             Test Case (Top View)
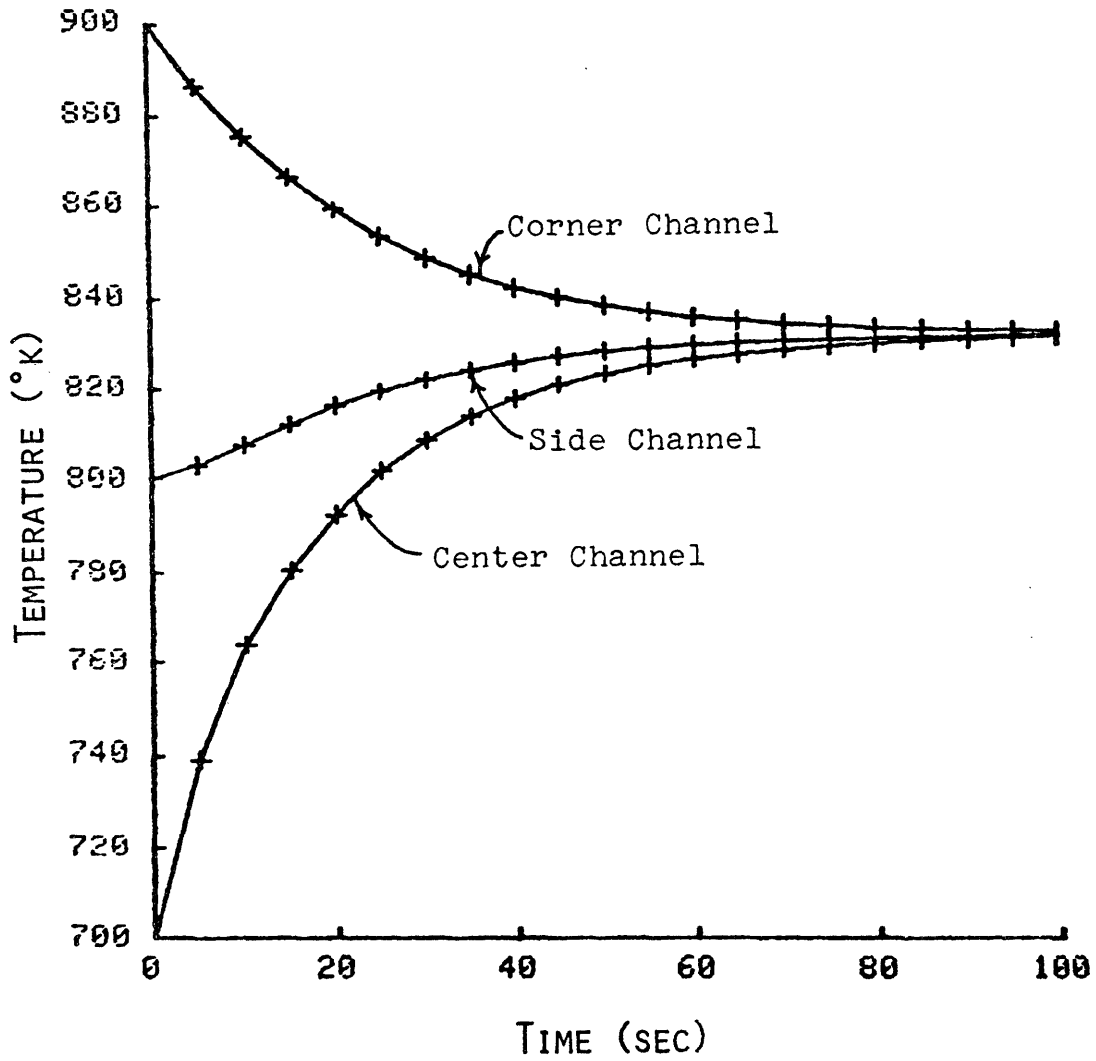
Figure 2.5   Fluid Conduction Test Case –
9 Channel (Explicit Run)
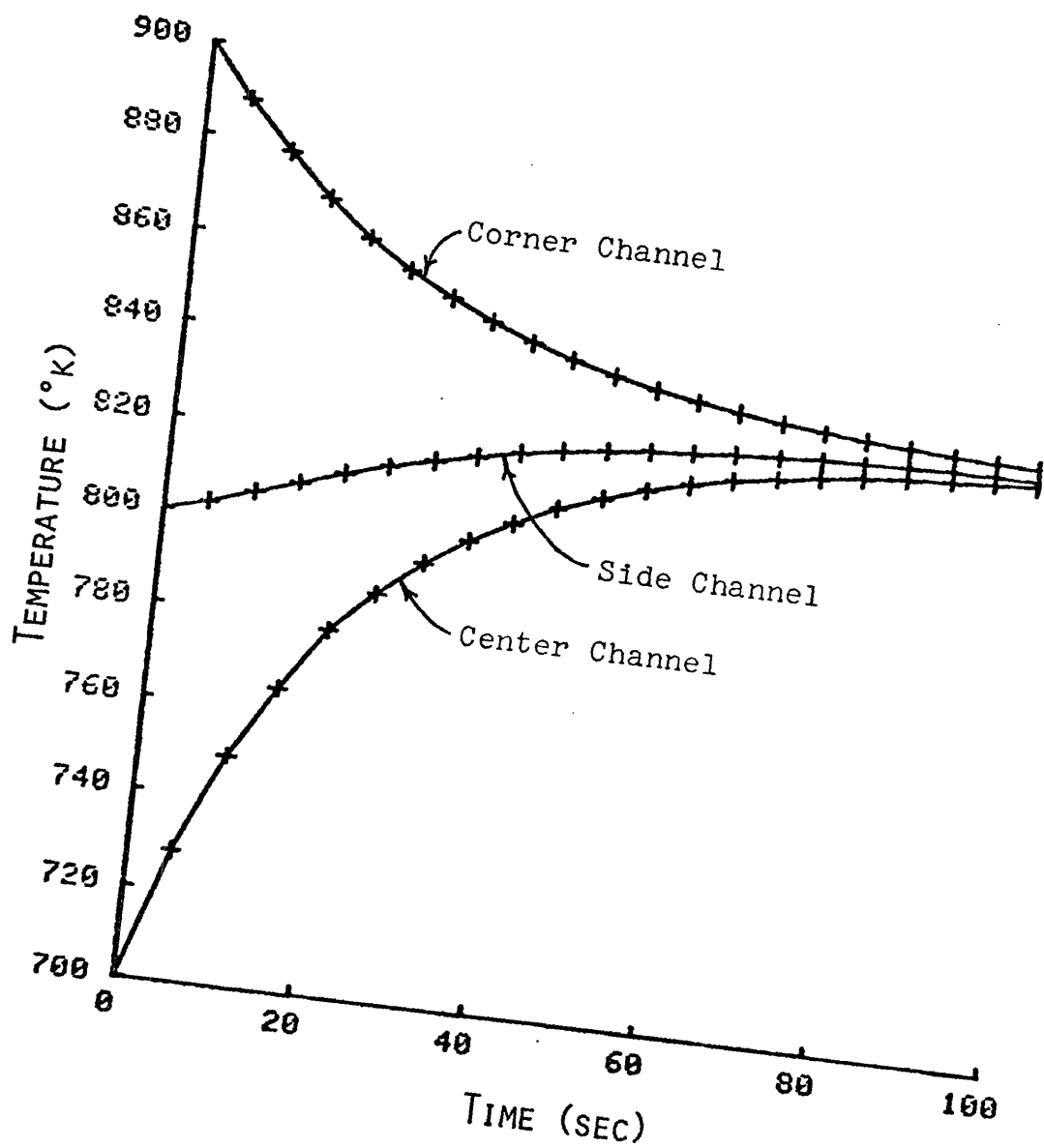
Figure 2.6 Fluid Conduction Test Case –
9 Channel (Semi-implicit Run)

Chapter 3:   STRUCTURE CONDUCTION MODEL

3.1 Basic Assumptions

The structure conduction model now in THERMIT permits
the user the option of taking into account the heat losses
to the structure surrounding the region of interest.   In
the previous version of THERMIT an adiabatic boundary con-
dition was assumed around the outer boundary of the region
modeled.   This option still exists, if so desired.   The heat
flow to the structure is calculated using a multi-layer
conduction model.   Several simplifying assumptions were
necessary in order to implement the model.

The major assumption made is that of azimuthal sym-
metry.   This assumption was made for two reasons.   First,
in most cases there will not be much of a temperature
variation around the outside of the region modeled.   Second,
far more computer storage space would be required if the
code were to calculate azimuthal temperature variations.
Therefore, only radial conduction is considered.   The
structure is broken up axially into sections which coincide
with the axial fluid cells.   Thus, the fluid cells at each
axial level transfer heat only to the section of the structure
that corresponds to that region.   Axial conduction within the
structure is neglected also.

As in the fluid conduction model described in Chapter 2,
the heat transfer from any fluid channel in which boiling
has occurred is neglected.   The rationale behind this is that

the dramatic drop in the thermal conductivity of sodium upon boiling reduces the heat transfer capability so much as to make it negligible. If some of the fluid channels touching the structure boil, those that remain in the single phase liquid regime continue to transfer heat to the structure.

The geometrical layout of the structure is specified by the user, with certain restrictions. Different materials may be used, but they must be in concentric rings around the inner region. For example, the user could construct a three region structure consisting of an annulus of stainless steel surrounded by rings of insulation and stainless steel again. The user also specifies the number of meshes desired within each region. The temperatures are calculated at the boundary of each mesh cell.

Only the fluid cells in physical contact with the structure are affected by the structure conduction model. Consider the example shown in Figure 3.1, which consists of a single assembly encased in a hex can and surrounded by a layer of insulation and another layer of stainless steel. Twelve of the sixteen fluid channels touch the structure through some portion of their perimter. These twelve may all lose heat directly to the structure. The four interior channels do not communicate directly with the structure, but they do communicate with the exterior channels through the fluid conduction model described in Chapter 2. Thus, heat generated in the interior of the region has a mechanism for being transferred radially outward to the structure.
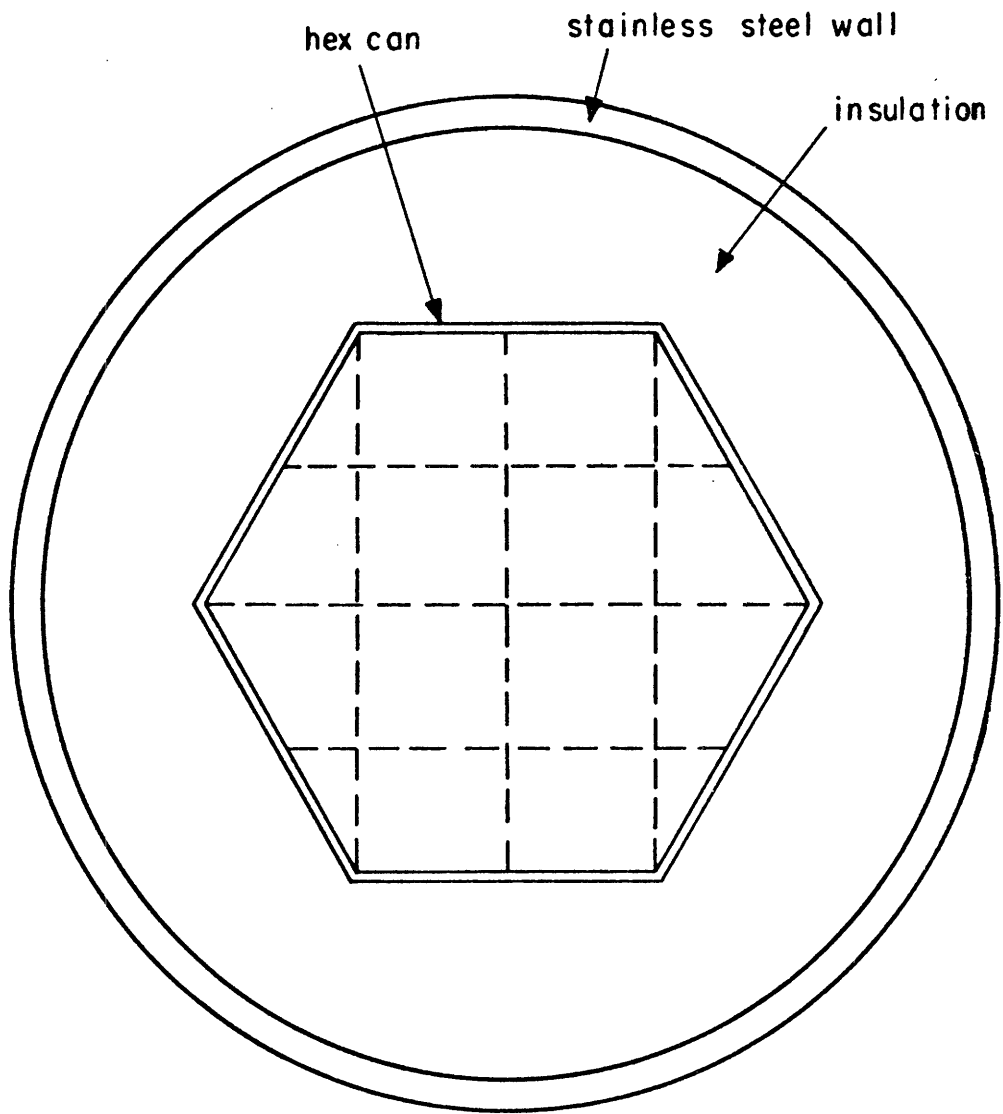
Figure 3. 1   Hex Can with Associated Structure

A close look at Figure 3.1 will reveal that some simplifications have to be made in order to represent this case using the structure conduction model in THERMIT. The hex can must be formed into an annulus, so as to maintain the azimuthal symmetry required. Figure 3.2 shows this case as it would be modeled on THERMIT. The inner boundary of the hex can is determined by summing up the perimeters of contact for all the exterior cells. The sodium in the fluid channels adjacent to the structure is combined and formed into an imaginary annulus inside the structure wall for the purposes of calculation. The inner radius of the sodium annulus is determined by setting the cross-sectional area of the annulus equal to the sum of the cross-sectional areas of the sodium in each of the fluid cells adjacent to the structure. This averaging scheme is necessary in order to preserve the azimuthal symmetry and to produce a geometry for which the heat transfer characteristics are known. More details will be given in the next section.

3.2 Boundary Conditions

In order to solve the conduction equation for the temperature distribution in the structure the conditions at the inner and outer boundaries are needed. These are provided in the form of a heat transfer coefficient and a temperature.
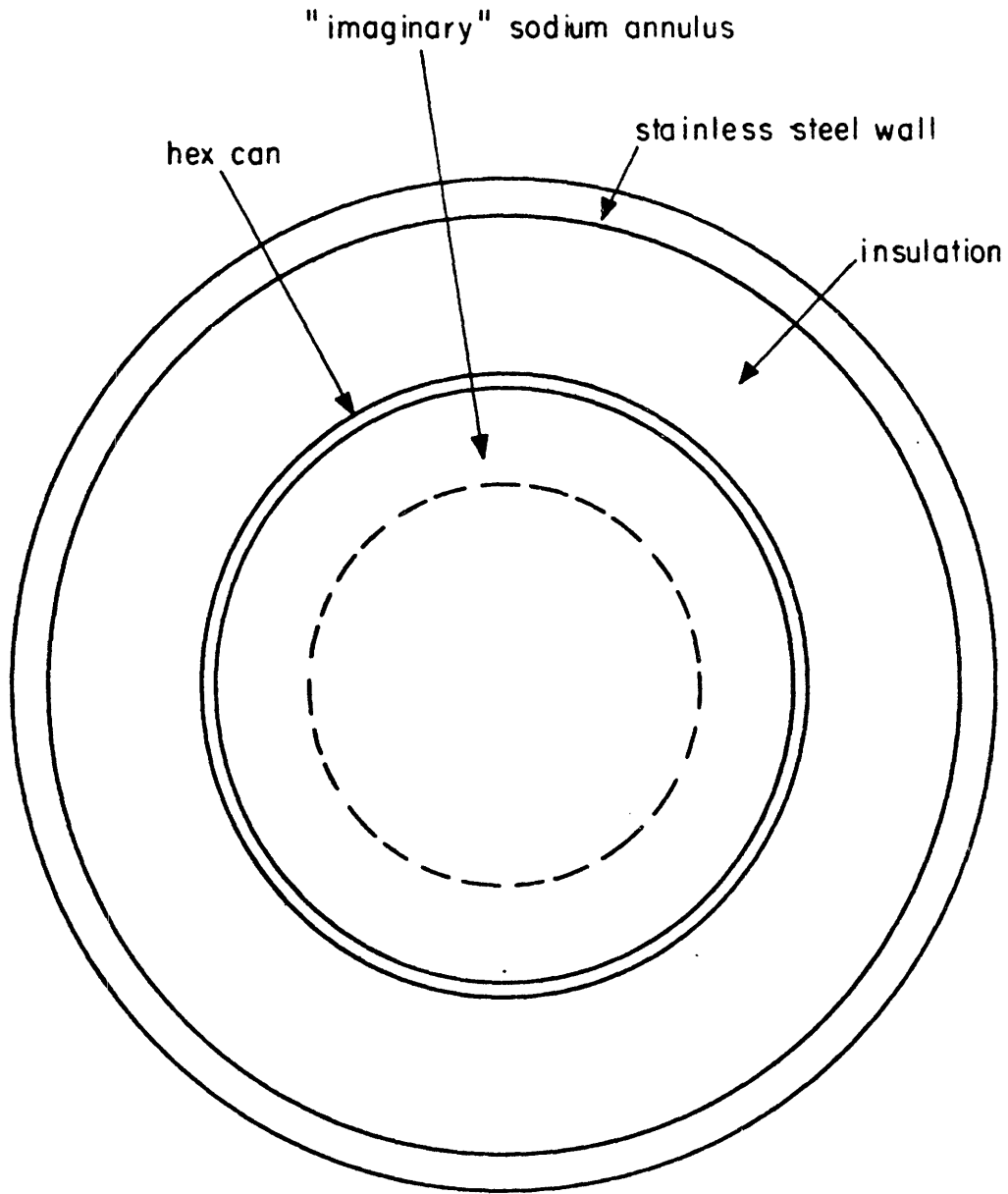
Figure 3.2 Thermit Model of Hex Can with Associated
Structure

For the outer boundary of the structure the user specifies a constant heat transfer coefficient and a constant temperature outside the structure. Thus, the heat flux on the outer boundary will be:

$$q''_{out} = h_{out}(T_\infty - T_{wall,out}) \qquad (3-1)$$

where $T_{wall,out}$ = the temperature at the outer boundary of the structure. If an adiabatic condition at the outer wall is desired, the user should set $h_{out} = 0.0$.

The boundary conditions at the inner surface of the structure are more complicated, however, because they involve heat transfer between the flowing liquid sodium and the stationary structure. As previously mentioned, the conditions of the sodium in each of the fluid channels in contact with the structure must be averaged, so as to maintain azimuthal symmetry. Therefore, a single temperature and pressure are calculated by taking the volume average of these quantities in each of the separate fluid channels in question.

Now that this "imaginary" annulus has been formed and its properties are known the problem is to obtain a heat transfer coefficient for the sodium/wall interface. Obviously, no correlation exists for the actual geometry encountered, so this explains why the sodium is placed in the "imaginary"

annulus described in the previous section. O.E. Dwyer [4]

developed a Nusselt Number correlation for liquid sodium

flowing in an annulus, transferring heat through its outer

boundary:

$$Nu = \frac{hDe}{k} = A + C(\bar{\psi}Pe)^{\beta}, \qquad (3-2)$$

where

$A = 5.54 + 0.023(r_2/r_1)$

$C = 0.0189 + 0.00316(r_2/r_1) + 0.0000867(r_2/r_1)^2$

$\beta = 0.758(r_2/r_1)^{-0.0204}$

r_2 = outer radius of annulus

r_1 = inner radius of annulus

$\bar{\psi}$ is assumed to be 1.0.

$$Pe = Re \cdot Pr = \frac{GDec_p}{k}$$

Given the temperature and pressure of the sodium and

the dimensions of the annulus, k, c_p, De, and G are known,

so the heat transfer coefficient, h, can be calculated.

The net heat flux on the inner boundary of the structure is

then:

$$q''_{in} = h_{in}(T_{sodium} - T_{wall,in}) \qquad (3-3)$$

where $T_{wall,in}$ = the temperature at the inner boundary of

the structure, and h_{in} is calculated from Equation (3-2).

This completes the list of boundary conditions necessary

to solve the radial heat conduction equations.

3.3 Method of Solution

The general equation of heat conduction is [3]:

$$\nabla \cdot (k \nabla T) + q''' = \rho c_p \frac{\partial T}{\partial t} \qquad (3-4)$$

The situation modeled in THERMIT is considerably simpler, though, because of the assumptions of negligible axial and azimuthal conduction, and zero heat generation within the structure. With these simplifications Equation (3-4) reduces to:

$$\rho c_p \frac{\partial T}{\partial t} = \frac{1}{r} \frac{\partial}{\partial r}(rk\frac{\partial T}{\partial r}) \qquad (3-5)$$

This equation, coupled with the boundary conditions (3-1) and (3-3), constitutes the analytical solution to the problem.

The finite difference scheme used to solve these equations on the computer is similar to that described in Ref. [1] for the fuel rod model, with some modifications. The structure is divided into a series of concentric rings (see Figure 3.3), each of which shall be called a mesh cell. The properties ρ, c_p, and k are evaluated at the centers of the mesh cells, while the temperatures of the structure are calculated at the boundaries of the mesh cells (called the nodes). Both sides of Equation (3-5) are multiplied by rdr and integrated between the centers of the two mesh cells around node i to yield:
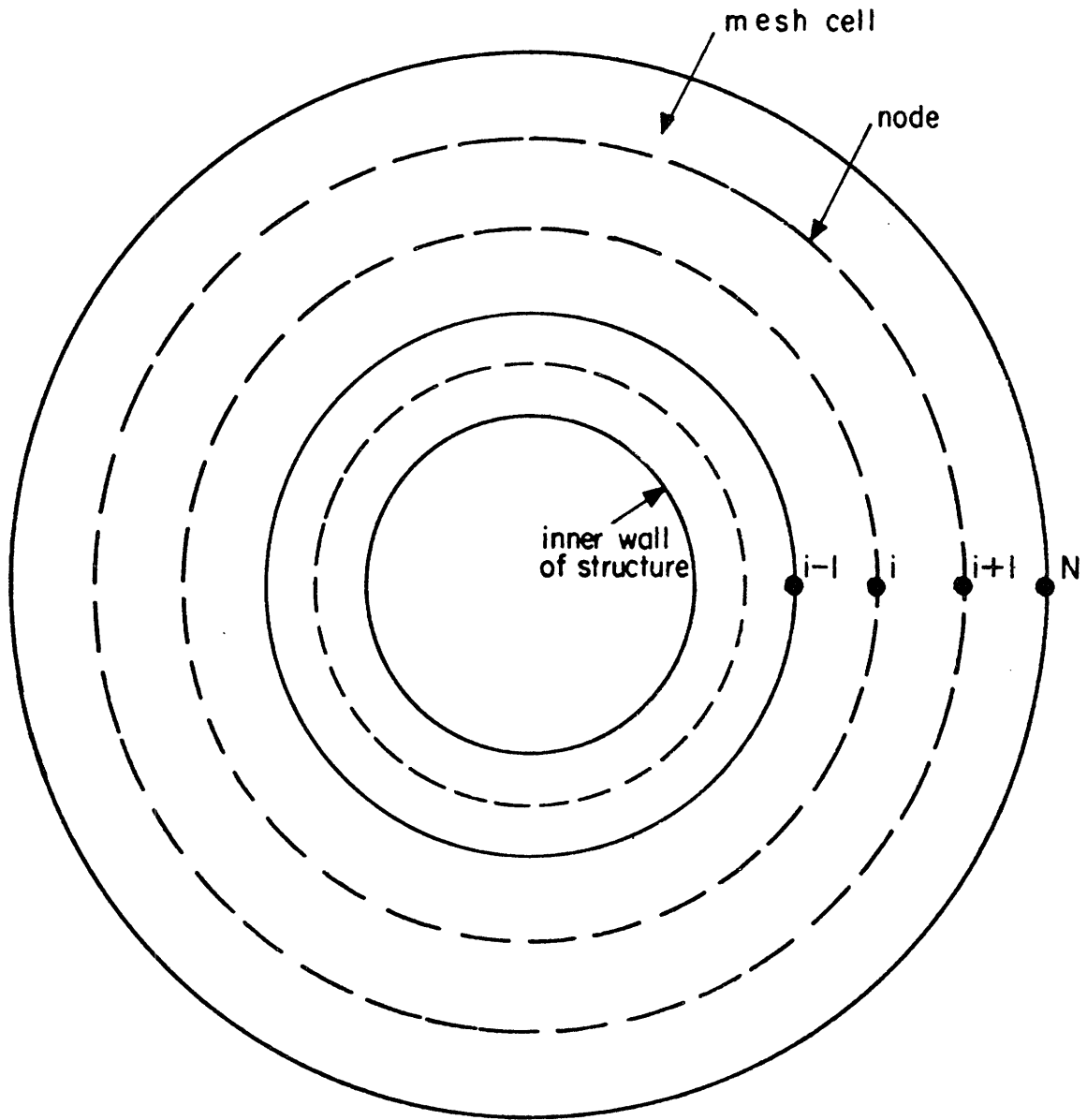
Figure 3.3 Mesh Cell Representation of Structure

$$\int_{r_{i-\frac{1}{2}}}^{r_{i+\frac{1}{2}}} \rho c_p \frac{\partial T}{\partial t}\, r\, dr - \int_{r_{i-\frac{1}{2}}}^{r_{i+\frac{1}{2}}} d(rk\frac{\partial T}{\partial r}) = 0 \qquad (3\text{-}6)$$

For the average cell, the numerical integration of (3-6) yields:

$$(\overline{\rho c_p})_i^{(n)}\left(\frac{T_i^{(n+1)} - T_i^{(n)}}{\Delta t}\right) - (\frac{rk}{\Delta r})_{i+\frac{1}{2}}(T_{i+1}^{(n+1)} - T_i^{(n+1)})$$

$$+ (\frac{rk}{\Delta r})_{i-\frac{1}{2}}(T_i^{(n+1)} - T_{i-1}^{(n+1)}) = 0 \qquad (3\text{-}7)$$

where

$$(\overline{\rho c_p})_i = \frac{r_{i+\frac{1}{2}}^2 - r_i^2}{2}(\rho c_p)_{i+\frac{1}{2}} + \frac{r_i^2 - r_{i-\frac{1}{2}}^2}{2}(\rho c_p)_{i-\frac{1}{2}} \qquad (3\text{-}8)$$

The superscripts refer to the time step at which the variables are evaluated, and the subscripts refer to the mesh cell positions at which the properties are taken. Integral values denote nodes, while half integral values denote mesh cell centers.

There are two locations at which Equation (3-7) is not valid. These are the inner surface of the structure (the first half-cell), and the outer surface of the structure (the last half-cell). For the inner surface of the structure Equation (3-6) is integrated from r_1 to $r_{3/2}$. This gives:

$$\frac{r_{3/2}^2 - r_1^2}{2}(\rho c_p)_{3/2}^{(n)}\left(\frac{T_1^{(n+1)} - T_1^{(n)}}{\Delta t}\right) - (\frac{rk}{\Delta r})_{3/2}(T_2^{(n+1)} - T_1^{(n+1)})$$

$$+ rq_{in}'' = 0 \qquad (3\text{-}9)$$

where q_{in}'' is given by Equation (3-3).

The outer half-cell is integrated from $r_{N-\frac{1}{2}}$ to r_N to obtain:

$$\frac{r_N^2 - r_{N-\frac{1}{2}}^2}{2}(\rho c_p)_{N-\frac{1}{2}}^{(n)} \left(\frac{T_N^{(n+1)} - T_N^{(n)}}{\Delta t}\right) + \left(\frac{rk}{\Delta r}\right)_{N-\frac{1}{2}} (T_N^{(n+1)} - T_{N-1}^{(n+1)})$$

$$+ r_N q_{out}'' = 0 \qquad\qquad (3-10)$$

where q_{out}'' is given by Equation (3-1), and N = the total number of nodes.

One further item has to be specified before Equations (3-9) and (3-10) can be considered complete, and that is the time step at which q_{in}'' and q_{out}'' are to be evaluated. The maximum degree of implicitness is desired. In order to satisfy this objective the following equations are used:

$$q_{in}''^{(n+1)} = h_{in}^{(n)} (T_{sodium}^{(n)} - T_{wall,in}^{(n+1)}) \qquad\qquad (3-11)$$

$$q_{out}''^{(n+1)} = h_{out} (T_{wall,out}^{(n+1)} - T_\infty) \qquad\qquad (3-12)$$

Note that h_{out} and T_∞ are constant, so they have no superscripts. One can see that both h_{in} and T_{sodium} are evaluated explicitly. This is necessary because of the fact that T_{sodium} is really the average temperature of all the fluid cells in contact with the structure. An attempt to include the T_{sodium} term implicitly would couple the fluid cells to each other through temperatures as well as pressures, and would therefore radically alter the entire fluid dynamics solutions scheme of the code.

The result of Equations (3-7) through (3-12) is a set
of N simultaneous linear equations in N unknowns (T_1 to T_N).
The solution of the matrix problem formed by these equations
is accomplished by the Gaussian (forward elimination-back
substitution) method.

Equations (3-7) through (3-12) thus provide a solution
to the temperature problem in the structure. Because the
only coupling with the fluid dynamics portion of the code
(through Equation (3-11)) is explicit, the structure con-
duction problem can be solved for the new time step <u>before</u>
the fluid dynamics portion is solved. Indeed, this must
be the case, because the heat flux term q''_{in} is implicit
in the wall temperature of the structure.

Equations (3-7), (3-9), and (3-10) are modified some-
what for steady state calculations. The object in obtaining
a steady state is to speed up the calculations as much as
possible, so the first term in each of the above equations
is dropped. This neglects the thermal inertia of the material,
and thus accelerates the rate at which steady state is obtained.
The same method is used in solving the fuel rod conduction
equations (see Ref. [1]).

Now that the new temperature distribution in the structure
has been obtained, its effect on the fluid must be determined.
The heat flux at the fluid/wall interface is known (Equation
(3-11)), but this is a total flux, averaged over the whole

surface at each axial section. Since THERMIT solves the fluid dynamics equations cell by cell, the total heat loss must be apportioned among the individual fluid cells in contact with the structure. This apportioning is done on the basis of the perimeter of contact of each of the cells. For example, if channel A has a perimeter of contact that is three times that of channel B, then the heat loss (or gain) experienced by channel A will be three times that of channel B.

As noted before, only channels in the single phase liquid regime lose a significant portion of heat. Thus, any channel in which vapor is present is excluded from both the averaging and apportioning schemes defined above.

3.4 Programming Information

The structure conduction model requires eleven additional input parameters above those described in Reference [1] (see Appendix A). There are three new integers, two real numbers, three integer arrays, and three real arrays, in addition to modifications in one other input parameter.

The first of the three integers, "nx", specifies the number of fluid channels whose perimeter includes some part of the structure wall. The second, "nrzs", sets the number of radial zones (i.e. different materials) in the structure. There is no restriction on the number of zones allowed. The third new integer input, "istrpr", specifies whether or not the temperature in the structure is to be printed on the

output file. A value of one is affirmative, while zero is negative. If the structure conduction option is requested the calculations are performed regardless of the value of "istrpr". One of the previously existent parameters, "iht", has also been modified. It now consists of two digits, the first of which specifies the type of structure conduction desired. If the first digit is omitted the structure conduction option is bypassed. A value of one in the tens place requests structure conduction with the thermal properties of the structure (k and ρc_p) invariant with temperature, while a value of two selects the full structure conduction calculation.

The two additional real numbers, "hout" and "tout", are the heat transfer coefficient to the outside and temperature of the outside environment, as written in Equation (3-1).

Six new arrays are necessary if the structure conduction option is requested (i.e. if the tens digit of "iht" is greater than zero). The first three are integer arrays. "inx(nx)" gives the index number of each of the fluid channels adjacent to the structure. See Reference [1] for a description of the index numbering system for the fluid channels. The integer array "mnrzs(nrzs)" specifies the material in each of the radial zones in the structure. Each of the integers one

through six represents a different material (see Section 4.2). "nrmzs(nrzs)" sets the number of mesh cells in each radial zone in the structure. As in the fuel rod model, the mesh size within each zone is uniform. The last three new inputs are real arrays. "pcx(nx)" contains the actual contact perimeter for each of the fluid channels adjacent to the structure. (Note: the order of the entries in this array must be the same as the order in "inx", so the code will match up the channels with their proper perimeters. For example, if channel seven is the third value in "inx" then the perimeter corresponding to that channel must be the third entry in "pcx".) The next array, "drzs(nrzs)", specifies the thickness (in the radial direction) of each of the radial zones in the structure. The last array, "tws(nz)", is the initial temperature of the inside wall of the structure. The entire structure is considered to be at this temperature at time zero.

In order to accommodate the structure conduction model four new subroutines were added to THERMIT and one existing one was modified extensively. The new subroutines paralleled the fuel rod subroutines to a certain extent.

The first subroutine, INITSC, is called from subroutine INIT, and performs a function analogous to that of INITRC. It sets up the geometry of the structure from the input parameters described above. This subroutine is called only

once, at the beginning of the calculation, and is bypassed if the structure conduction option is not requested. The geometry of the structure cannot be changed once it is set.

The main structure conduction subroutine, QLOSS, performs the same functions as HCOND0 and HCOND1 perform for the fuel rod conduction. This subroutine, which is called from subroutine NEWTON, averages the fluid properties in the exterior fluid cells, calls subroutine HXCOR, which calculates the heat transfer coefficient defined in Equation (3-2), calls subroutine CPROP to get the thermal properties of the structure, calls subroutine STEMPF to solve the matrix equation for the structure temperatures (as RTEMPF does for the fuel rod temperatures), and apportions the heat loss among the exterior fluid cells according to the procedure described in the previous section. The array "qlss", containing the heat losses from each exterior cell due to structure conduction, is passed into subroutine QCOND, where it is combined with the array "qcnd" (which contains the heat losses from each cell due to conduction between fluid cells), to produce a single array containing the net heat flow into each cell due to both liquid conduction and structure conduction. This array is then passed on to the liquid phase energy equation in subroutine JACOB.

The subroutine CPROP mentioned in the previous paragraph is not really a new subroutine, but a modification of the old

subroutine RPROP, which calculated the thermal properties of the fuel rod. Subroutine CPROP is called in both the structure and fuel rod conduction models, and will be described in more detail in Section 4.2.

3.5 Sample Cases

Before the above-mentioned structure conduction model was incorporated in THERMIT it was tested separately, to insure the accuracy of its predictions. Two transient cases were run.

The purpose of the first case was to test the method in which the conduction equations are finite differenced and solved, so a de-emphasis was placed on the boundary conditions. In fact, the geometry used in this case is a solid cylinder of 5.0 cm radius, so the inner boundary condition is adiabatic, and the heat flux apportioning scheme is bypassed. The situation modeled is that of a cylinder at 500°k placed in a 200°k environment, with a constant heat transfer coefficient of 342.06W/m^2°k on the outer boundary. The calculations were continued for 500 seconds, using ten second time steps. The results are plotted in Figure 3.4. The temperature histories at the center and surface of the cylinder were then compared with the analytical solutions [5]. The results of this comparison are displayed in Figures 3.5 and 3.6. As one can see, the model simulates the analytical results quite closely. If a smaller time step were used the model would become even more accurate.
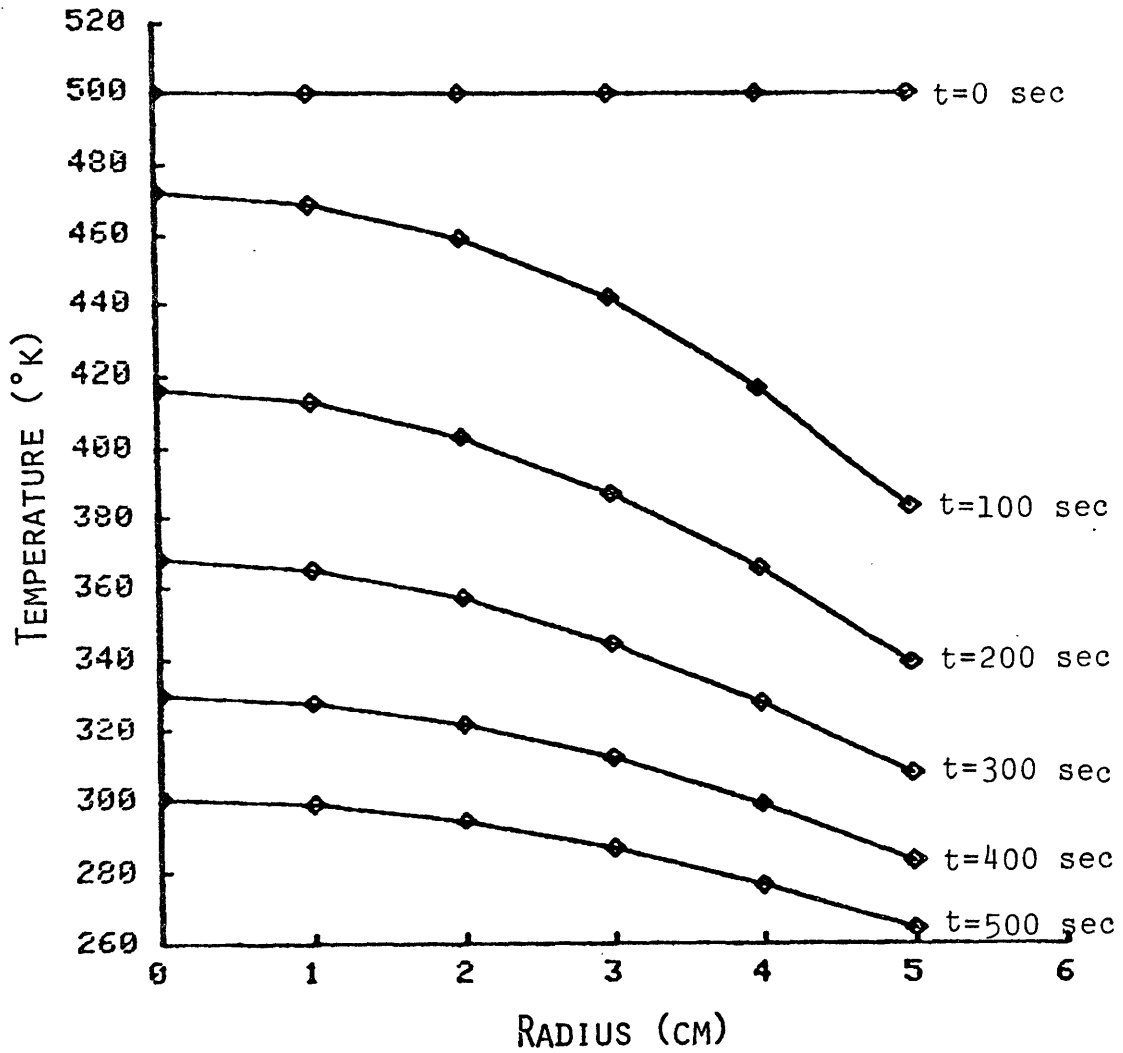
Figure 3.4   Temperature Distribution of Cylinder
Initially at 500°k, Placed in a 200°k
Environment
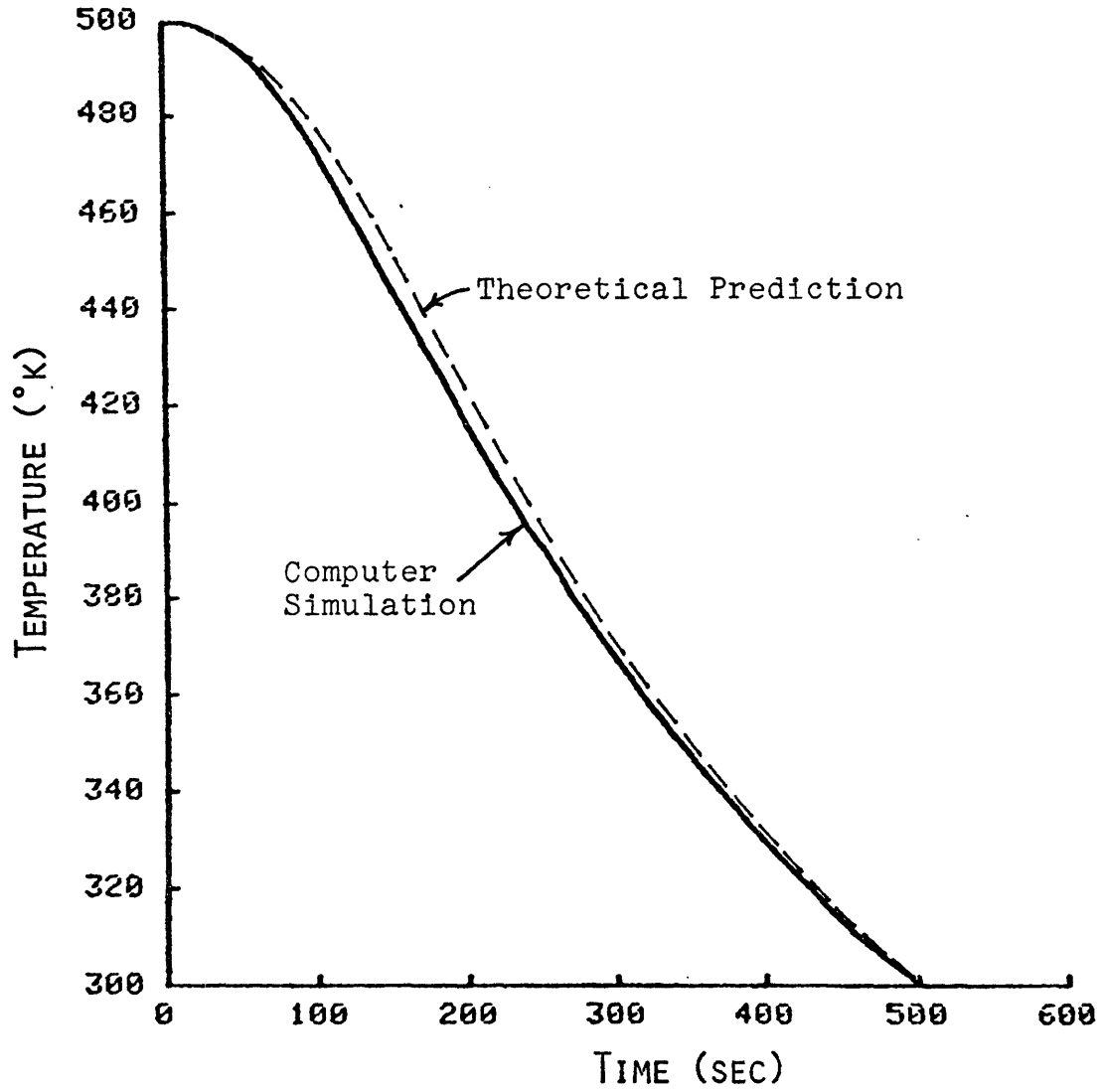
Figure 3.5 Centerline Temperature of Cylinder
vs. Theoretical Prediction
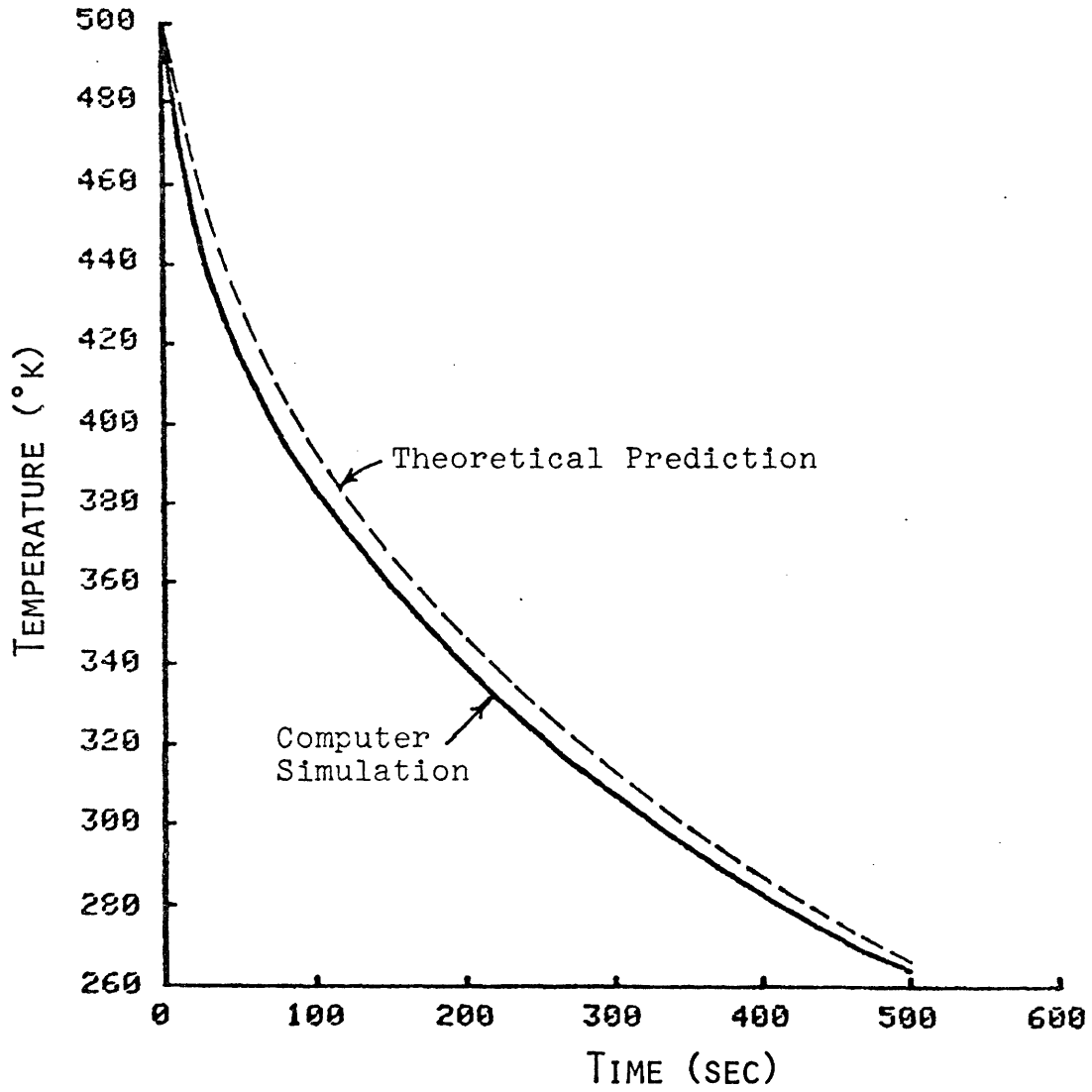
Figure 3.6   Surface Temperature of Cylinder
vs. Theoretical Prediction

The second test case was of a more complicated nature, so no comparison with an analytical result was possible. It consisted of a two-component annulus with stainless steel on the inside and an insulating material called Marimet* on the outside. The annulus, initially at 500°k, was subjected to an outer boundary condition of 200°k and a 342.06W/m²°k heat transfer coefficient. The inner boundary consisted of three fluid mesh cells fixed at 800, 810, and 820°k. The volume-average temperature was 805.71°k. The purpose of this simulation was to test the code logic which deals with multi-zone geometry, inner boundary conditions, and heat apportioning among fluid cells. Figure 3.7 shows the temperature distribution within the annulus at several different points in time. One can see that as steady state was approached the inner section of the annulus had a much smaller temperature gradient than the outer one. This is due to the fact that the thermal conductivity of stainless steel is much greater than that of the Marimet insulation.

After these two separate tests were run, the structure conduction model was incorporated in THERMIT. In most cases the effect of including structure conduction is inversely proportional to the size of the region modeled. For example, the inclusion of structure conduction would have a far greater

---

*Marimet is a Johns-Manville trade name for calcium-silicate block insulation.
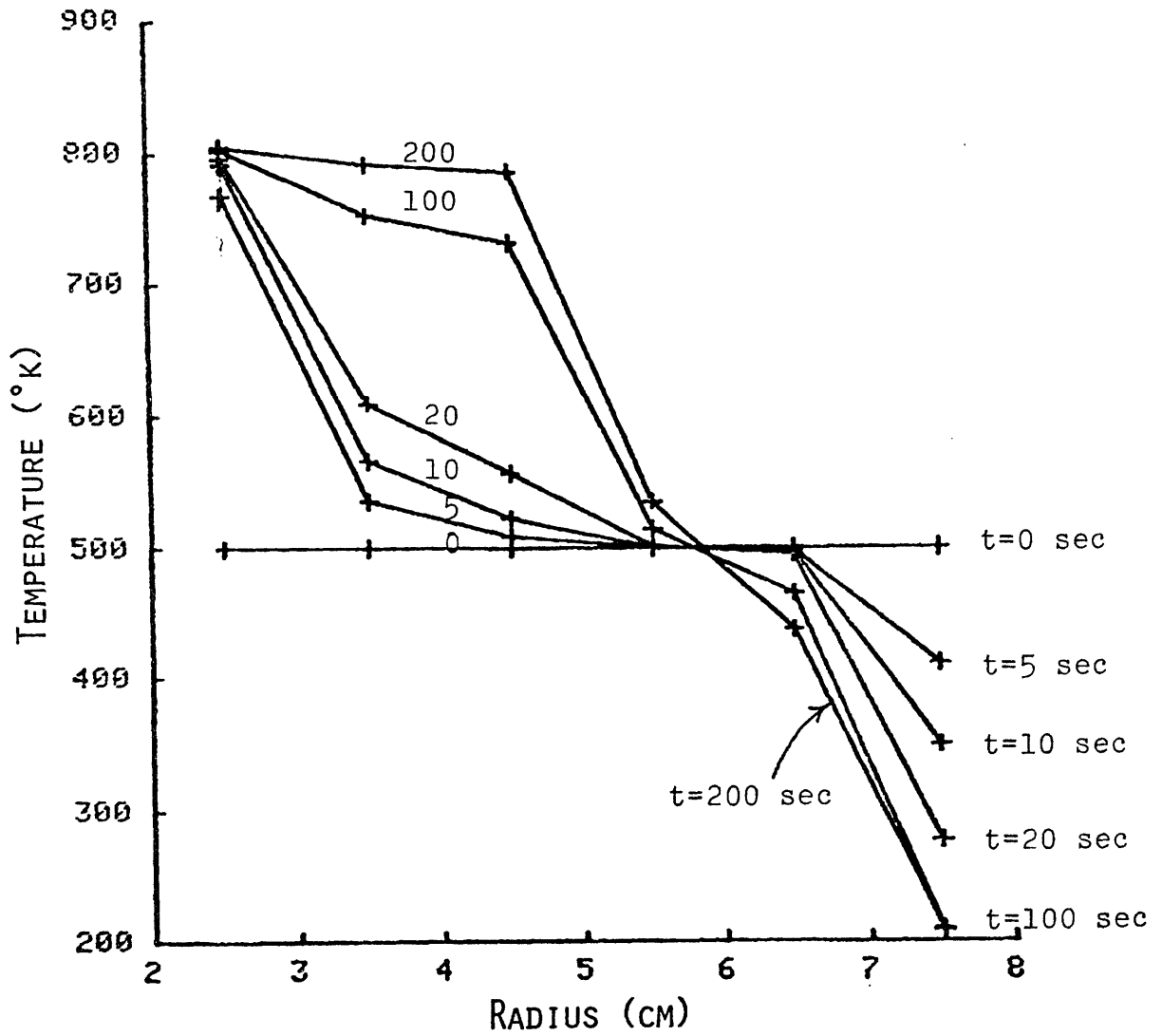
Figure 3.7   Temperature Distribution of Two-component
             Annulus Initially at 500°k, Subjected to
             Different Boundary Conditions at the Inner
             and Outer Surfaces

effect when modeling heat transfer in a single rod array
than when modeling heat transfer in an entire reactor
core. In order to test the effect of including heat trans-
fer to the structure, THERMIT was run to simulate the re-
sults of the THORS Bundle 6A Experiments done at Oak Ridge
National Laboratory [6]. The code was run both with and
without the structure conduction option, so as to see
whether the inclusion of structure conduction significantly
improved the results. The results of this comparison
are presented in Chapter 7.
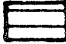
Chapter 4: FUEL ROD CONDUCTION MODEL

4.1 Features of Model

The new fuel rod conduction model incorporated in the sodium version of THERMIT allows the user a considerable amount of flexibility in modeling the heat transfer from the fuel rod to the sodium coolant. Previously the user was restricted to three radial zones: fuel, gap, and clad. Now the user may specify the number of radial zones desired and the material in each zone, in addition to the number of mesh cells per zone. This capability becomes especially important in the case of radially variable fuel rod properties. The old three-zone model could not handle anything more complicated than the fuel rod shown in Figure 4.1. Suppose, however, that it was necessary to model the fuel rod in Figure 4.2, in which sintering has occurred. Now five zones are needed, to represent the central void, the denser sintered region, the outer fuel region, the gap, and the clad. The latter case could not be adequately modeled with only three radial zones. Another advantage of the new fuel rod model is that the user may vary the mesh spacing within one material region by dividing it up into subregions. For example, given the fuel rod in Figure 4.1, the user might want to use a finer mesh spacing on the outer half of the fuel pellet than on the inner half, in order to more accurately represent the temperature gradi-

KEY

☒ = fuel pellet

▤ = cladding

☐ = gap
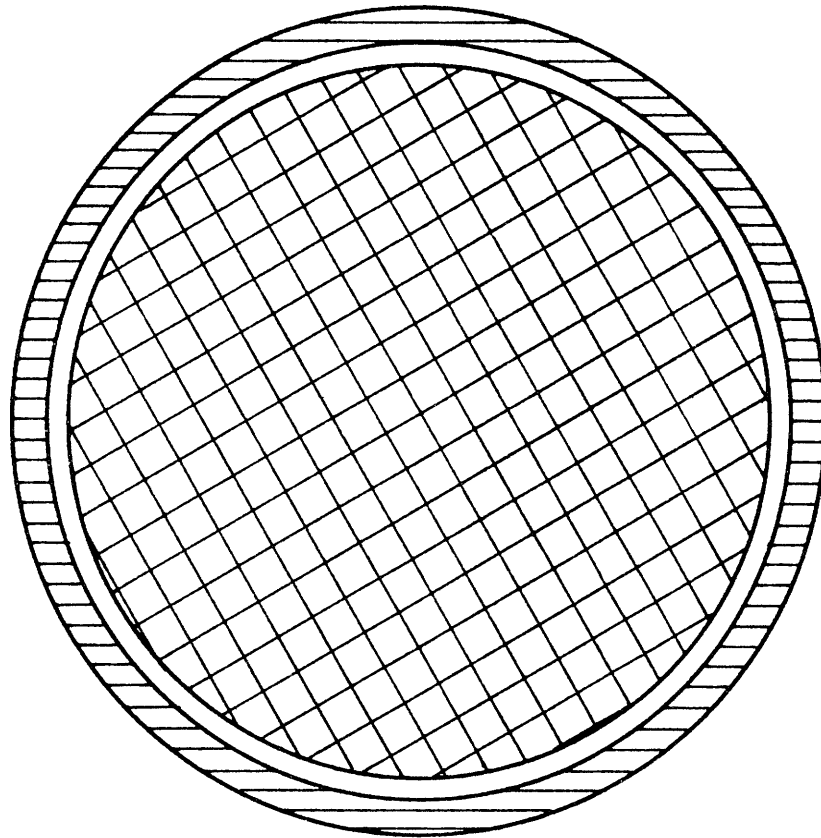
Figure 4.1 Three Zone Fuel Rod (Top View)
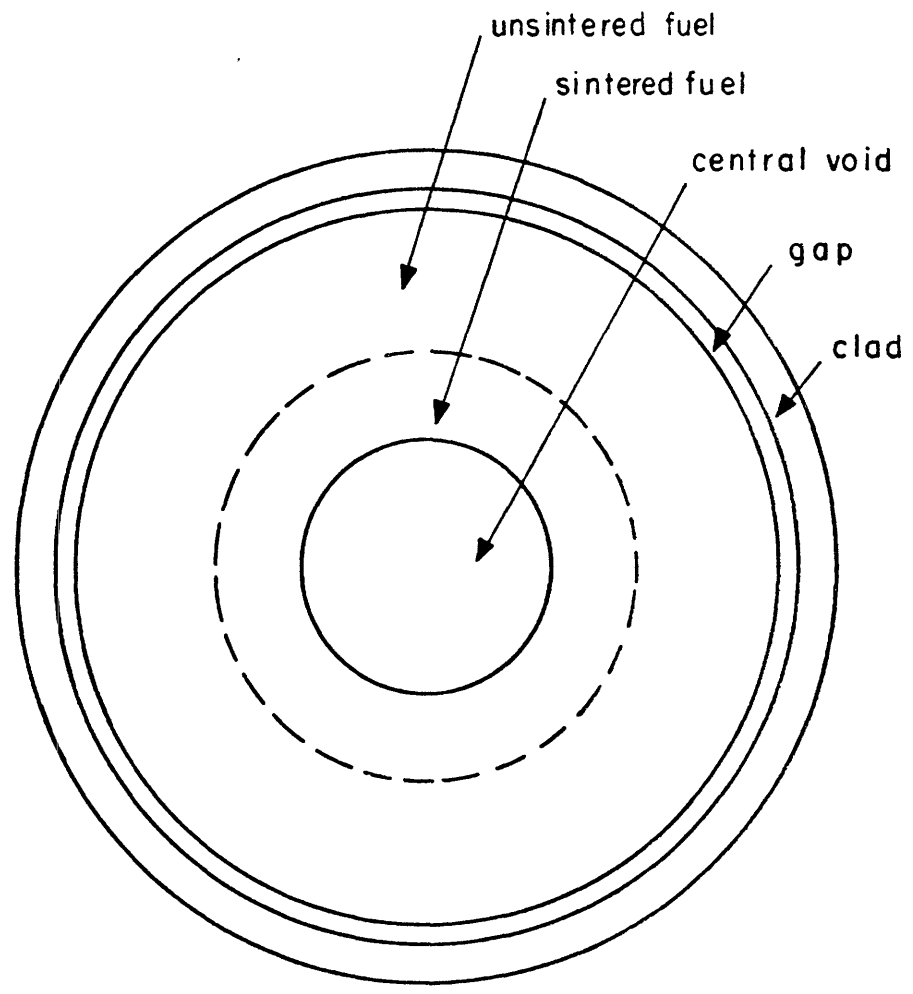
Figure 4.2   Five Zone Fuel Rod (Top View)

ient. With the new model the user may split up the fuel pellet into two radial zones, each of which will contain the same material, but with a different mesh spacing.

In addition to providing for a variable number of radial zones in the fuel, the new fuel rod model contains the option of specifying as many axial regions as desired. This is extremely important in modeling such features as a fission gas plenum (see Figure 4.3). In the previous version of THERMIT the geometrical layout of the fuel rod was assumed to extend axially all the way up the channel. The new model, however, allows the user to "construct" a fuel rod in each axial region. The number of radial zones, material composition, and even the number of fuel rods per channel may vary from one axial region to the next. The next section describes the input variables to the new model in more detail.

4.2 Programming Information

The incorporation of the new fuel rod model in the sodium version of THERMIT involved extensive revisions of the required input data, because instead of having a fixed number of radial zones and only one axial region, both of these parameters were variable.

Two new integer inputs were added. The first, "narf", denotes the number of axial regions in the fuel. A separate set of geometrical inputs is required for each axial
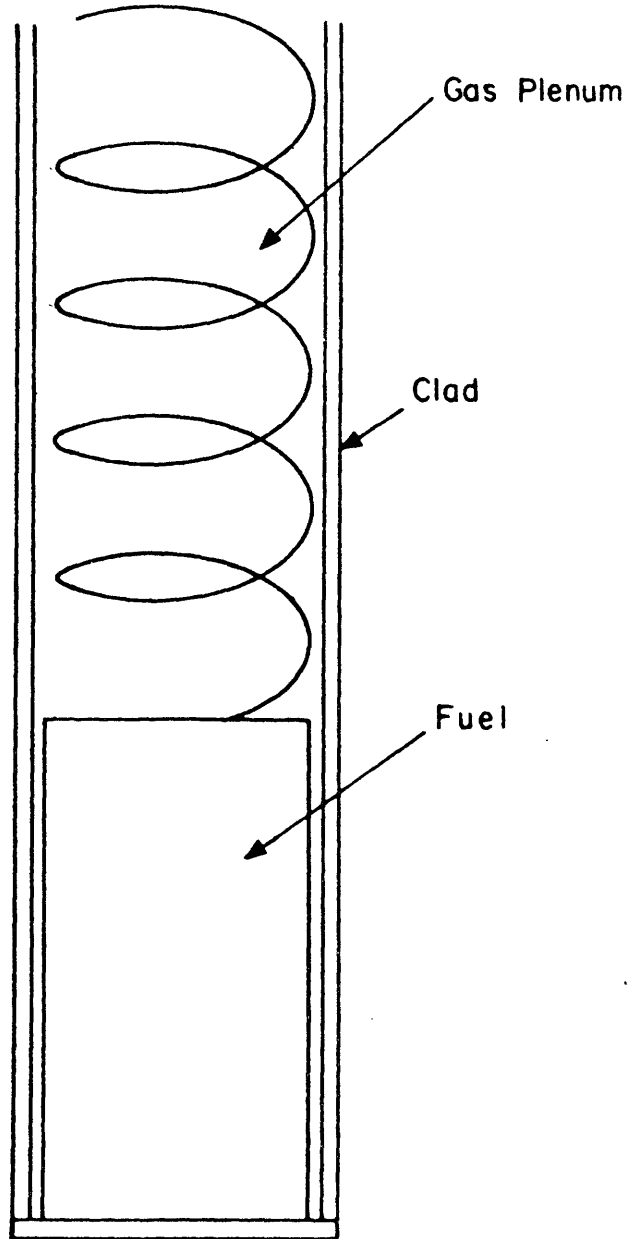
Figure 4.3   Fuel Rod with Gas Plenum   (Side View)

region. The parameter "ihtpr" is analogous to "istrpr", described in Section 3.4. It is an indicator for the printing of the temperatures and heat fluxes within the fuel rod. A value of one requests printout, while a value of zero bypasses printing (the calculations themselves are still performed, however). Section 3.4 described the tens digit of the parameter "iht". The units digit controls the fuel heat transfer. A value of zero bypasses the fuel rod conduction mechanism, a value of one requests fuel heat transfer with all thermal properties of the rod constant with temperature, a value of two keeps only the gap properties constant, and a value of three allows all thermal properties to vary with temperature.

The configuration of the fuel rod is specified by four new integer arrays. "ifcar(narf)" contains the axial level number of the first mesh cell (i.e. lowest) in each of the axial regions specified in the fuel. For example, if there are twelve axial cells ("nz"=12), and three axial regions, extending from cells 1-4, 5-8, and 9-12, then "ifcar" contains the numbers 1, 5, and 9. (Note: the first entry in "ifcar" must always be one, and the entries must be in increasing order. For example, the order 1, 9, 5 is unacceptable.) The array "nrzf(narf)" specifies the number of radial zones in the fuel for each axial region. Note that the capability of varying the number of radial

zones between axial regions exists. "nrmzf(nrzfmx,narf)" sets the number of radial meshes in each radial zone of the fuel at each axial level. The first index, "nrzfmx", represents the maximum value in the array "nrzf". The user must be cautious when inputting this array. Consider the following example: three axial regions are desired ("narf"=3), which have 3, 4, and 1 radial zones, respectively. This makes "nrzfmx"=4, so the array "nrmzf" is dimensioned (4,3). The order of input is: (1,1), (2,1), (3,1), (4,1), (1,2), (2,2), ..., where the second index denotes the axial region number. Because region one has only three radial zones, entry (4,1) is superfluous, as are entries (2,3), (3,3), and (4,3), since region three has only one radial zone. Any value may be input for these entries (zero makes the most sense), but it is important to remember that <u>they</u> <u>must</u> <u>be</u> <u>entered</u>. This same argument applies to the next array: "mnrzf(nrzfmx,narf)" which specifies the material in each radial zone of the fuel, at each axial level. Each available material is given an integer number, and when that number is entered in "mnrzf" the appropriate radial zone is associated with that material. The numbering scheme is identical for the structure conduction array "mnrzs". Currently six materials exist, and are given the following numbers:

1 = fuel (UO_2/PuO_2)

2 = the fuel-clad gap in the fuel

3 = type 316 stainless steel

4 = type 304 stainless steel

5 = liquid sodium

6 = a degraded form of an insulating material

called Marimet, Ref. [6]

More materials may be added by the user as needed.

Three of the existing real arrays dealing with fuel rod conduction were modified, and one new one was added. The modifications in the existing arrays were in how they were dimensioned. The array "qt(narf,nc)", which controls the transverse power shape, may now vary in each axial region. The same is true of "rn(narf,nc)", which sets the number of fuel rods in each channel. The array that controls the fuel rod radial power shape, "qr(nfmlmx,narf)" (where "nfmlmx"=the maximum number of mesh cells in the fuel, taken over all axial regions), may also vary with the axial region. Note that the order of input to the latter array presents the same subtlety as in the arrays "nrmzf" and "mnrzf". The final array connected with the fuel rod conduction model is "drzf(nrzfmx,narf)", which contains the thickness of each radial zone in the fuel, at each axial region. This replaces the old real inputs "thc" and "thg" (see Ref. [1]).

This completes the list of new and revised heat conduction input variables. A short summary of these variables is presented in the THERMIT Input Description in Appendix A.

The implementation of the new fuel rod conduction model in THERMIT required modifications in the input and initialization portions of the code. Subroutine INPUT was modified extensively, so as to incorporate the many new and revised input variables. The major changes occurred in subroutine INITRC, however. This subroutine, which initializes the geometrical parameters involved in the solution scheme, was rewritten in a much more general form.

The only other subroutine that required major changes was subroutine RPROP, which is now called CPROP, and is used for the structure conduction calculation, too. This subroutine calculates the parameters ρc_p, and k for each fuel rod mesh cell by calling the appropriate material property subroutine corresponding to the radial zone of the fuel rod. For example, if CPROP is called for a three-zone geometry consisting of fuel, gap, and type 304 stainless steel clad (material numbers 1, 2, and 4), then it will first call subroutine MP1 to get the fuel thermal properties, then subroutine MP2 to get the gap properties,

and finally subroutine MP4 to get the clad properties.
The logic was intentionally set up so as to facilitate
the addition of subroutines modeling materials not
currently represented. Thus the user may easily add a
subroutine MP7, MP8, etc., until all the necessary
materials are included.

The effect of the new fuel rod model was tested
for the THORS Bundle 6A Experiments run at Oak Ridge [6].
The results are presented in Chapter 7.

Chapter 5: INTERFACIAL EXCHANGE COEFFICIENTS

5.1 Mass Exchange Coefficient

The z-direction mass conservation equations (in two-fluid form) are the following:

$$\frac{\partial}{\partial t}(\alpha \rho_v) + \frac{\partial}{\partial z}(\alpha \rho_v u_v) = \Gamma \tag{5-1}$$

$$\frac{\partial}{\partial t}[(1-\alpha)\rho_\ell] + \frac{\partial}{\partial z}[(1-\alpha)\rho_\ell u_\ell] = -\Gamma \tag{5-2}$$

where Γ is the mass exchange coefficient, defined as the net rate of mass transfer per unit volume from the liquid to the vapor phase ($kg/m^3 sec$). If Equations (5-1) and (5-2) are added together the gamma term disappears, and the mixture form of the mass conservation equation is produced. Gamma may be split into two components as follows:

$$\Gamma = \Gamma_e - \Gamma_c \tag{5-3}$$

where Γ_e = rate of liquid evaporation per unit volume
($kg/m^3 sec$)

Γ_c = rate of vapor condensation per unit volume
($kg/m^3 sec$)

The model for mass exchange used in THERMIT is a modified version of the Nigmatulin Model described in References [7] and [8]:*

$$\Gamma_e = \begin{cases} \rho_\ell A \alpha (1-\alpha) \sqrt{R_g} \lambda_e \left(\dfrac{T_\ell - T_s}{\sqrt{T_s}} \right) & \text{for } T_\ell > T_s \\ \\ 0 & \text{for } T_\ell \leqslant T_s \end{cases} \qquad (5-4)$$

$$\Gamma_c = \begin{cases} -\rho_v A \alpha (1-\alpha) \sqrt{R_g} \lambda_c \left(\dfrac{T_v - T_s}{\sqrt{T_s}} \right) & \text{for } T_v < T_s \\ \\ 0 & \text{for } T_v \geqslant T_s \end{cases} \qquad (5-5)$$

where R_g = gas constant for sodium = 361.49J/kg°K

λ_e and λ_c are calibration constants = 0.1

A is proportional to the interfacial area of mass exchange per unit volume (m^{-1}).

In the original Nigmatulin Model, A was calculated by assuming bubbly flow with a constant bubble density:

$$A = \begin{cases} \left(\dfrac{4\pi N}{3} \right)^{1/3} \alpha^{2/3} & \text{for } \alpha \leqslant 0.5 \\ \\ \left(\dfrac{4\pi N}{3} \right)^{1/3} (1-\alpha)^{2/3} & \text{for } \alpha > 0.5 \end{cases} \qquad (5-6)$$

where N = bubble density = 10^7 bubbles/m^3.

---

*Also see pages 34 and 35 of Ref. [1]. Note, however, that errors are present in some of the equations on these pages and in the previous version of THERMIT. The correct equations are given in this chapter.

Note that A is proportional (not equal) to the interfacial area. For example, consider the situation where $\alpha \leqslant 0.5$ (vapor bubbles in a liquid continuum).

$$A_{true} = \frac{Surface\ Area\ of\ Bubbles}{Unit\ Volume\ of\ Fluid} = 4\pi r_b^2 N \qquad (5-7)$$

where r_b = radius of bubbles

A_{true} = the true interfacial area

To get r_b as a function of void fraction use the definition of the latter:

$$\alpha = \frac{Volume\ of\ Vapor}{Unit\ Volume} = \frac{4}{3}\pi r_b^3 N \qquad (5-8)$$

Rearranging (5-8),

$$r_b^2 = \left(\frac{3\alpha}{4\pi N}\right)^{2/3} \qquad (5-9)$$

Substituting (5-9) into (5-7) we obtain

$$A_{true} = 3\left(\frac{4\pi N}{3}\right)^{1/3}\alpha^{2/3} = 3A \qquad (5-10)$$

Thus the true interfacial area of mass exchange per unit volume is three times that calculated in Equation (5-6).

The model introduced in the current version of THERMIT is identical to the model just described in all respects but one: the interfacial area, A. The original Nigmatulin Model assumes a constant bubble density, which is unrealistic. Not only will the number of bubbles change with the void fraction, but in sodium boiling at low pressures (as in LMFBR's) one finds that the large void fractions en-

countered dictate annular flow over most of the region of interest. The modified version of THERMIT takes these factors into account in developing a methodology for calculating the interfacial area as a function of flow regime and channel geometry.

First consider the bubbly flow regime, which exists at low void fractions. For reasons to be explained later in this section, it will be assumed that for a void fraction less than 0.6 bubbly flow prevails. Bubbles are assumed to form in the middle of each subchannel, packed on top of each other (see Figure 5.1). The geometry considered is that of a triangular array of cylindrical fuel rods, as in LMFBR's.

Take a volume of height dz. In this volume there are $dz/2r_b$ bubbles. Thus the total surface area of all the bubbles is:

$$A_{bubbles} = 4\pi r_b^2 \frac{dz}{2r_b} = 2\pi r_b \, dz \qquad (5-11)$$

The volume of fluid in this height dz is $A_x \, dz$, where A_x is the cross-sectional area of the fluid in the subchannel. For the triangular subchannel of Figure 5.1,

$$A_x = \frac{P^2\sqrt{3}}{4} - \frac{\pi D^2}{8} \qquad (5-12)$$

Therefore,

$$V_{fluid} = A_x \, dz = \left[\frac{P^2\sqrt{3}}{4} - \frac{\pi D^2}{8}\right] dz \qquad (5-13)$$

Top View
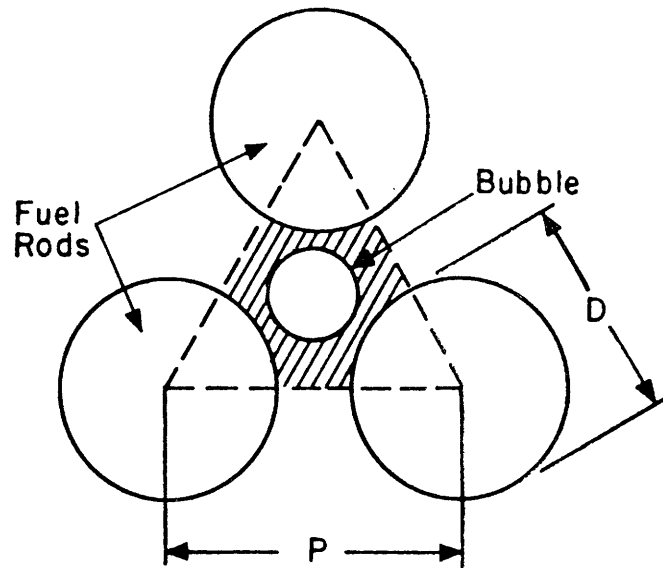
Side View
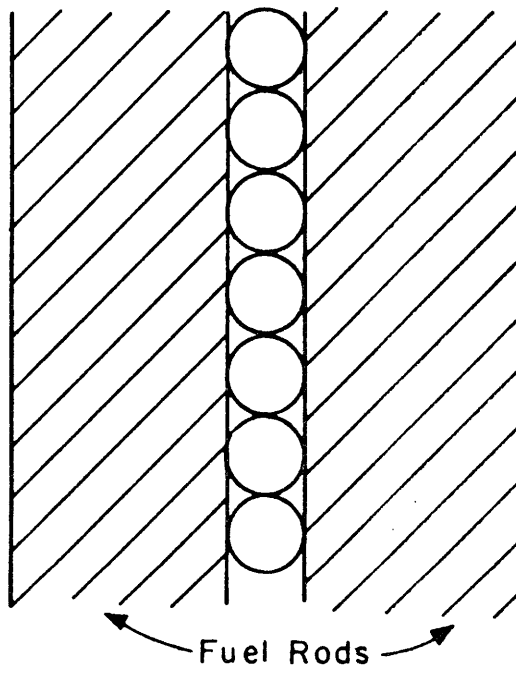
Figure 5.1   Bubbly Flow in Triangular Rod Arrays

From Equations (5-10), (5-11), and (5-13),

$$A = \frac{A_{true}}{3} = \frac{1}{3}\left[\frac{16\pi r_b}{2P^2\sqrt{3} - \pi D^2}\right] \qquad (5-14)$$

Once again, an expression for r_b as a function of void fraction and geometry is needed:

$$\alpha = \frac{\text{Volume of vapor}}{\text{Volume of fluid}} = \frac{\frac{4}{3}\pi r_b^3 \frac{dz}{2r_b}}{\left[\frac{P^2\sqrt{3}}{4} - \frac{\pi D^2}{8}\right]dz} \qquad (5-15)$$

Solving for r_b,

$$r_b = \sqrt{\frac{3\alpha}{16\pi}(2P^2\sqrt{3} - \pi D^2)} \qquad (5-16)$$

Equation (5-16) is substituted into (5-14) to yield:

$$A = \frac{4}{D}\sqrt{\frac{\pi\alpha}{3[2\sqrt{3}(P/D)^2 - \pi]}} \qquad \text{for } \alpha < 0.6 \qquad (5-17)$$

Equation (5-17) is the formulation used to determine the value of A in Equations (5-4) and (5-5), for the bubbly flow regime.

Because of the uncertainty involved in trying to identify a slug flow regime (and also the similarity in surface area between bubbly and slug flow), it is assumed that for a void fraction greater than 0.6 and less than an

upper dryout value of 0.957 (to be explained later), the
flow is of an annular nature. Therefore, the liquid flows
in an annulus around the fuel rods, with the vapor in the
center of the channel (see Figure 5.2). For r_a = the outer
radius of the liquid annulus,

$$A = \frac{A_{true}}{3} = \frac{\frac{1}{2} \cdot 2\pi r_a \, dz}{3 \left[\frac{P^2\sqrt{3}}{4} - \frac{\pi D^2}{8}\right] dz} = \frac{8\pi r_a}{3(2P^2\sqrt{3} - \pi D^2)} \qquad (5\text{-}18)$$

and

$$\alpha_\ell = 1 - \alpha = \frac{\frac{1}{2}\pi (r_a^2 - \frac{D^2}{4}) \, dz}{\left[\frac{P^2\sqrt{3}}{4} - \frac{\pi D^2}{8}\right] dz} \qquad (5\text{-}19)$$

Solving the latter for r_a,

$$r_a = \sqrt{\frac{(1-\alpha)(2P^2\sqrt{3} - \pi D^2) + \pi D^2}{4\pi}} \qquad (5\text{-}20)$$

Substituting (5-20) into (5-18),

$$A = \frac{4\sqrt{\pi}}{3D(2\sqrt{3}(P/D)^2 - \pi)} \sqrt{(1-\alpha)2\sqrt{3}(P/D)^2 + \pi\alpha} \qquad (5\text{-}21)$$

$$\text{for } 0.6 \leqslant \alpha \leqslant 0.957$$

Physically, one would expect the interfacial area of
mass transfer to approach zero as $\alpha \to 1.0$. It is clear
that Equation (5-21) does not satisfy this limit. This is
because, in deriving that equation, it was assumed that
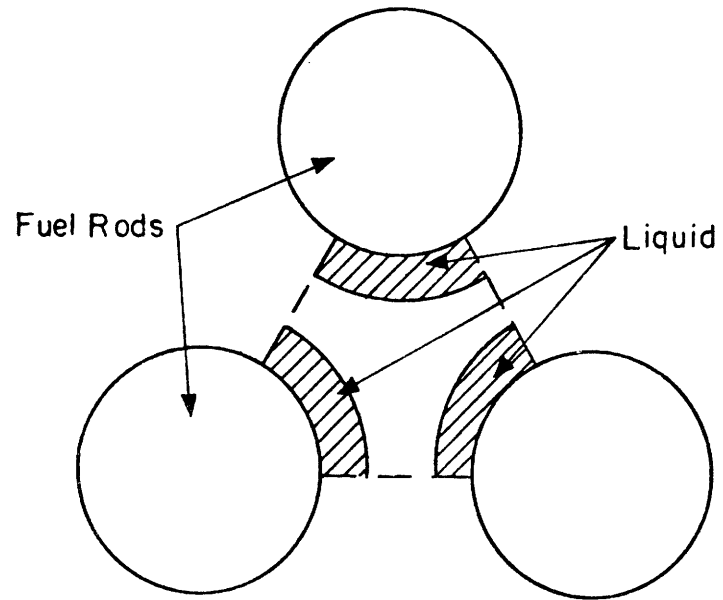
Figure 5.2   Annular Flow in Triangular Rod Arrays

the liquid remains in contact with the wall at all times.
In reality there is a void fraction below 1.0 at which
vapor begins to come in contact with the wall. Experiments dealing with steady state flow of sodium in a heated
tube (see Ref. [9]) have shown that this dryout void fraction is approximately equal to 0.957. Therefore, for
$\alpha > 0.957$, Equation (5-21) is modified so as to approach
zero as $\alpha \to 1.0$:

$$A = \frac{4\sqrt{\pi}}{3D\left(2\sqrt{3}\,(P/D)^2 - \pi\right)} \sqrt{(1-\alpha)\,2\sqrt{3}\,(P/D)^2 + \pi\alpha}\ \sqrt{\frac{1-\alpha}{1-0.957}}$$

$$\text{for } \alpha > 0.957 \qquad\qquad (5\text{-}22)$$

Equations (5-17), (5-21), and (5-22) constitute a
continuous, flow-regime-dependent methodology for calculating the interfacial area of mass exchange required in the
Nigmatulin Model for gamma. These equations are plotted
as a function of void fraction for different P/D ratios
in Figure 5.3 (for a fuel rod assembly with D = 0.25"),
and in Figure 5.4 (for a blanket assembly with D = 0.50").
For comparison, the original Nigmatulin expression for A
(Equation (5-6)), is also plotted.

The discontinuity at $\alpha = 0.6$ represents the transition
from bubbly to annular flow. Note that the "jump" is quite
small for $1.2 < P/D < 1.3$, which is the normal value for
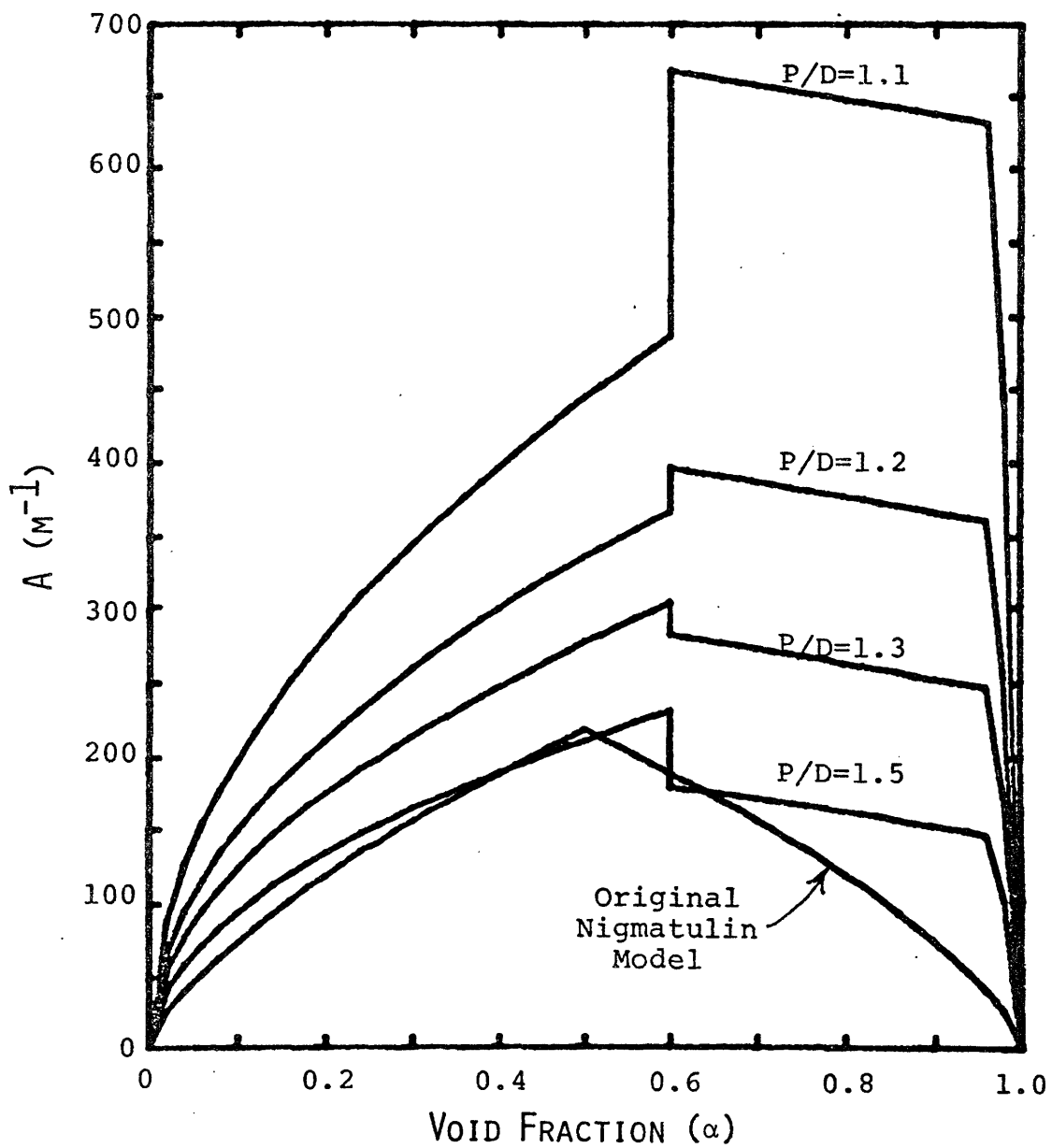
Figure 5.3   Interfacial Area of Mass Exchange
vs. α (D=0.25")
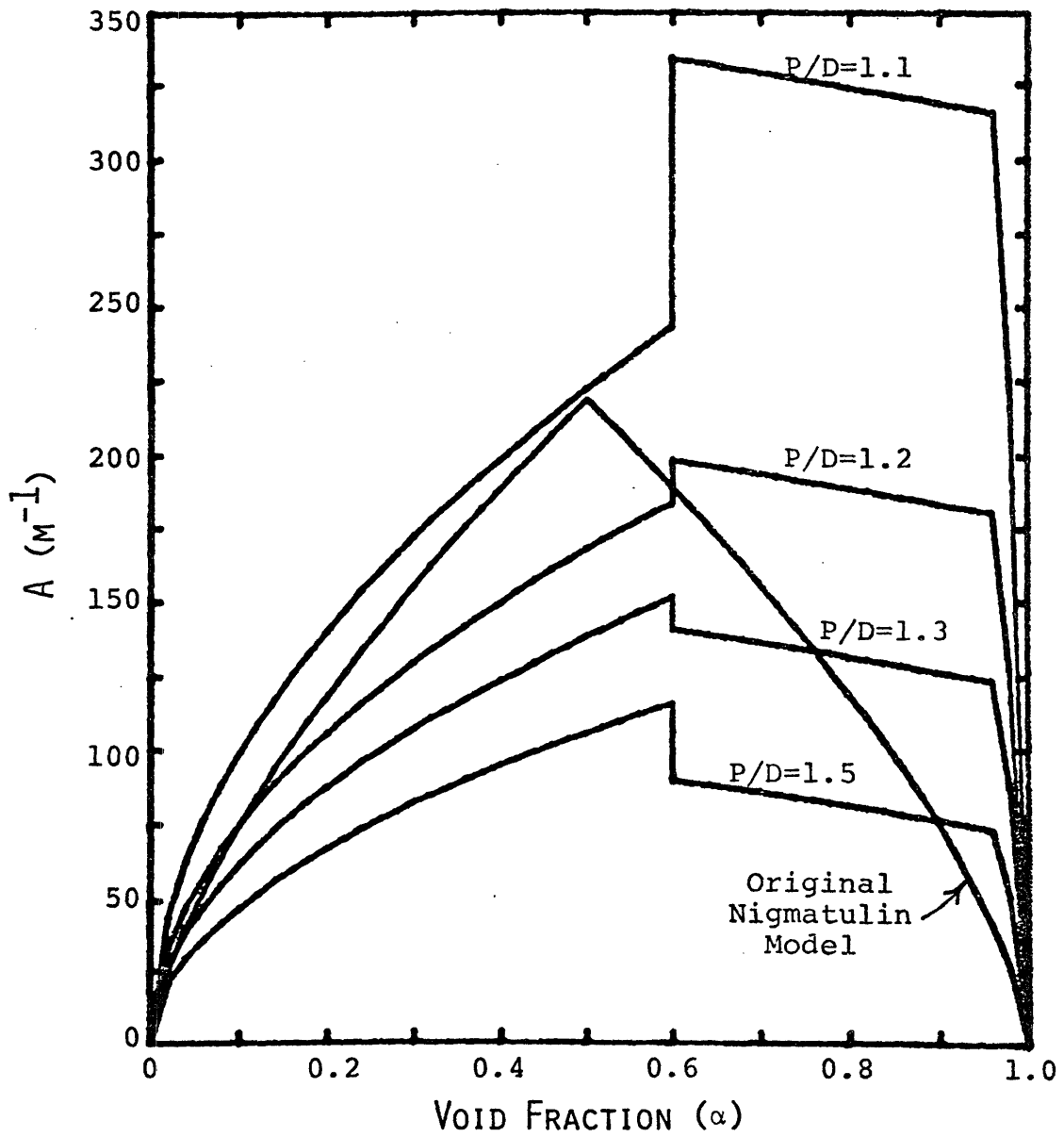
Figure 5.4   Interfacial Area of Mass Exchange
vs. α (D=0.50")

LMFBR's. In fact, there is no discontinuity at all for P/D ≈ 1.25. This was a consideration in choosing 0.6 as the void fraction at which transition occurs, because a large "jump" could cause numerical problems when running the code (see Section 5.3). The main reason for selecting this value, however, is that it represents a good guess at the actual bubbly/slug - annular transition void fraction. Various correlations for calculating these transition void fractions exist, but they all are geometry-dependent, and as yet no generally accepted correlation exists for sodium flow in triangular rod bundles. Even if one existed, though, the increase in accuracy would be meaningless, because far greater uncertainties exist in the Nigmatulin Model, particularly in the values of λ_e and λ_c: the calibration constants.

The manner in which the new model for gamma was incorporated in THERMIT is discussed in more detail in Section 5.3.

5.2 Momentum Exchange Coefficient

Just as the two-fluid mass conservation equations have a coefficient that determines the rate of mass exchange between phases, so the momentum equations have a coefficient that determines the rate of momentum exchange between phases

due to interfacial shear. The general form of the two-fluid momentum equations (in the z-direction) is:

$$\frac{\partial}{\partial t}(\alpha \rho_v u_v) + \frac{\partial}{\partial z}(\alpha \rho_v u_v^2) + \alpha \frac{\partial p}{\partial z} =$$

$$u_\ell \Gamma_e - u_v \Gamma_c - K(u_v - u_\ell) - \alpha \rho_v g - F_{w,v} \qquad (5-23)$$

$$\frac{\partial}{\partial t}[(1-\alpha)\rho_\ell u_\ell] + \frac{\partial}{\partial z}[(1-\alpha)\rho_\ell u_\ell^2] + (1-\alpha)\frac{\partial p}{\partial z} =$$

$$u_v \Gamma_c - u_\ell \Gamma_e + K(u_v - u_\ell) - (1-\alpha)\rho_\ell g - F_{w,\ell} \qquad (5-24)$$

where $F_{w,v}$ = wall friction term acting on the vapor (N/m^3)

$F_{w,\ell}$ = wall friction term acting on the liquid (N/m^3)

K = momentum exchange coefficient due to inter-facial shear (kg/m^{3}sec)

Γ_c and Γ_e are defined as in the previous section.

Once again, if these two equations are summed together the interfacial terms will cancel. Because of this property Equations (5-23) and (5-24) are called the conservative form of the momentum equations. For reasons connected with facilitating the selection of a finite difference strategy, THERMIT uses a non-conservative form of the momentum equations. This form is obtained by differencing the first two terms in Equations (5-23) and (5-24) by parts to obtain:

$$\alpha \rho_v \frac{\partial u_v}{\partial t} + u_v \frac{\partial}{\partial t}(\alpha \rho_v) + \alpha \rho_v u_v \frac{\partial u_v}{\partial z} + u_v \frac{\partial}{\partial z}(\alpha \rho_v u_v) \qquad (5\text{-}25)$$

and

$$(1-\alpha)\rho_\ell \frac{\partial u_\ell}{\partial t} + u_\ell \frac{\partial}{\partial t}[(1-\alpha)\rho_\ell] + (1-\alpha)\rho_\ell u_\ell \frac{\partial u_\ell}{\partial z} +$$

$$u_\ell \frac{\partial}{\partial z}[(1-\alpha)\rho_\ell u_\ell] \qquad (5\text{-}26)$$

Now the mass conservation equations ((5-1) and (5-2)) are substituted for the second and fourth terms of Equations (5-25) and (5-26) to yield:

$$\alpha \rho_v \frac{\partial u_v}{\partial t} + \alpha \rho_v u_v \frac{\partial u_v}{\partial z} + u_v(\Gamma_e - \Gamma_c) \qquad (5\text{-}27)$$

and

$$(1-\alpha)\rho_\ell \frac{\partial u_\ell}{\partial t} + (1-\alpha)\rho_\ell u_\ell \frac{\partial u_\ell}{\partial z} + u_\ell(\Gamma_c - \Gamma_e) \qquad (5\text{-}28)$$

When these expressions are substituted back into Equations (5-23) and (5-24) the non-conservative form of the momentum equations is formed:

$$\alpha \rho_v \frac{\partial u_v}{\partial t} + \alpha \rho_v u_v \frac{\partial u_v}{\partial z} + \alpha \frac{\partial p}{\partial z} = -F_{i,v}(u_v - u_\ell) - \alpha \rho_v g - F_{w,v}$$

$$(5\text{-}29)$$

and

$$(1-\alpha)\rho_\ell \frac{\partial u_\ell}{\partial t} + (1-\alpha)\rho_\ell u_\ell \frac{\partial u_\ell}{\partial z} + (1-\alpha)\frac{\partial p}{\partial z} = F_{i,\ell}(u_v - u_\ell) -$$

$$(1-\alpha)\rho_\ell g - F_{w,\ell} \qquad (5\text{-}30)$$

where

$$F_{i,v} = K + \Gamma_e \qquad (5-31)$$

$$F_{i,\ell} = K + \Gamma_c \qquad (5-32)$$

These equations are non-conservative as long as $F_{i,v} \neq F_{i,\ell}$, which is true unless $\Gamma_e = \Gamma_c = 0$. Equations (5-31) and (5-32) show that the total interfacial momentum exchange coefficients must consider both the momentum exchange due to shear forces and the momentum exchange caused by mass transfer between phases.

The old version of THERMIT ignores the momentum exchange due to mass transfer and sets $F_{i,v} = F_{i,\ell} = K$. This can be done when an unheated, insulated test section is considered, because very little evaporation and condensation is taking place. But when one is modeling something like a reactor core, where the heat flux and thermal effects of the channel walls are significant, these factors can no longer be ignored.

The correlation used in THERMIT for the momentum exchange due to interfacial shear, K, was developed by M.A. Autruffe [9], from the KFK Experiments [10] in Germany. These experiments reported data of two-phase vertical flow of sodium in a circular tube, under steady state conditions. The sodium entered the bottom of the tube at a predetermined flow rate and inlet temperature and passed

through a heating coil, where a known quantity of heat was transferred to the fluid, causing it to boil. Along a 120 mm test section downstream from the heated section the inlet and outlet pressures and the void fractions were measured. The value of K was determined from the finite difference form of Equations (5-29) and (5-30). Because the data was taken in an unheated section of the channel, Γ_e and Γ_c were negligible. Autruffe developed the following correlation to fit the data from the KFK Experiments:

$$K = \frac{4.31}{2D_h}\rho_v |u_v - u_\ell| \{(1-\alpha)[1 + 75(1-\alpha)]\}^{0.95} \qquad (5-33)$$

where D_h = hydraulic diameter = $\dfrac{4 \times A_f}{P_w}$

Equation (5-33) was tested against data from another experiment, performed at Ispra [11], and was found to be quite adequate. See Reference [9] for more details. Accordingly, Equation (5-33) was incorporated in the sodium version of THERMIT.

In order to determine how significant the momentum exchange due to mass transfer is when compared to K, two parametric comparisons were made. The first comparison simulated sodium boiling in a typical LMFBR undergoing a rapid transient (such as an overpower transient). Table 5.1 summarizes the parameters used. Both Γ_e and K are

plotted in Figure 5.5 as a function of void fraction, for different liquid superheats. Γ_e is calculated according to the flow-regime-dependent form of the Nigmatulin Model described in Section 5.1. Note that as the void fraction increases above 0.6 the value of K decreases more rapidly than Γ_e, so even for low superheats (like 0.5°C) the momentum exchange due to Γ_e becomes significant when compared to K. Since high void fractions are invariably encountered in sodium soon after boiling incipience, it can be concluded that the effect of mass transfer between phases cannot be neglected in the momentum equations under transient conditions.

The second comparison between K and Γ_e simulated boiling conditions in an LMFBR at steady state. The only difference between this case and the previous one is that a higher slip ratio (defined as u_v/u_ℓ) is expected, because the flow is fully-developed. A slip ratio of ten was chosen, so $u_v = 45.0$ m/sec. Table 5.1 contains the other values used. The results of this case are shown in Figure 5.6. One can see that in this case the ratio of K to Γ_e is greater, but for superheats greater than 0.5°C, as α gets up in the 0.8 - 1.0 region, Γ_e becomes significant once again. Therefore, the mass transfer term cannot be safely neglected even in steady state.
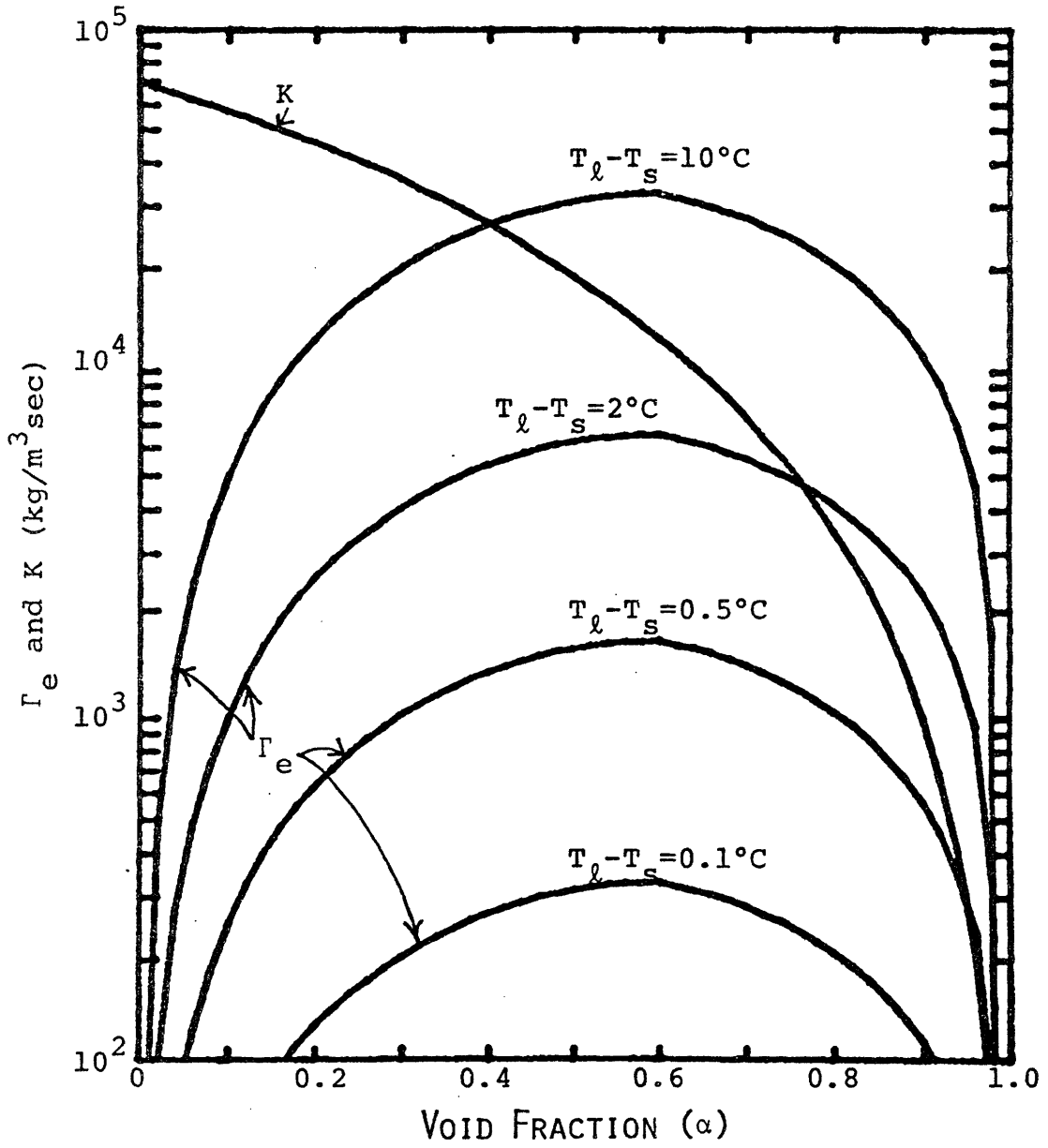
Figure 5.5   Values of Γ_e and K for a Transient
in a Typical LMFBR
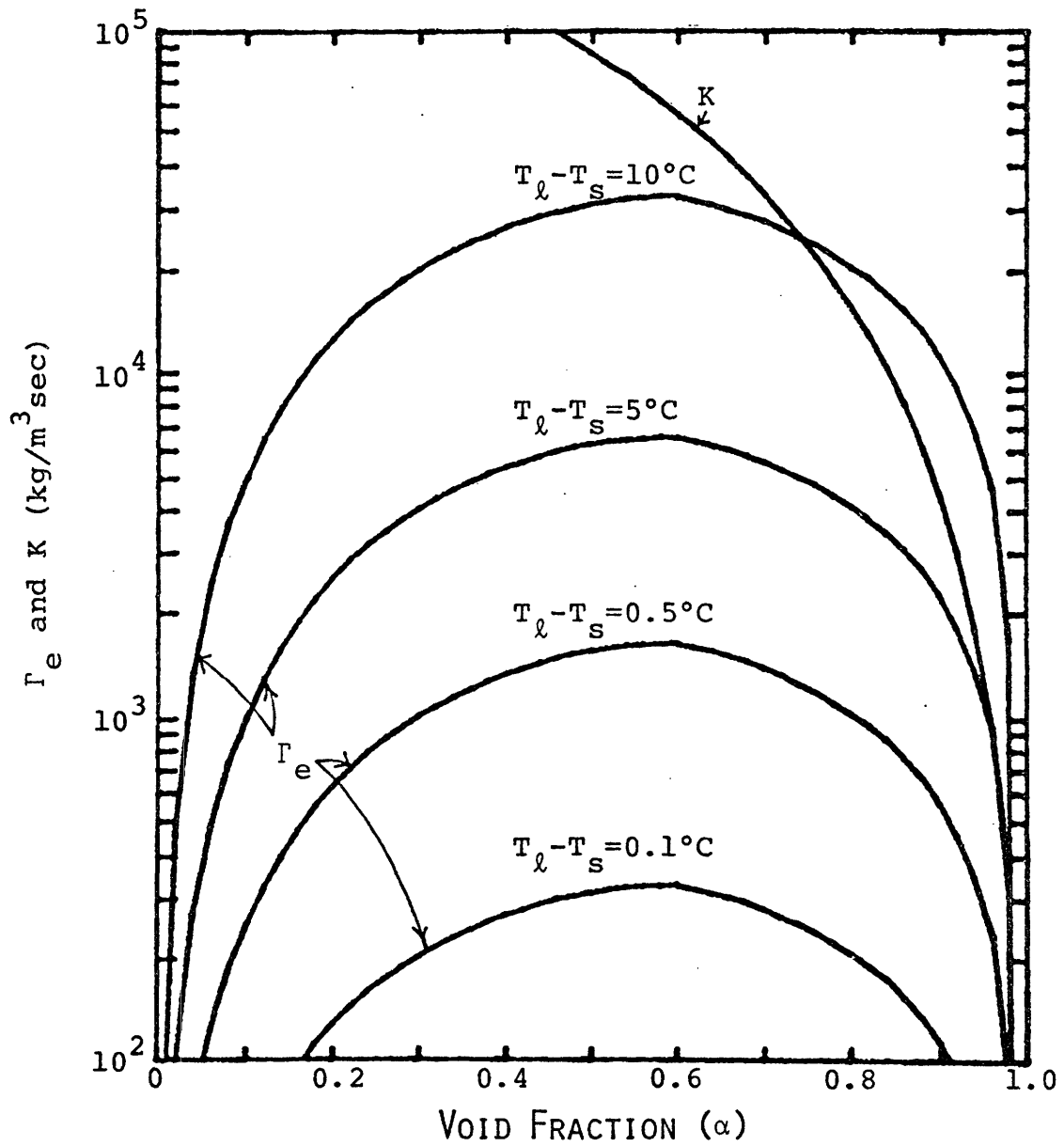
Figure 5.6 Values of Γ_e and K at Steady State
in a Typical LMFBR

TABLE 5.1

Parameter Used in Comparison of K vs. Γ_e

PARAMETER	TRANSIENT CASE	STEADY STATE
P/D	1.25	1.25
D_{rod}	6.35×10^{-3} m	6.35×10^{-3} m
u_ℓ	4.50 m/sec	4.50 m/sec
u_v	13.50 m/sec	45.00 m/sec
T_{sat}	884°C	884°C
ρ_ℓ	741.96 kg/m^3	741.96 kg/m^3
ρ_v	0.2706 kg/m^3	0.2706 kg/m^3

$$D_h = \frac{4 \times A_f}{P_w} = \frac{2P^2 \sqrt{3} - \pi D^2}{\pi D} = 4.59 \times 10^{-3} \text{ m}$$

5.3 Programming Information

As described in Reference [1], the Nigmatulin Model for gamma is incorporated in a partially implicit manner in THERMIT. The only difference between the old and the new versions of THERMIT is in the interfacial area of mass exchange. In the old version this was an explicit term (see Equation (5-6)), so to be consistent it was made explicit in the new version, too. Thus, Equations (5-17), (5-21), and (5-22) directly replace Equation (5-6) in subroutine GAMMA, which calculates the value of gamma and its derivatives.

The only potential problem with the new formulation for gamma is the discontinuity in the interfacial area at a void fraction of 0.6 (see Figures 5.3 and 5.4). As previously stated, this could cause a numerical instability when the void fraction passes this value, but for normal fuel assembly values of P/D this is not a problem. Only for very tight pitch (P/D < 1.1) or very loose pitch (P/D > 1.5) rod bundles could this problem exist. In the case of blanket assemblies (P/D ≈ 1.08) this could present a problem. In the future, if necessary, a "transition" region could be established (for example, $0.5 < \alpha < 0.7$) over which the bubbly flow expression could be phased out while the annular expression is phased in. This would eliminate the discontinuity in the expression for A.

In order to be able to incorporate the effect of mass transfer between phases upon the momentum exchange coefficient, subroutine FINTER had to be modified. Because FINTER is called from subroutine EXPLCT, which determines the explicit terms in the conservation equations for the fluid, K, Γ_e, and Γ_c were all required to be calculated entirely explicitly. This introduces a small inconsistency in the fluid equations, because the gamma term in the mass equations, being partially implicit, will not be the same as the gamma term in the momentum equations, which is explicit. Therefore, care must be exercised in keeping the time step size down to a reasonable level, so as to minimize this effect. Experience with running THERMIT has shown, however, that upon initiation of boiling the time step will automatically reduce to a small value, due to the Courant stability criterion. Because of this, no measurable loss of accuracy is expected.

Chapter 6: FRICTION FACTOR CORRELATIONS

6.1 Axial Friction Factor - Single Phase Liquid

In order to solve the liquid momentum equation for the axial direction of fluid flow it is necessary to calculate the pressure drop due to friction. This change in pressure is defined in terms of the Darcy friction factor, f, as:

$$\Delta p = f\frac{L}{De} \frac{\rho v^2}{2} \tag{6-1}$$

where

   L = length in the axial (z) direction

   De = equivalent diameter

   v = velocity in the axial direction

   Δp = pressure drop

Under most conditions of interest it is not possible to develop a precise expression for the friction factor that is entirely based upon theory. Hence, we must rely upon empirical correlations developed from experimental results. Care must be taken not to apply these formulas beyond their range of applicability.

Several factors must be considered when choosing a correlation, and each constraint further restricts the number of choices available. In searching for an axial friction factor for the sodium version of THERMIT the first constraint was that only data for sodium could be

used. The second constraint was the geometry. Because
THERMIT models conditions in an LMFBR core the best fric-
tion factor is one which is developed for flow in a wire-
wrapped triangular rod array. This considerably reduces
the number of choices. It is desirable to choose a cor-
relation which is valid over a wide range of pitch-to-dia-
meter ratios, so one correlation could be used for both
blanket assemblies (P/D ≈ 1.08) and fuel assemblies
(P/D ≈ 1.25). It is also necessary to cover as wide a
range of Reynolds number as possible, so both low flow and
high flow cases may be simulated.

The final distinction that must be made is whether to
use a subchannel friction factor or a bundle friction fac-
tor. The difference between the two is that for a subchan-
nel friction factor the variables in Equation (6-1) are
evaluated based on the subchannel velocity, density, equiv-
alent diameter, etc., while for the bundle friction factor
these variables are all averaged over the entire bundle.
Unfortunately, neither of these two options is ideal for
THERMIT, because a bundle may be represented by only one
channel (in which case the bundle friction factor is more
accurate), by many channels (in which case the subchannel
friction factor is more accurate), or by anything in be-
tween. In practice, however, it would be extremely ex-
pensive to operate THERMIT with a subchannel sized mesh

spacing*, so bundle friction factors are more desirable.

Friction factor correlations for sodium flow have been developed by Autruffe [9], Markley [12], Novendstern [13], and Hawley and Chiu [14, 15]. None of these correlations satisfies all of the above-mentioned criteria. The data range over which each is valid is presented in Table 6.1.

Autruffe's correlation was developed for two-phase flow of sodium in a single tube, under turbulent conditions. For a void fraction of zero it yields the following:

$$f = \frac{0.18}{Re^{0.2}} \tag{6-2}$$

The disadvantages of this correlation from the point of view of THERMIT are numerous. First, it was developed for flow in a single tube, so its applicability to rod bundles is questionable. Secondly, it is not valid in the laminar region. Finally, it was developed primarily for two-phase flow. It is mentioned, however, because it will be shown to be of some value in the next section.

The second correlation is that of R.A. Markley and F.C. Engel [12]. As can be seen from Table 6-1, it is applicable in the laminar regime as well as in the turbulent. Its formulation is as follows:

---

*An average 217 pin fast reactor assembly contains 438 subchannels--far too many to model each individually.

TABLE 6.1

Range of Data for Various Axial Friction Factor Correlations

PARAMETER	AUTRUFFE	MARKLEY	NOVENDSTERN	HAWLEY AND CHIU
P/D	---	1.067-1.125	1.06-1.42	1.06-1.34
T_{sat} (°C)	800-950	316	204-593	?
Quality (x)	0.004-0.98	---	---	---
Void Fraction (α)	0.55-1.0	---	---	---
Re	3,300-155,000	0-40,000	2,600-200,000	400-300,000
Number of pins	---	19-61	19-217	19-217
Diameter of Pins (cm)	---	1.2-1.325	0.498-1.2	0.498-1.27
H/D	---	7.7-15.4	8-96	7.6-96

$$f_{Turbulent} = \frac{0.55}{Re^{0.25}} \qquad \text{for } 5000 \leqslant Re \leqslant 40,000 \qquad (6-3)$$

$$f_{Laminar} = \frac{32}{\sqrt{H}} \left(\frac{P}{D}\right)^{1.5} \frac{1}{Re} \qquad \text{for } Re \leqslant 400 \qquad (6-4)$$

$$f_{Transition} = f_{Turbulent}\sqrt{\psi} + f_{Laminar}\sqrt{1-\psi}$$

$$\text{for } 400 < Re < 5000 \qquad (6-5)$$

where

$$\psi = \frac{Re - 400}{4600}$$

H = wire wrap lead length (meters)

P/D = pitch to diameter ratio

Equations (6-3), (6-4), and (6-5) are applicable in the turbulent regime, laminar regime, and transition regime, respectively. The disadvantage of the Markley/Engel correlation is that the turbulent formula is only applicable up to Re = 40,000 and is based entirely on blanket assembly data, where P/D ≈ 1.08 and D ≈ 0.50". Thus the applicability of the turbulent formula (Equation (6-3)) to fuel assemblies (P/D ≈ 1.25, D ≈ 0.25") is questionable. The laminar formulation (Equation (6-4)) has been tested against fuel assembly test data, though, and agrees reasonably well with the data.

The remaining two correlations are basically subchannel friction factors, from which bundle friction factors may be deduced, given the flow split parameters. In order to understand the notation involved, refer to the nineteen pin bundle shown in Figure 6.1, which has been divided up
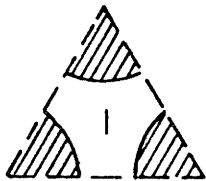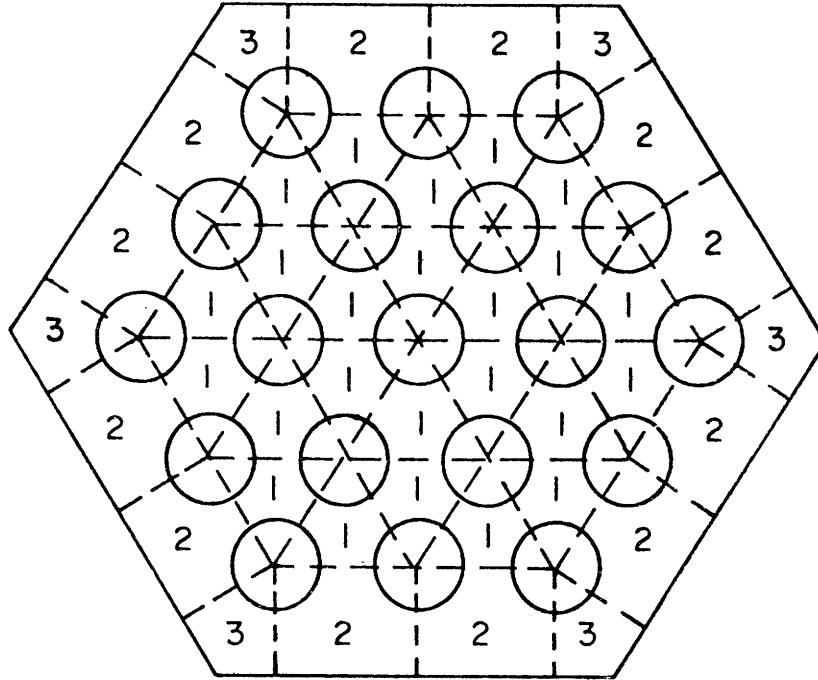
= Center Subchannel
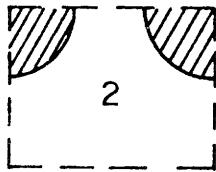
= Side Subchannel

= Corner Subchannel

Figure 6. 1   Different Types of Subchannels in a 19 Pin Bundle

into subchannels. Note that there are three different types of subchannels, numbered one, two, and three. These are also referred to as center, side, and corner subchannels, respectively. A nineteen pin bundle contains six corner, twelve side, and 24 center subchannels. By contrast, a 217 pin fast reactor bundle contains six corner, 48 side, and 384 center subchannels, so it can be seen that as the number of pins in the assembly increases the percentage of center subchannels also increases. The flow split parameter, X, is defined as follows:

$$X = \frac{v_1}{v_T} \tag{6-6}$$

where

v_1 = velocity of fluid in a center subchannel

v_T = total bundle-average velocity

In both of the aforementioned subchannel correlations a subchannel friction factor for center subchannels is defined as follows:

$$\Delta p_1 = f_1 \frac{L}{De_1} \frac{\rho v_1^2}{2} \tag{6-7}$$

Since the pressure drop in any one subchannel must equal the pressure drop in the rod bundle as a whole we obtain:

$$\Delta p_1 = f_1 \frac{L}{De_1} \frac{\rho v_1^2}{2} = \Delta p_T = f_T \frac{L}{De_T} \frac{\rho v_T^2}{2} \qquad (6-8)$$

Solving for f_T (and substituting $v_T = v_1/X$):

$$f_T = f_1 \left(\frac{De_T}{De_1}\right) X^2 \qquad (6-9)$$

Therefore, if f_1 is known and if an expression can be found for X^2, f_T can be calculated.

The Novendstern correlation is the simplest of the two. It is applicable for single phase flow of sodium in a wire-wrapped triangular rod bundle under turbulent conditions (Re > 2600), and is the following:

$$f_T = \frac{0.316M}{\left[X\left(\frac{De_1}{De_T}\right)Re_T\right]^{0.25}} \left(\frac{De_T}{De_1}\right) X^2 \qquad (6-10)$$

where

$$M = \left\{ \frac{1.034}{(P/D)^{0.124}} + \frac{29.7(P/D)^{6.94}Re_T^{0.086}}{(H/D)^{2.239}} \right\}^{0.885} \qquad (6-11)$$

and

$$X = \frac{A_T}{N_1A_1 + N_2A_2\left(\frac{De_2}{De_1}\right)^{0.714} + N_3A_3\left(\frac{De_3}{De_1}\right)^{0.714}} \qquad (6-12)$$

where

N_1, N_2, N_3 are the numbers of center, side, and corner subchannels, respectively,

A_1, A_2, A_3 are their cross-sectional fluid areas,

De_1, De_2, De_3 are their equivalent diameters,

A_T is the total cross-sectional area of flow.

By comparison, Novendstern's correlation is plotted in Figure 6.2 with both Markley and Autruffe for a 61 pin blanket assembly. Note the reasonably close agreement between Novendstern and Markley. Figure 6.3 compares the three correlations for a 217 pin fuel assembly. Markley's correlation significantly overpredicts Novendstern's turbulent friction factor, while Autruffe slightly underpredicts it.

The correlation of Hawley and Chiu will not be presented here, for several reasons. First of all, considering the geometry employed by THERMIT, the additional accuracy provided by this correlation would be meaningless. This is because the rectangular mesh cells utilized by THERMIT do not correspond in size or shape to the triangular subchannels for which this correlation was developed. Infact, it will be shown that even the Novendstern correlation can be simplified before utilization. Furthermore, at the time that this work was done some difficulties existed with Hawley's laminar friction factor. These difficulties have since been solved, however, so it is ready for use, if desired. The interested reader is referred to References [14] and [15] for more information on this subject.
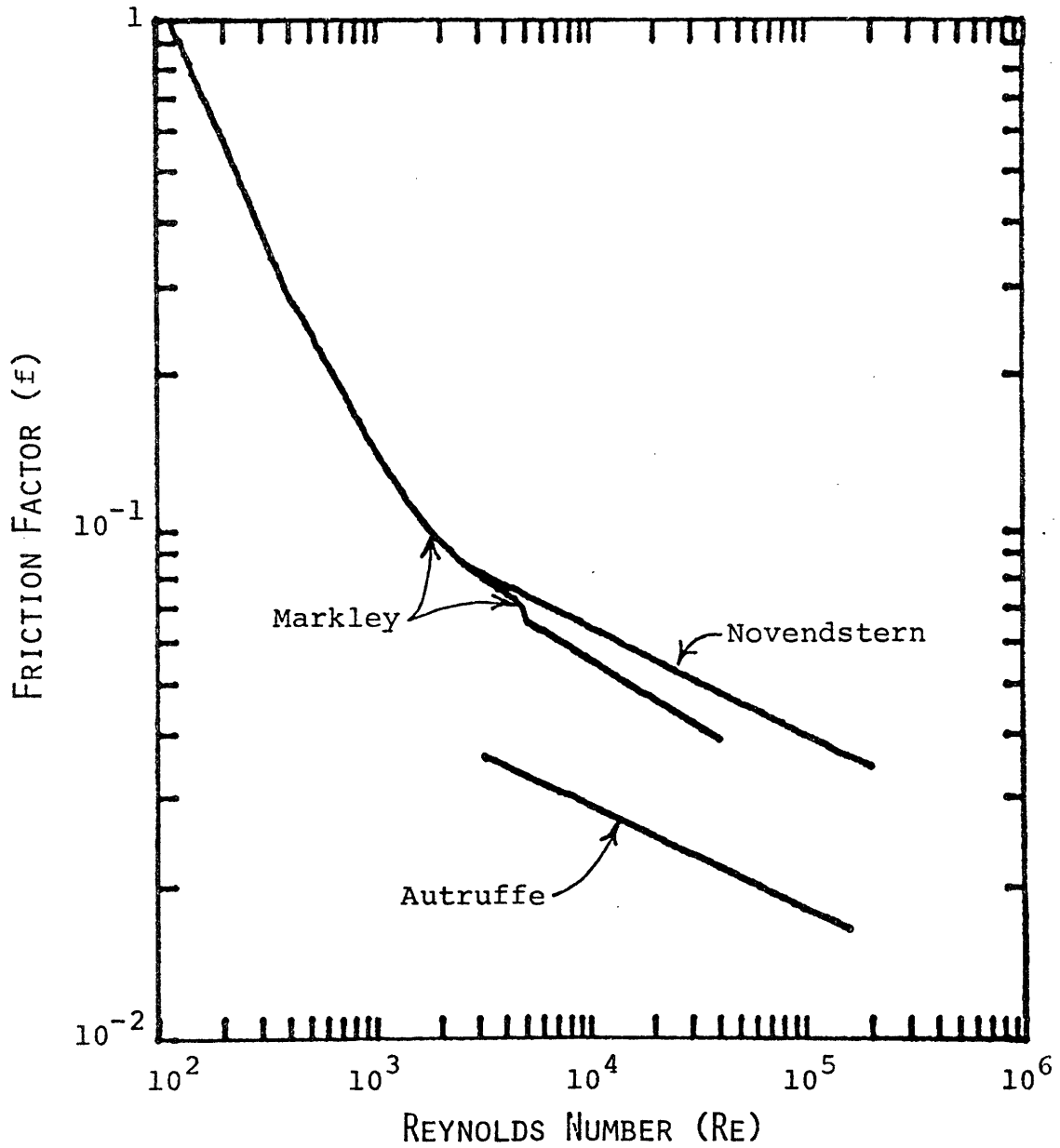
Figure 6.2 Axial Friction Factor vs. Re for a 61 Pin
Blanket Assembly
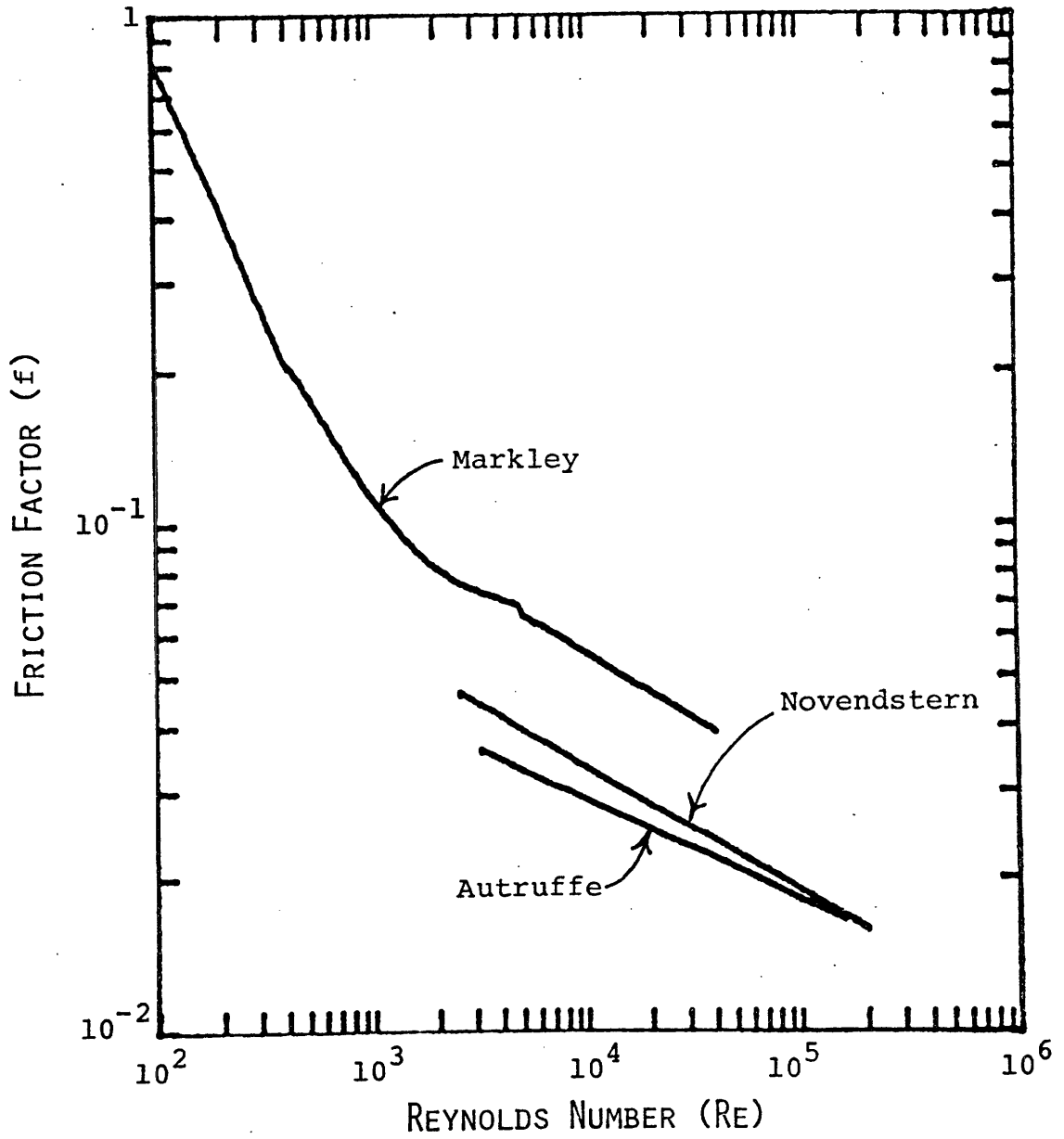
Figure 6.3   Axial Friction Factor vs. Re for a 217 Pin
             Fuel Assembly

Now let's summarize the correlations presented. Autruffe's correlation covers only the turbulent regime, and does not represent the desired geometry. The Markley/ Engel correlation covers the turbulent and laminar regime, but the turbulent formulation is not applicable over a wide range of P/D ratios. Novendstern's correlation is valid over the entire P/D range, but is applicable only for turbulent flow. Obviously, none of these correlations can provide a complete solution by itself. We can maximize accuracy, however, by using Markley's laminar correlation with Novendstern's turbulent correlation, and connecting the two via a transition formula similar to Equation (6-5). But first several simplifications will be made in Novend- stern's correlation. It will be assumed that $X \approx 1.0$. This assumption becomes more and more accurate as the num- ber of pins in the bundle increases. For an average 217 pin bundle (P/D=1.25, H/D=51.72, D=0.232 in), X=0.9701. Even if a bundle as small as nineteen pins is considered, X=0.9367 (for the same P/D, H/D, and D). The second as- sumption made is that $De_T/De_1 \approx 1$. For our 217 pin bundle De_T/De_1=1.037, while in the nineteen pin bundle De_T/De_1= 1.085. If Equation (6-10) is rearranged we get:

$$f_T = \frac{0.316M}{Re_T^{0.25}} \cdot \xi \qquad (6-13)$$

where

$$\xi = \left(\frac{De_T}{De_1}\right)^{1.25} X^{1.75} \tag{6-14}$$

Thus, for the 217 pin bundle $\xi = 0.9923$, and for the nineteen pin bundle $\xi = 0.9876$. (Note that since $De_T/De_1 > 1.0$ and $X < 1.0$ the errors cancel each other out, to some extent.) It is therefore quite valid to assume $\xi \approx 1.0$. This simplifies Equation (6-13) considerably. Since (6-13) is valid down to $Re = 2600$, the transition region between this correlation and Markley's laminar correlation (Equation (6-4)) is $400 < Re < 2600$. The following is the formulation employed in THERMIT:

$$f_{Turbulent} = \frac{0.316M}{Re^{0.25}} \quad \text{for } 2600 \leqslant Re \leqslant 200,000 \tag{6-15}$$

$$f_{Laminar} = \frac{32}{\sqrt{H}}(\frac{P}{D})^{1.5} \frac{1}{Re} \quad \text{for } Re \leqslant 400 \tag{6-16}$$

$$f_{Transition} = f_{Turbulent}^{\sqrt{\psi}} + f_{Laminar}^{\sqrt{1-\psi}} \tag{6-17}$$

$$\text{for } 400 < Re < 2600$$

where

$$\psi = \frac{Re - 400}{2200},$$

H is in meters, and M is calculated from Equation (6-11).

One further stipulation is made. A glance at Equation (6-16) shows that $f_{Laminar} \to 0$ as $H \to \infty$. This is clearly unrealistic. Reference [12] reports that for a bare rod bundle ($H = \infty$) with P/D = 1.08, $f \cdot Re = 60$. Therefore, to avoid problems the condition $f_{Laminar} \cdot Re \geq 60$ is imposed for all values of H and P/D. Equations (6-15), (6-16), and (6-17) represent the best available methodology for calculating single phase axial liquid friction factors in wire-wrapped triangular rod arrays. These equations are plotted in figure 6.4 for both a 61 pin blanket assembly and a 217 pin fuel assembly. The next task is to find axial friction factors for two-phase sodium flow.

6.2 Axial Friction Factor - Two Phase Flow

In the previous section it was stated that it is rarely possible to develop precise expressions for the friction factor that are based entirely upon theory. This statement is even more valid when applied to two phase flow of sodium in rod bundles. Unfortunately, the data base for two phase flow is even smaller than that of single phase flow. Of the previously mentioned friction factor correlations only Autruffe's was tested in the two phase region, and it was developed for flow in a single tube.

THERMIT uses the two-fluid formulation of the conservation equations, and therefore requires both a liquid wall friction factor (f_ℓ) and a vapor wall friction factor (f_v).
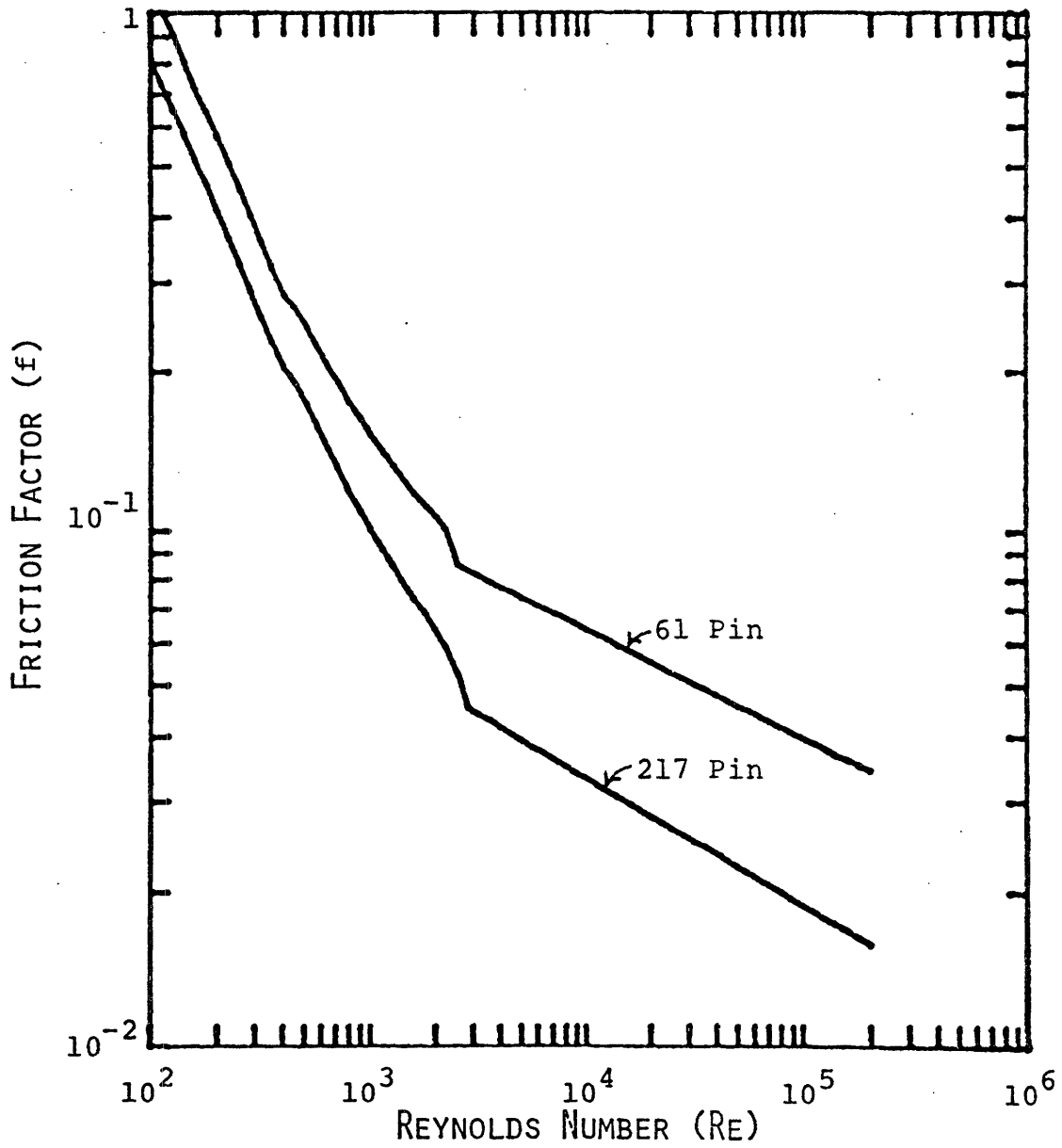
Figure 6.4 THERMIT Axial Friction Factor vs. Re for
61 and 217 Pin Assemblies

The interfacial friction between the liquid and vapor phases was discussed in Chapter 5.

When developing a correlation for two phase flow it is often important to consider the flow regime that is likely to exist. As stated in Chapter 5, one expects annular flow over most of the region of interest. In fact, the experiments analyzed by Autruffe [9] indicated that vapor did not come into contact with the wall until the void fraction exceeded 0.957. Therefore, the axial friction factors for two phase flow in THERMIT are multiplied by parameters called contact fractions, which represent the percentage of the surface of the fuel rod in contact with the liquid or vapor. It is assumed that for a void fraction below 0.957 the entire surface of the rod is coated with liquid. As the void fraction increases from 0.957 to 1.0 the liquid contact fraction decreases linearly from 1.0 to 0.0, while the vapor contact fraction goes from 0.0 to 1.0. In mathematical notation,

$$cf_\ell = \begin{cases} 1.0 & \text{for } \alpha \leq 0.957 \\ \dfrac{1.0-\alpha}{0.043} & \text{for } 0.957 < \alpha \leq 1.0 \end{cases} \qquad (6\text{-}18)$$

$$cf_v = \begin{cases} 0.0 & \text{for } \alpha \leq 0.957 \\ \dfrac{\alpha-0.957}{0.043} & \text{for } 0.957 < \alpha \leq 1.0 \end{cases} \qquad (6\text{-}19)$$

These factors insure that $f_\ell \rightarrow 0.0$ as $\alpha \rightarrow 1.0$, and $f_v = 0.0$ for $\alpha \leqslant 0.957$.

The next question is what form f_ℓ and f_v take in two phase flow. Autruffe's correlation, which is valid in the turbulent region only, is the following:

$$f_\ell = \frac{0.18}{Re_\ell^{0.2}} \qquad \text{and} \qquad f_v = \frac{0.2\alpha}{Re_v^{0.2}} \qquad (6\text{-}20)$$

where

$$Re_\ell \equiv \frac{(1-\alpha)\rho_\ell v_\ell De}{\mu_\ell} \qquad \text{and} \qquad Re_v \equiv \frac{\alpha\rho_v v_v De}{\mu_v} \qquad (6\text{-}21)$$

Note that the only difference between f_ℓ and the standard correlation for single phase flow in a pipe is the inclusion of the $(1-\alpha)$ factor in the Reynold's Number. This leads one to believe that Equations (6-15), (6-16), and (6-17) would be valid in the two phase region if the Reynold's Number were multiplied by $(1-\alpha)$, and the entire result were multiplied by cf_ℓ (so as to approach the correct limit as $\alpha \rightarrow 1.0$). This was incorporated in THERMIT. In all places where Re appears, the old definition is replaced by Re_ℓ from Equations (6-21). This yields:

$$f_{Turbulent,\ell} = \frac{0.316M}{Re_\ell^{0.25}} \cdot cf_\ell \qquad \text{for } 2600 \leqslant Re_\ell \leqslant 200,000 \qquad (6\text{-}22)$$

$$f_{Laminar,\ell} = \frac{32}{\sqrt{H}}(\frac{P}{D})^{1.5} \frac{cf_\ell}{Re_\ell} \quad \text{for } Re_\ell \leq 400 \qquad (6\text{-}23)$$

$$f_{Transition,\ell} = f_{Turbulent,\ell}^{\sqrt{\psi}} + f_{Laminar,\ell}^{\sqrt{1-\psi}}$$

$$\text{for } 400 < Re_\ell < 2600 \qquad (6\text{-}24)$$

where

$$\psi = \frac{Re_\ell - 400}{2200}$$

and the Re factor in M (Equation (6-11)) is replaced by Re_ℓ.

Equations (6-22), (6-23), and (6-24) provide a consistent methodology for calculating the axial two phase liquid friction factor. The next step is to obtain the vapor friction factor. As stated before, it is assumed that no vapor comes in contact with the wall for void fractions below 0.957. Therefore $f_v = 0.0$ in this range. Of all the authors investigated, Autruffe was the only one who proposed a vapor friction factor. His correlation has two major drawbacks, however. First, it was developed for flow in a single tube, and thus has no P/D or H/D effect. Second, it applies only to turbulent flow. For these reasons it was decided not to employ the Autruffe friction factor for vapor. Instead, the Markley-Novendstern correlation described above was implemented, with vapor properties being substituted for the liquid. Once again, because of the lack of available data this correlation cannot be tested for verification, but it does have the advantage of including the geometrical

effects that are not present in Autruffe's correlation. In addition, the two correlations predict quite similar results for turbulent flow in fuel assemblies (P/D $\approx$ 1.25). Therefore, the following formulas are used for vapor friction:

$$f_{Turbulent,v} = \frac{0.316M}{Re_v^{0.25}} cf_v \quad \text{for } 2600 \leq Re_v \leq 200,000 \tag{6-25}$$

$$f_{Laminar,v} = \frac{32}{\sqrt{H}} \left(\frac{P}{D}\right)^{1.5} \frac{cf_v}{Re_v} \quad \text{for } Re_v \leq 400 \tag{6-26}$$

$$f_{Transition, v} = f_{Turbulent,v}\sqrt{\psi} + f_{Laminar,v}\sqrt{1-\psi}$$
$$\text{for } 400 < Re_v < 2600 \tag{6-27}$$

$$\text{where } \psi = \frac{Re_v-400}{2200}$$

and the Re factor in M (Equation (6-11) is replaced by Re_v.

6.3   Transverse Friction Factor

The momentum equations in the x and y directions also require a friction pressure drop term. In this case, however, the geometry is different from the axial direction. Instead of flow along rods we have flow across rods.

The correlation employed in THERMIT was developed by Gunter and Shaw[16], for the single phase region. The two phase multiplier of Ishihara, Palen and Taborek[17] was used. These correlations are documented in Reference [1].

This section will expand upon the description in Reference [1], showing the derivations of the correlations in greater detail.

The single phase friction factor in the x (or y) direction is defined by:

$$\Delta p_\ell = f_\ell \frac{L}{D_v} \frac{\rho_\ell V^2_{max}}{2}$$ (6-28)

where

Δp_ℓ = pressure drop in the transverse direction due to friction;

L = length in the transverse (x or y) direction;

V_{max} = transverse velocity at the point of maximum flow constriction between rods;

D_v = volumetrically defined transverse hydraulic diameter;

$$D_v \equiv \frac{4 \times \text{Volume of sodium in tube bank}}{\text{Exposed surface area of tubes}}$$ (6-29)

Gunter and Shaw define both a laminar and a turbulent correlation for the liquid friction factor, f_ℓ, with the transition occuring at a Reynolds Number of 202.5. Thus,

$$f_\ell = \begin{cases} \dfrac{180}{Re_\ell} & \text{for } Re_\ell \leq 202.5 \\ \dfrac{1.92}{Re_\ell^{0.145}} & \text{for } Re_\ell > 202.5 \end{cases}$$ (6-30)

$$\text{where } Re_\ell = \frac{\rho_\ell |V_{max}| D_v}{\mu_\ell}$$

For two phase flow with both liquid and vapor Reynolds

Numbers in the laminar regime (where $Re_\ell \equiv (1-\alpha)\rho_\ell |v_{\ell,max}|^{Dv}/\mu_\ell$

and $Re_v \equiv \alpha\rho_v |v_{v,max}|^{Dv}/\mu_v$),

$$\Delta p_\ell = f_\ell \frac{L}{D_v} \frac{\rho_\ell v_{\ell,max}^2}{2} \quad \text{and} \quad \Delta p_v = f_v \frac{L}{D_v} \frac{\rho_v v_{v,max}^2}{2} \quad (6\text{-}31)$$

where

$$f_\ell = \frac{180}{Re_\ell} cf_\ell \quad \text{and} \quad f_v = \frac{180}{Re_v} cf_v \quad \begin{matrix} (\text{for } Re_\ell < 202.5 \\ \text{and } Re_v < 202.5) \end{matrix}$$

cf_ℓ and cf_v are defined as in Equations (6-18) and (6-19).

(Note: this is a departure from Reference [1], which uses the

single phase Reynolds Numbers and omits the contact fractions.)

If either the liquid or vapor is in the turbulent regime,

a two phase multiplier is applied to the friction pressure

drop, to yield the following equation:

$$\Delta p_{TP} = f \frac{L}{D_v} \frac{G^2}{2\rho_\ell} \phi_{\ell o}^2 \quad (6\text{-}32)$$

where

G = total mass flow rate (at the point of maximum flow constriction) = $G_\ell + G_v$

G_ℓ = $(1-\alpha)\rho_\ell v_{\ell,max}$

G_v = $\alpha\rho_v v_{v,max}$

f = two phase friction factor $\equiv \dfrac{1.92}{Re^{0.145}}$ (6-33)

Re = two phase Reynolds Number $\equiv \dfrac{GD_v}{\mu_\ell}$ (6-34)

$\phi_{\ell o}^2$ = $1 + \dfrac{8}{X_{tt}} + \dfrac{1}{X_{tt}^2}$ (from Ref. [17]) (6-35)

$$\frac{1}{X_{tt}^2} = \left(\frac{x}{1-x}\right)^{2-.145} \left(\frac{\rho_\ell}{\rho_v}\right) \left(\frac{\mu_v}{\mu_\ell}\right)^{.145} \tag{6-36}$$

Because THERMIT uses a two-fluid formulation, both a liquid and a vapor friction factor are required, so Equation (6-32) must be split into two parts before implementation is possible. This is done by splitting $\phi_{\ell 0}^2$ into two pieces. When doing this one must be certain that the proper limits are maintained as the void fraction approaches zero or one. It shall be shown that if the first two terms in the expression for $\phi_{\ell 0}^2$ are associated with the liquid phase and the third term is associated with the vapor phase the proper limits are maintained. Thus we have:

$$\Delta p_\ell = f \frac{L}{D_v} \frac{G^2}{2\rho_\ell} \{1 + \frac{8}{X_{tt}}\}cf_\ell \tag{6-37}$$

and

$$\Delta p_v = f \frac{L}{D_v} \frac{G^2}{2\rho_\ell} \{\frac{1}{X_{tt}^2}\}cf_v \tag{6-38}$$

Once again, the contact fractions appear for the reasons outlined in Section 6.2.

Before these equations can be solved, the expression for $\frac{1}{X_{tt}^2}$ (Equation [6-36]) is modified, eliminating x. Keeping in mind that $xG = G_v$ and $(1-x)G = G_\ell$,

$$\frac{1}{X_{tt}^2} = \frac{G_v{}^2}{G_\ell{}^2} \left[\frac{f_v}{f_\ell}\right] \left[\frac{\rho_\ell}{\rho_v}\right] \tag{6-39}$$

where

$$f_\ell \equiv \frac{1.92}{Re_\ell{}^{0.145}} \text{ and } f_v \equiv \frac{1.92}{Re_v{}^{0.145}} \tag{6-40}$$

The results of Equation (6-39), when inserted in Equations (6-37) and (6-38), yield:

$$\Delta p_\ell = f \frac{L}{D_v} \frac{G^2}{2\rho_\ell} \left\{1 + \frac{8G_v}{G_\ell}\left(\frac{f_v}{f_\ell}\right)^{\frac{1}{2}}\left(\frac{\rho_\ell}{\rho_v}\right)^{\frac{1}{2}}\right\}cf_\ell \tag{6-41}$$

and

$$\Delta p_v = f \frac{L}{D_v} \frac{G^2}{2\rho_\ell} \left\{\frac{G_v{}^2}{G_\ell{}^2}\left(\frac{f_v}{f_\ell}\right)\left(\frac{\rho_\ell}{\rho_v}\right)\right\}cf_v \tag{6-42}$$

At this point several approximations are made. First, it is assumed that $G \approx G_\ell$. This approximation is made for two reasons. First, because $\rho_\ell \gg \rho_v$, $G_\ell \gg G_v$ except at very high void fractions. Second, the numerical scheme in the code is greatly simplified by making this assumption. The second approximation made is that $f \approx f_\ell$, which follows from the previous assumption (see Equations [6-33] and [6-34]). This ensures that the formulas go to the correct limit as the void fraction approaches zero or one. With these simplifications,

$$\Delta p_\ell = \left\{f_\ell \frac{L}{D_v} \frac{(1-\alpha)^2\rho_\ell v_{\ell,max}^2}{2}\right.$$

$$\left.+ \frac{4L}{D_v}(f_\ell f_v \rho_\ell \rho_v)^{\frac{1}{2}} \alpha(1-\alpha)v_{v,max}v_{\ell,max}\right\}cf_\ell \tag{6-43}$$

and

$$\Delta p_v = \{ f_v \; \frac{L}{D_v} \; \frac{\alpha^2 \rho_v v_{v,max}^2}{2} \} c f_v \qquad (6\text{-}44)$$

for $Re_\ell > 202.5$ <u>or</u> $Re_v > 202.5$

In summary, if both the liquid and the vapor phases are in laminar flow ($Re_\ell < 202.5$ and $Re_v < 202.5$), Equations (6-31) are used for Δp_ℓ and Δp_v. If either or both of the phases are in the turbulent regime, Equations (6-43) and (6-44) are employed.

6.4   Programming Information

The implementation of the new friction factor correlations in THERMIT required only a few modifications in the code. One new input parameter was required: the helical pitch to diameter ratio (H/D) used in Equations (6-16) and 6-23). Subroutine FWALL, which calculates the axial and transverse friction factors for both the liquid and vapor phases, was rewritten to incorporate the correlations described in Sections 6.1 to 6.3. In order to be consistent with the numerical scheme used in THERMIT, the friction factors are calculated explicitly.

Chapter 7: VERIFICATION OF MODELS

AND APPLICATION TO LMFBR CONDITIONS

7.1 Purpose

The purpose of this chapter is three-fold. First, and most importantly, it attempts to verify some of the models described in the previous chapters. In particular, the structure conduction model (Chapter 3), and the fuel rod conduction model (Chapter 4) are tested. The fluid conduction model was tested separately (see Section 2.5). Although comments will be made about the interfacial exchange coefficients (Chapter 5) and the friction factors (Chapter 6), the nature of the simulations made did not permit the formulation of any concrete generalizations about these correlations.

The second purpose of this chapter is to compare the predictions of the sodium version of THERMIT with an actual experiment that was run. For this purpose the THORS Bundle 6A experiments performed at Oak Ridge National Laboratory [6] were chosen. Section 7.2 describes the experiments in more detail.

By comparing THERMIT's predictions with the actual experimental results, the performance of the aforementioned models can be evaluated, and their importance can be deter-

mined. It must be stressed, however, that the sodium

version of THERMIT is still in the process of development,

and is not expected to give extremely accurate results at

this point. Several difficulties arose with the performance

of THERMIT in the two phase region. These difficulties will

be explained in more detail in the following sections, and

Chapter 8 will suggest some possible solutions.

The third purpose of this chapter is to apply THERMIT

to LMFBR conditions, and make some generalizations about

the importance of such factors as radial heat loss in a 217

pin bundle during a loss-of-flow transient. This subject

will be explored in Section 7.4.

Because of the fact that THERMIT for sodium is still

in the development stage, the focus of this chapter will be

on the verification of models, rather than the simulation

of experimental results. The latter task will be taken up

in the future, when the modeling process is complete.

7.2 Description of the THORS Bundle 6A Experiments

The THORS Bundle 6A experiments were performed in 1978

at Oak Ridge National Laboratory. This section will briefly

describe the experimental setup and the parameters for the

one run which will be analyzed (Test 71h, Run 101). For

more details, see Reference [6].

The THORS Facility is a high-temperature sodium facility

for thermal-hydraulic testing of simulated LMFBR subassem-

blies under steady state and transient conditions. Heat
generation in the simulated subassemblies is provided by
electrically heated fuel pin simulator units. Bundle 6A
consisted of 19 pins of 0.230 in. diameter spaced by 0.056
in. diameter helical wire-wrap spacers on a 12.0 in. helical
pitch. The bundle hex can of 0.020 in. thickness was sur-
rounded by approximately 1 in. of insulation, and rings of
stainless steel, sodium and stainless steel again (see
Figure 7.1).

The results of the tests indicated that the thermal
inertia of the structure surrounding the bundle was higher
than expected. Upon inspection it was discovered that there
was significant sodium leakage into the insulation. There-
fore, the heat losses to the insulation were far greater
than expected.

Bundle 6A had a heated length of 36 in., with a chopped
cosine axial power distribution (peak-to-mean power ratio =
1.3). The fuel pin simulators (FPS's) were constructed of
a core of compacted boron nitride wrapped by a heater wire,
another layer of boron nitride, and a cladding of type 316
stainless steel (see Figure 7.2). Downstream from the heated
length the FPS contained four different structural regions
within the stainless steel clad. The first consisted of a
boron nitride core (of .125 in. diameter) with a ring of
type 304 stainless steel, the second was solid boron nitride,
the third was solid nickel, and the fourth simulated the
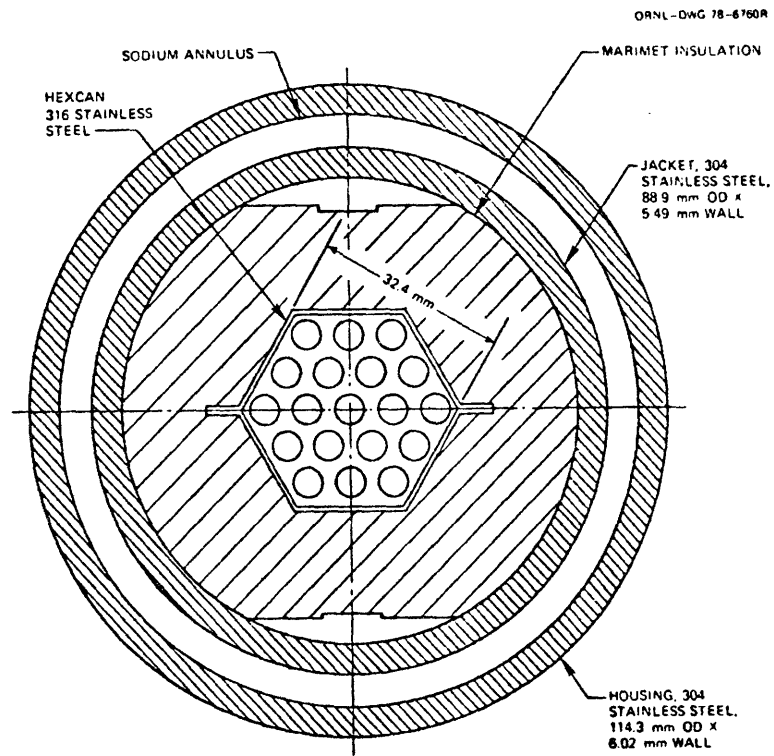
Figure 7.1 - Cross Section of THORS Bundle 6A

ORNL-DWG 76-2978

CENTRAL BN INSULATION — 120° — ANNULAR BN INSULATION

INTERNAL THERMAL ELEMENTS

EXTERNAL THERMOCOUPLE

SECTION A-A

ALIGNMENT PLUG

GROUNDING PLUG

PI-8% W HEATING ELEMENT, 0.013×0.125 in. RIBBON 0.125 in. OD (0.32×3.18 mm) VARIABLE PITCH

BN INSULATION

TYPE 316 STAINLESS STEEL SHEATH, 0.230-in.-OD, 0.015-in.-WALL (5.8×0.38 mm)

A

INTERMEDIATE MATERIAL TYPE 304 STAINLESS STEEL

COPPER TERMINAL

GROUND LEAD EXTENSION TYPE 304 STAINLESS STEEL

THERMAL ELEMENT A JUNCTION

EXTERNAL WIRE WRAP THERMOCOUPLE

INTERNAL SHEATHED THERMAL ELEMENT 0.015-in.-OD (0.38 mm)

36 in (0.91 m)

63 7/8 in (1.62 m)

Figure 7.2 - THORS Bundle 6A Fuel Pin Simulator

fission gas plenum. These regions had lengths of 1 1/16",
7/16", 6", and 42", respectively.

The particular run studied in this chapter was Test 71h,
Run 101. At a constant power of 127 kw and inlet temperature
of 661°K the test section flow was reduced from 6.2 gpm at
3.2 seconds to 1.9 gpm at 13.7 seconds, when boiling incep-
tion occurred. Local dryout was recorded at 28.5 seconds,
but permanent dryout did not occur until 36.3 seconds. The
test was terminated at 40.0 seconds. Figure 7.3 shows the
inlet flow and inlet and outlet pressures as a function of
time. Note the wild oscillations in the flow after boiling
inception. This demonstrates the unstable nature of sodium
boiling.

7.3   THERMIT Simulation of THORS Bundle 6A, Test 71h, Run 101

Three different runs were made using THERMIT to simulate
the THORS transient. This section will describe some of the
approximations made in modeling the experiment, and will
compare the results obtained with those observed in the
actual experiment.

All of the runs contained several basic approximations.
First of all, the runs were made with one dimensional geometry.
In other words, the entire cross section of the rod bundle was
lumped into one mesh cell. This was done in order to simplify
the geometry, and because the main purpose of these runs was
to test the models employed. Certain problems still exist in
the code, and it would not be cost-effective to run a more
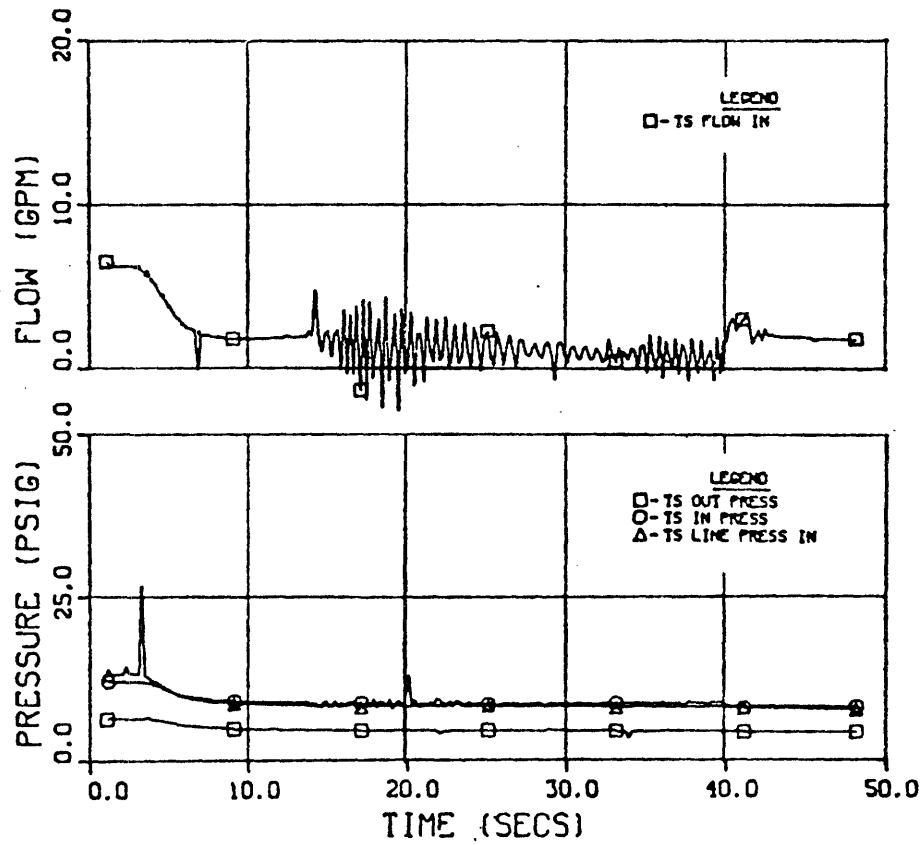
Figure 7.3 - Temperature and Pressure vs. Time
For Test 71h, Run 101

complicated case at this point in time. The second approxi-mation consisted of the choice of boundary conditions at the inlet and outlet. Either pressure or velocity conditions may be set. In these runs the inlet velocity and outlet pressure were specified. This is fine until boiling incep-tion, but after that point the inlet velocity oscillates wildly (as shown in Figure 7.3). It would be better to spe- cify inlet and outlet pressures after boiling, but when this is done flow reversal is seen almost immediately (0.08 seconds after boiling), and the code fails. In fact, at this moment in time there is a numerical problem of some sort with flow reversal. This problem will be discussed in more detail in Chapter 8. For this reason inlet velocity was specified throughout the transient. In the two phase region an average velocity midway between the maxima and minima of the oscilla-tions was used. The third approximation was that the thermal properties of the fuel pin simulator (FPS) were assumed to be independent of temperature. The FPS was divided up into four radial zones, representing the inner boron nitride, the heater wire, the outer boron nitride, and the cladding. For each of these regions a constant thermal conductivity and heat capacity was assumed. The length of the bundle was divided up into 14 mesh cells, for calculational purposes.

The inlet consisted of one cell of 12 inches in length, the heated section contained nine cells of four inches in length, and the gas plenum contained four cells of 12 inches

in length. In the third run the nodal spacing was slightly different. See Figure 7.4 for details.

The first of the runs was the most restrictive in terms of assumptions. It ignored condensation in the gas plenum by cutting off all heat transfer to the fuel rod in that region, and it assumed an adiabatic boundary around the outside of the bundle. In other words, the thermal inertia of the hex can and insulation was ignored. The simulation was run in three steps. First a steady state was obtained by running an "unperturbed" transient until all parameters remained constant (this is the only way to obtain a steady state result using THERMIT). The second step used the restart option of THERMIT (see Reference [1], and went through the first seven seconds of the transient, which contains the steepest part of the flow reduction. The third step continued the transient for another ten seconds. It was during this final step that boiling inception occurred. Appendix B.4 contains the input file and the two restart files used for this run, which will hereafter be called Case A.

The second run, Case B, was identical in all respects but one. The assumption of an adiabatic boundary condition was removed. The surrounding structure was modeled as five radial zones (see Figure 7.1). The first was the hex can. The second zone, the insulation, was divided into four mesh cells. Because it was reported that sodium had permeated the entire region, the design values for the thermal

SIDE VIEW OF FUEL PIN SIMULATOR
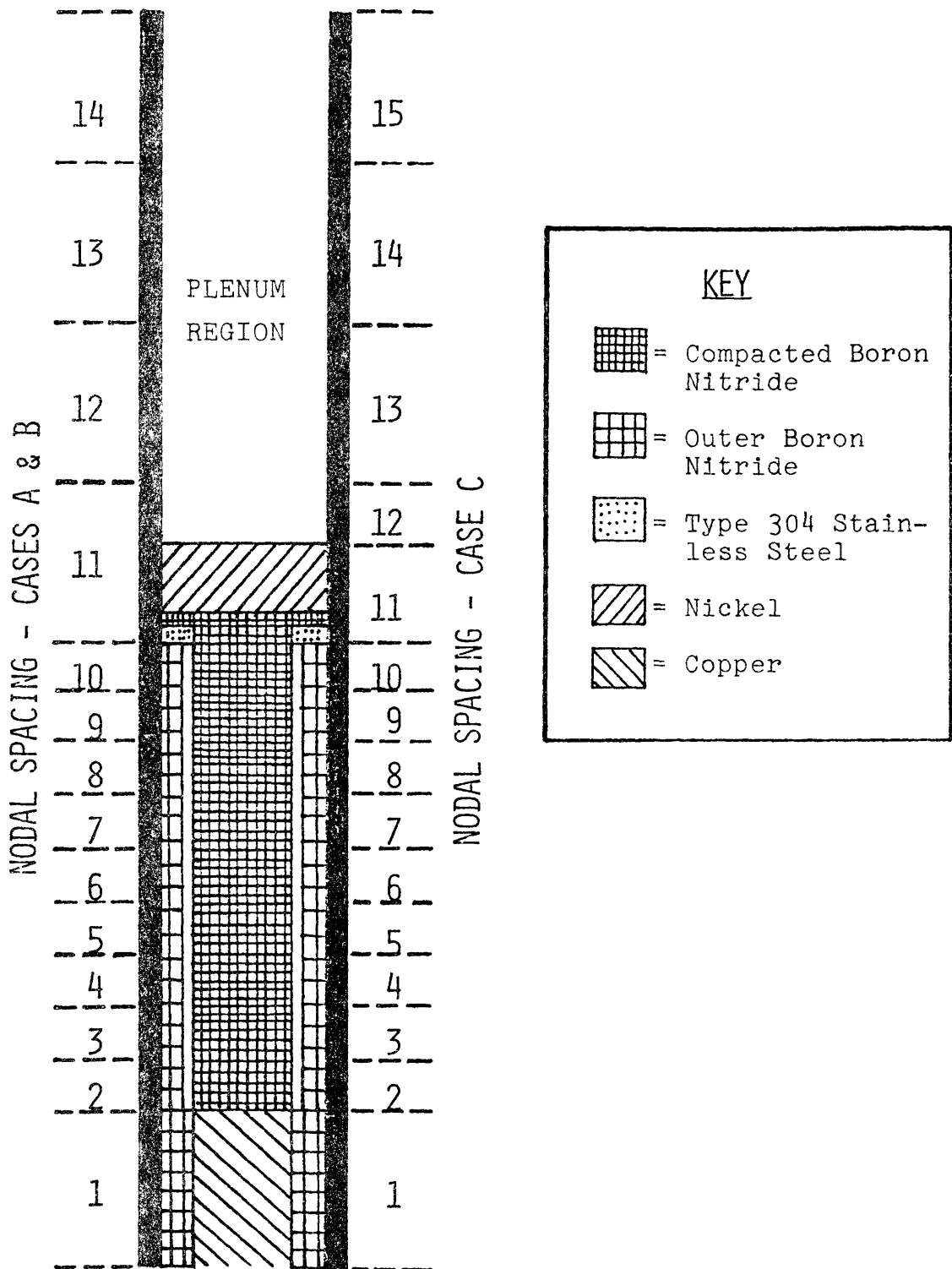
Figure 7.4 - Mesh Spacing Used in THERMIT Simulations
of THORS Bundle 6A Experiments

properties of the insulation could not be used. Given a porosity of 53% for the insulation, Reference [6] calculates the thermal properties of the sodium-soaked insulation by assuming that all void space is filled with sodium. These properties were used in Case B. The final three radial zones consisted of one mesh cell each. They represented the two rings of stainless steel and the sodium annulus in between. The boundary condition around the exterior of the structure was taken to be adiabatic. The input file for Case B is presented in Appendix B.5. The two restart files were the same as in Case A.

The third run, denoted Case C, was identical to Case B, except that in this case the thermal inertia effects of the gas plenum were taken into account. The fuel rod was divided up into three axial regions. The first region modeled the heated zone, and was described earlier in this section. The second region lumped the three short sections between the gas plenum and the heated zone into one region. This region contained the thermal properties of nickel, which constituted 80% of the material. The third region modeled the gas plenum, which was assumed to have a negligible heat capacity, so only the cladding was considered to have any thermal inertia. This case, unlike the previous two, allowed for heat transfer to the fuel rod in the unheated region. The input file for Case C is contained in Appendix B.6. Unfortunately, Case C developed a numerical problem upon initiation of boiling,

and was only able to advance 0.3 seconds into boiling before it failed. It is believed that the failure of this case was due to the instability of the code in boiling rather than any defect in the fuel rod conduction model, because the latter operated well in the single phase region. Experience with THERMIT has shown that the code is extremely sensitive in the two phase region, and any minor perturbations can be sufficient to cause the code to fail. This problem is understandable, considering the extremely large void fractions and vapor velocities encountered in sodium boiling, and the numerical instabilities these cause.

All three simulations gave identical results at steady state, as expected. This is because the outer boundary of the structure was adiabatic, and thus no heat was lost from the system. Figure 7.5 shows the steady state temperature distribution as a function of axial height, where zero represents the bottom of the heated zone. The results from the experiment are displayed also. No thermocouples were placed less than ∿53 cm. from the bottom of the heated section, so no data is available in that range. It should be noted that it is difficult to compare the THERMIT temperature predictions with the thermocouple readings, because THERMIT treats an entire plane as one lump, while the thermocouples record a temperature at one point only. It is therefore advisable when making comparisons to compare the shape of the curve and the approximate value of the numbers, rather
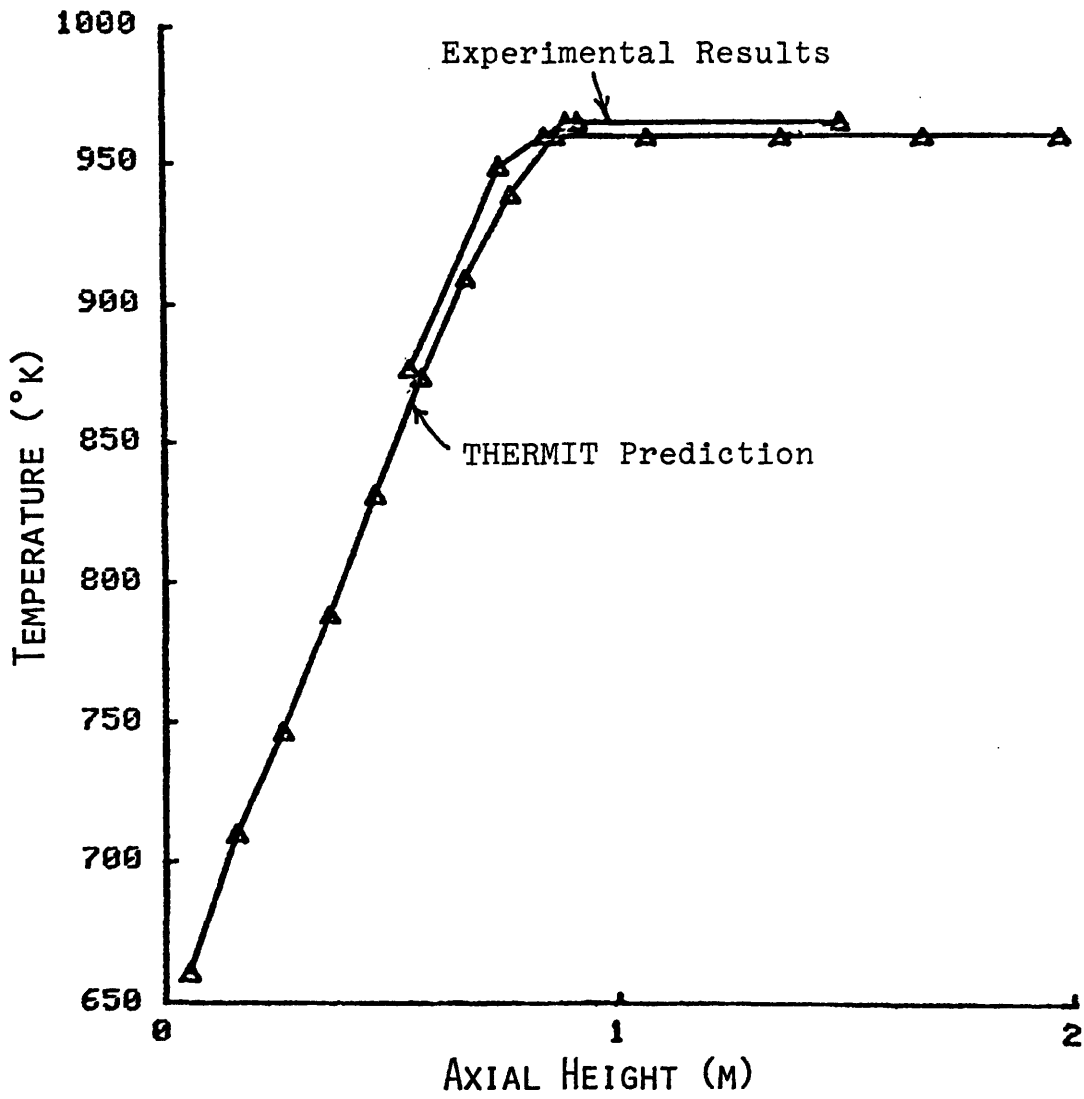
Figure 7.5   THORS Bundle 6A - Axial Temperature Distribution
at Start of Transient (Test 71h, Run 101)

than trying to get an exact match.

Figure 7.5 shows that THERMIT predicts the steady state temperatures pretty well, given the uncertainties mentioned previously. The next question is: how well do the different simulations predict boiling incipience? Cases A, B, and C were run for 20.2 seconds on the time scale shown in Figure 7.3, where the transient begins at 3.2 seconds. In the experiment boiling inception occurred at 13.7 seconds, as can be seen from the flow history plotted in Figure 7.3. One would expect that Case A would boil prematurely, since it does not allow for heat loss to the surrounding structure. It is also to be expected that Cases B and C would boil late, for two reasons. First, it was assumed that the insulation was fully sodium-soaked, which may over-estimate the heat losses. Secondly, because these runs are all single channel, no boiling occurs until the average temperature at some axial level exceeds saturation. In reality there is a fairly steep radial temperature gradient, and boiling occurs in the center of the bundle far earlier than on the periphery.

Figures 7.6 to 7.8 compare the temperature histories predicted by THERMIT with the experimental results, at three different axial locations. Figure 7.6 displays the temperature 30 inches above the bottom of the heated section, where boiling occurs first in the THERMIT runs. Figure 7.7 shows the temperature at 34 inches, nearer the top of the heated section (36 inches). Finally, Figure 7.8 displays the temperature at 54 inches, or 18 inches above the top of the
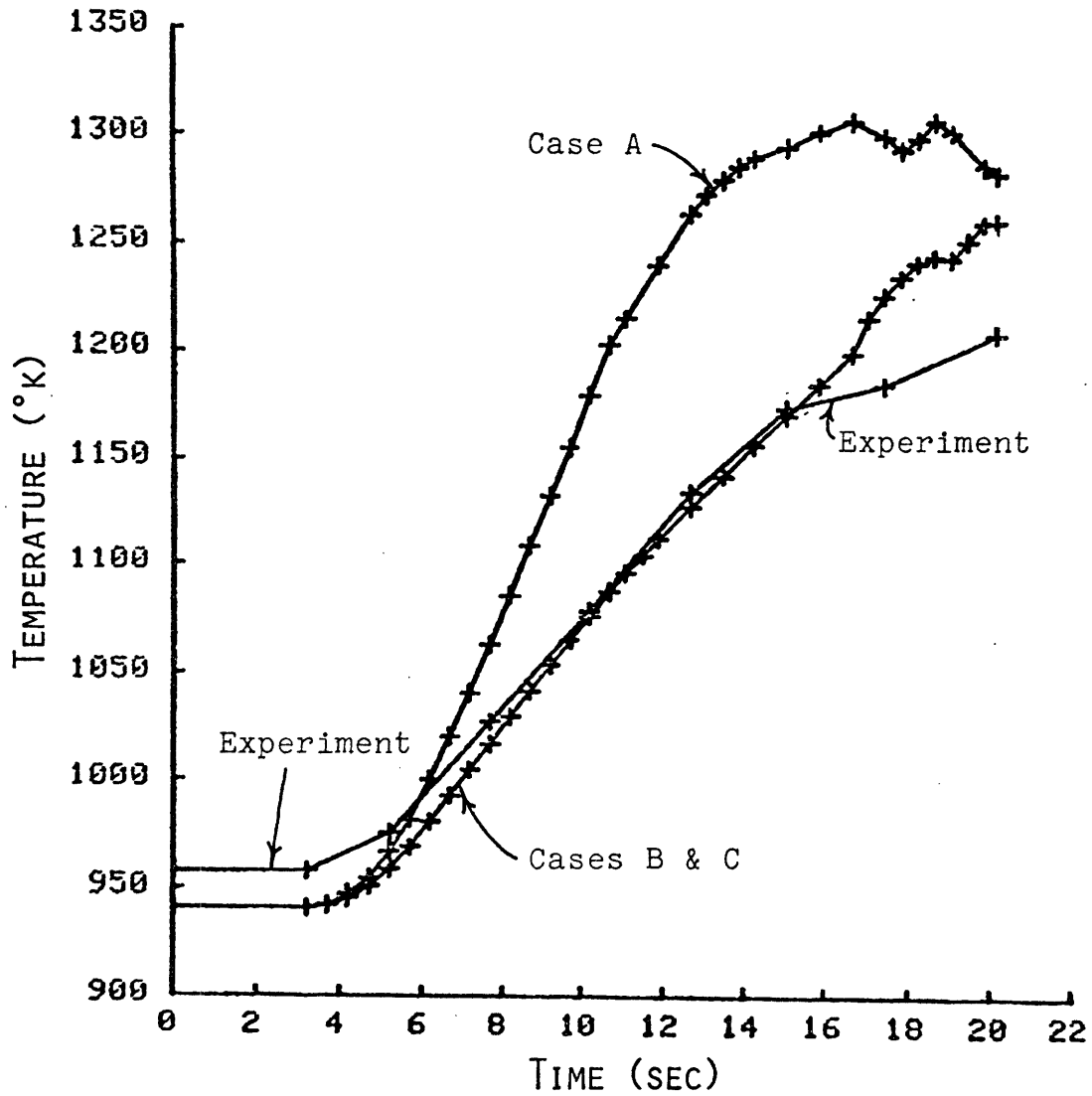
Figure 7.6 THORS Bundle 6A – Temperature History
at z=30 inches (Test 71h, Run 101)
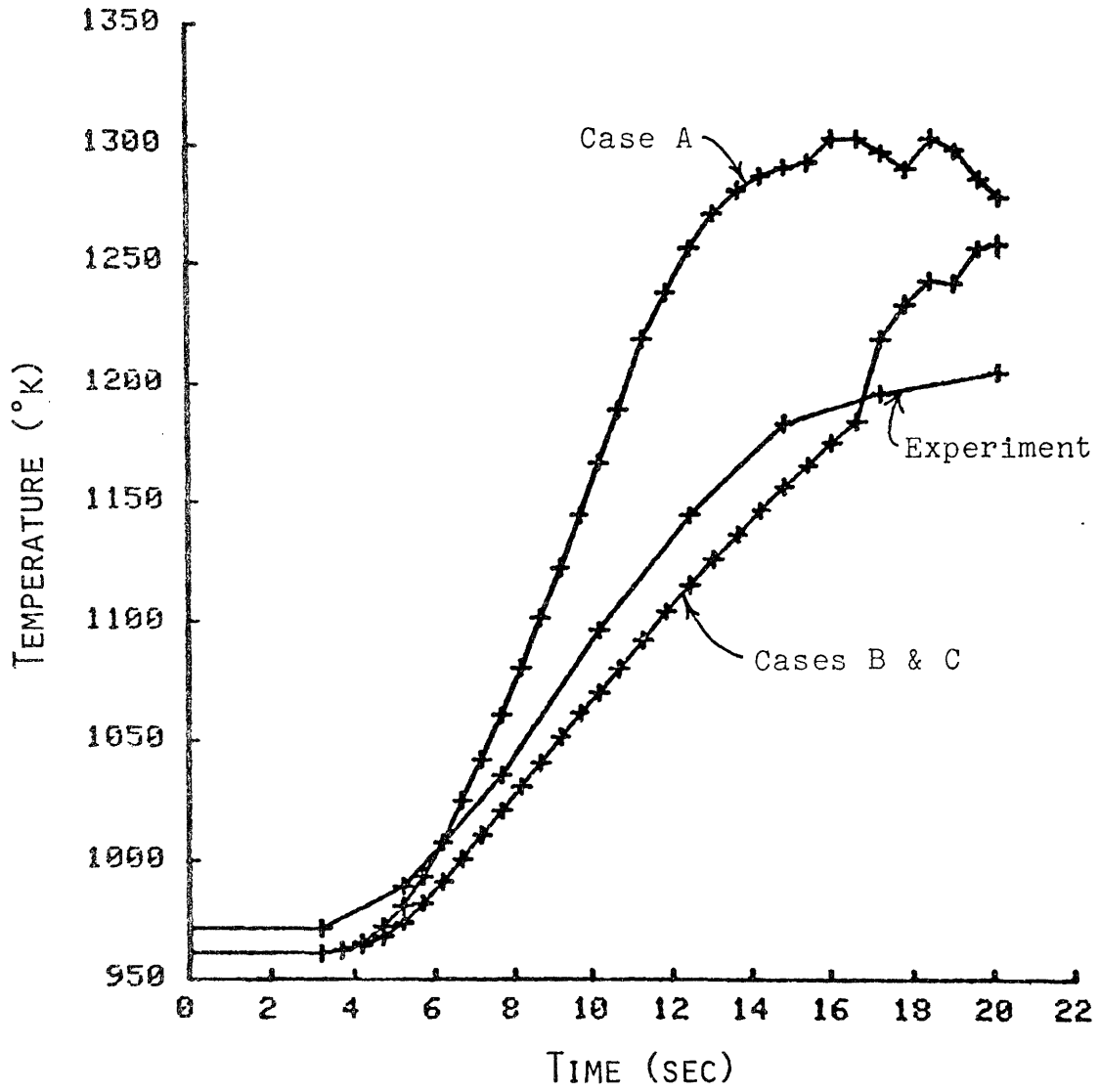
Figure 7.7   THORS Bundle 6A – Temperature History
             at z=34 inches (Test 71h, Run 101)
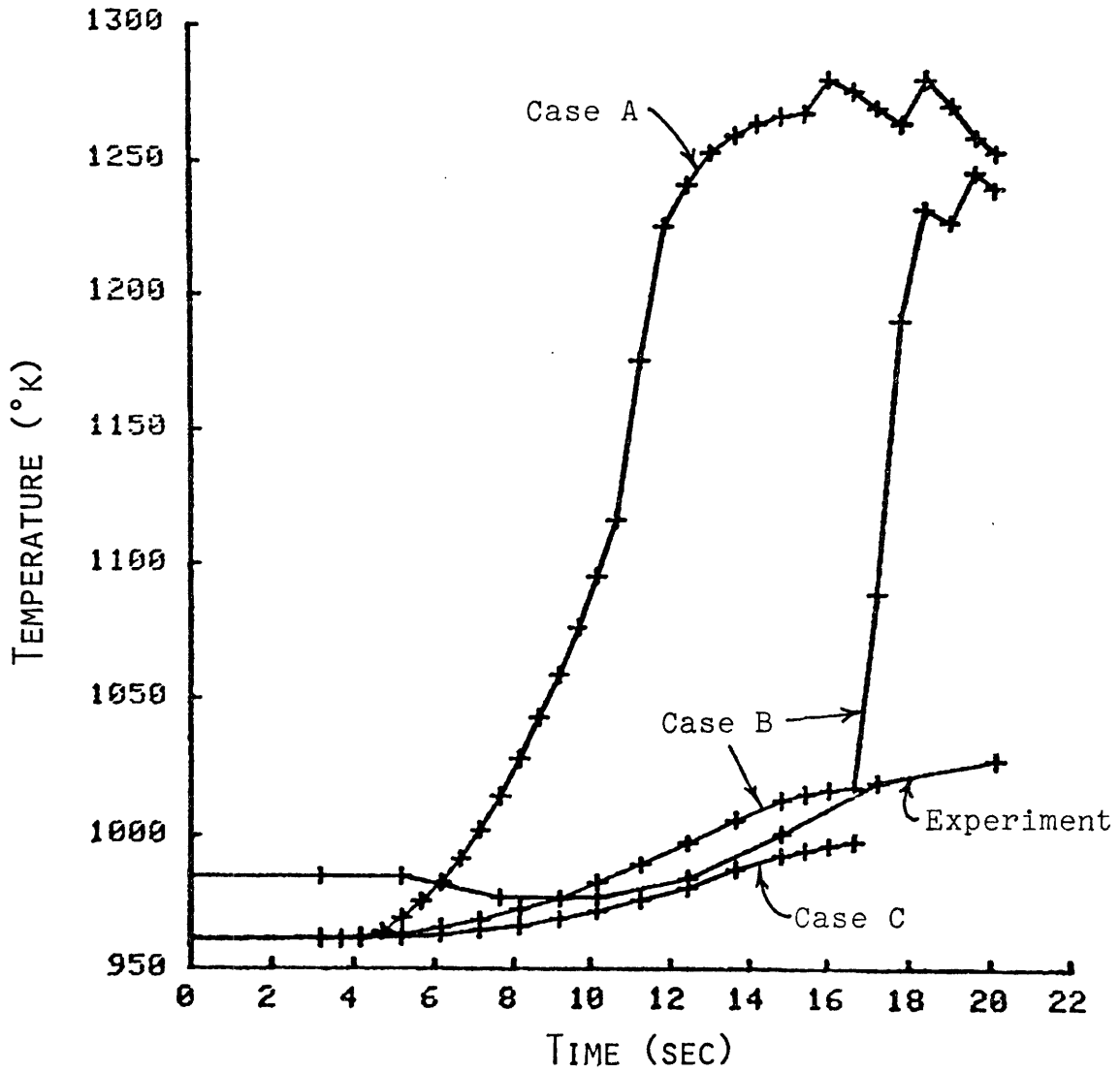
Figure 7.8   THORS Bundle 6A – Temperature History
at z=54 inches (Test 71h, Run 101)

heated section. No comparisons are made for z<30 inches, because there were very few thermocouples in this region, and it is therefore difficult to get a good comparison.

From these figures it can be seen that the inclusion of heat losses to the structure (Cases B and C) significantly improves the predictions. (Note that Cases B and C give the same results for both Figures 7.6 and 7.7. In other words, the inclusion of heat transfer to the fuel rod in the gas plenum region has a negligible effect on the temperature in the heated zone.) The boiling inception time for each of the runs is displayed in Table 7.1.

It is expected that if a multi-channel simulation (including heat losses) with a finer axial mesh spacing were run, boiling would occur earlier that in Cases B and C, and would thus match the experimental results more closely. Nevertheless, Figures 7.6 and 7.7 show that Cases B and C match the experimental results pretty closely, for axial levels within the heated zone. Case A significantly over-predicts the temperature, as expected.

Figure 7.8 is expecially interesting, becuase it shows the temperature history in the plenum region, 18 inches above the heated zone. At this height Cases B and C do predict different temperatures, and the experimental results can be seen to fall in between these two cases over a good portion of time. Cases C ends abruptly at about 16.8 seconds, because at that point numerical instabilities devel-

Table 7.1

Boiling Inception Times for THORS Bundle 6A Simulations

	Assumptions		Boiling Inception
Case	Radial Heat Losses	Gas Plenum	Time
A	No	No	10.7 sec
B	Yes	No	16.7 sec
C	Yes	Yes	16.7 sec
Experiment			13.7 sec

oped, and the code failed.

One feature present in all three figures is the sharp temperature rise in Cases B and C right after boiling inception (16.7 sec). This rise is especially pronounced in the plenum region. The reason for this is that soon after boiling the void is propagated downstream, and appears in the gas plenum and upper heated zones fairly quickly, even though they may be quite subcooled. As soon as the void appears at any axial level the conduction to the structure is assumed to be negligible (see Chapter 3), and the temperature then rises rapidly to saturation. In the plenum region this rise is quite large, as shown by Figure 7.8. This phenomenon could be corrected by phasing out structure conduction more slowly, as the void fraction increases.

Part of the explanation for the large difference between Case A and the experiment is that after boiling THERMIT shows a large rise in inlet pressure (outlet pressure is held nearly constant by the boundary conditions). Because the pressure increases, the saturation temperature increases also, and thus the liquid temperature keeps rising to a higher value before leveling off. The experiment shows only a minor increase in pressure drop upon boiling, so the temperatures do not reach such high levels. This behavior of THERMIT bears some investigation. Chapter 8 deals with the subject more fully.

Despite some of the problems encountered in THERMIT

after boiling, Cases A, B, and C are very useful in many ways. First of all, they show the importance of taking into account heat losses to the hex can and surrounding structure in a 19 pin bundle. Secondly, they show the value of considering the thermal inertia effects of the fuel cladding in the plenum region when calculating fluid temperatures in the plenum. Since the main purpose of Cases A, B, and C was to evaluate the effect of the models discussed previously, no more detailed simulations were run. However, all indications are that more rigorous geometrical modeling will give even better results.

7.4 LMFBR Fuel Assembly Simulation

The discovery that heat losses can be significant in a 19 pin bundle under transient conditions leads naturally to the question of whether heat losses are significant in a full-sized LMFBR fuel assembly of 217 pins. Heat losses would undoubtedly be less important in a 217 pin bundle, as compared to a 19 pin bundle, since the surface/volume ratio is much smaller (S/V = 291.5 for the THORS 19 pin bundle, while S/V = 87.6 for a 217 pin LMFBR bundle, where S = surface area of inside of hex can, and V = volume of sodium in the bundle).

In order to evaluate the importance of radial heat losses in loss-of-flow transients in a 217 pin bundle, three cases were run using THERMIT. These cases were similar to

those described in the previous section in that they were
single channel runs using inlet velocity and outlet pressure
as boundary conditions. The power-to-flow ratio was the same
as the THORS experiments, and the flow decay rate was identi-
cal also. The geometry of the fuel rods was unchanged. Be-
cause the new LMFBR fuel rod properties were not available
in THERMIT at the time of this writing, the properties of the
fuel pin simulator (see Section 7.2) were used. This scaled-
up version of the 19 pin THORS Bundle 6A assembly corresponds
very nearly to the 217 pin fuel assembly in the Clinch River
Breeder Reactor design (see Reference [19]).

The first run (referred to as Case D) was identical to
Case A, described in the previous section. It assumed no
radial heat losses, and no condensation in the plenum region.

The second run, Case E, included radial heat losses to
the hex can only. The hex can thickness was taken to be 3.0
mm. (as in CRBR), rather than the 0.51 mm. thickness present
in THORS Bundle 6A. The hex can was represented as one mesh
cell by the code, and its outer boundary was taken to be
adiabatic.

The final run, Case F, added an annulus of sodium-soaked
insulation around the hex can, in order to see how much this
affected heat loss. The thickness of the insulation was the
same as in the THORS experiments. This case can be thought
of as similar to a fuel assembly adjacent to a cold blanket
assembly in a fast reactor core, where heat losses from the

outer boundary of the hex can may be significant. The input files for Cases D, E, and F are reproduced in Appendices B.7, B.8, and B.9, respectively. The restart files were identical to those in Cases A, B, and C.

Once again, all three cases give identical results at steady state. In fact, the steady state temperature distribution is nearly identical to that predicted by Cases A-C. This is to be expected, since the power-to-flow ratios are identical.

Figures 7.9, 7.10, and 7.11 show the temperature histories for each of the cases, at axial heights of 22, 30, and 54 inches, respectively. As in the previous cases, the transient begins at 3.2 seconds. Note the sharp differences between these runs and those in Figures 7.6-7.8. Only in the plenum region (Figure 7.11) is there any major difference between the adiabatic and non-adiabatic cases. As expected, the adiabatic case predicts the highest temperatures, followed by Cases E and F. Surprisingly enough, the addition of the sodium-soaked insulation around the outside of the hex can does not affect the temperature to a great degree. The boiling inception times for Cases D, E, and F are shown in Table 7.2.

In the 19 pin bundle at z = 30 inches, the temperature predictions of Case C deviate from Case A by as much as 10.9%, whereas the 217 pin bundle shows deviations of only 3.9% between Cases D and F, at that axial level. It is interesting to note that the ratio of these deviations, 2.8, is
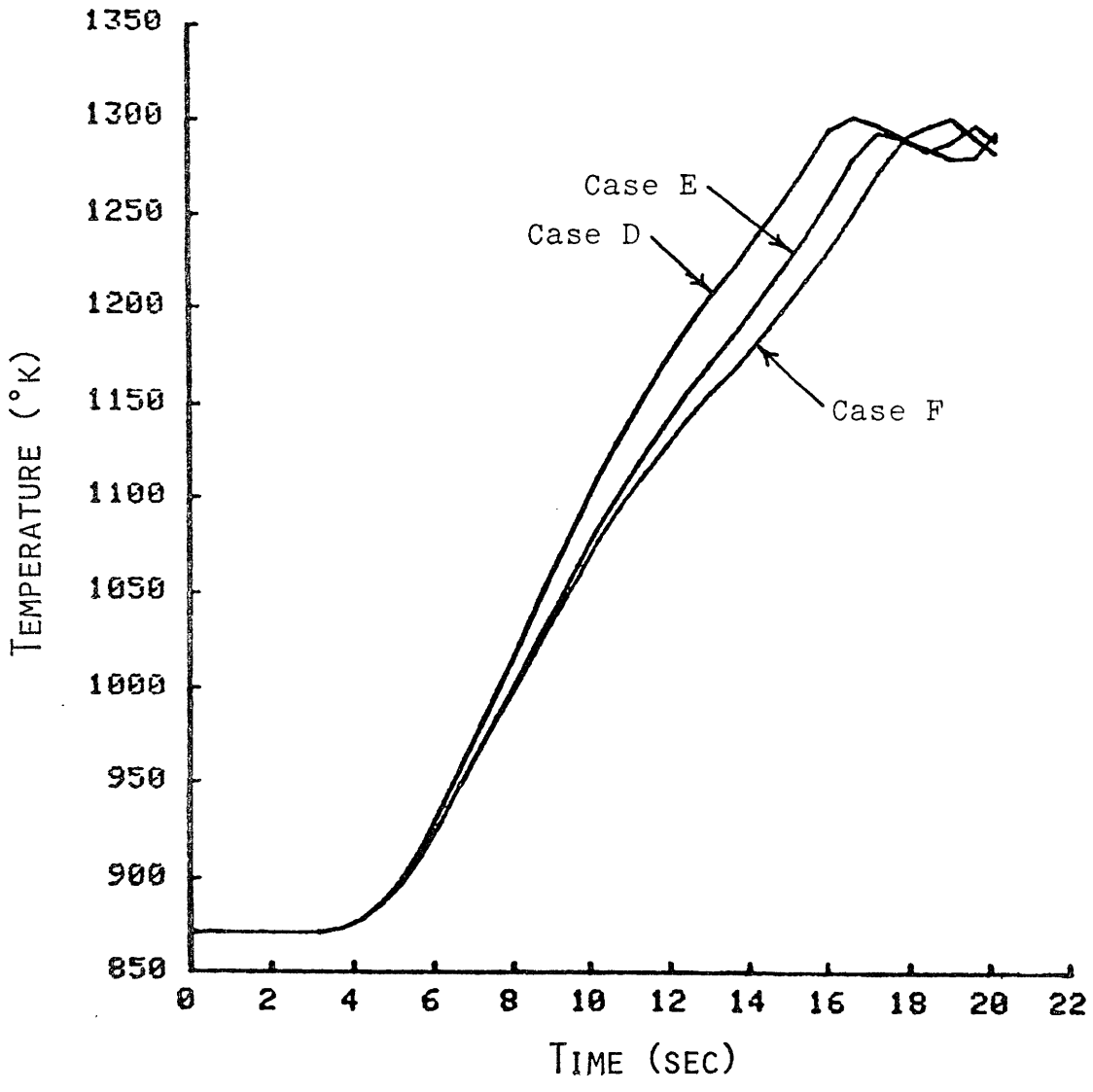
Figure 7.9   217 Pin Bundle - Temperature History
at z=22 inches
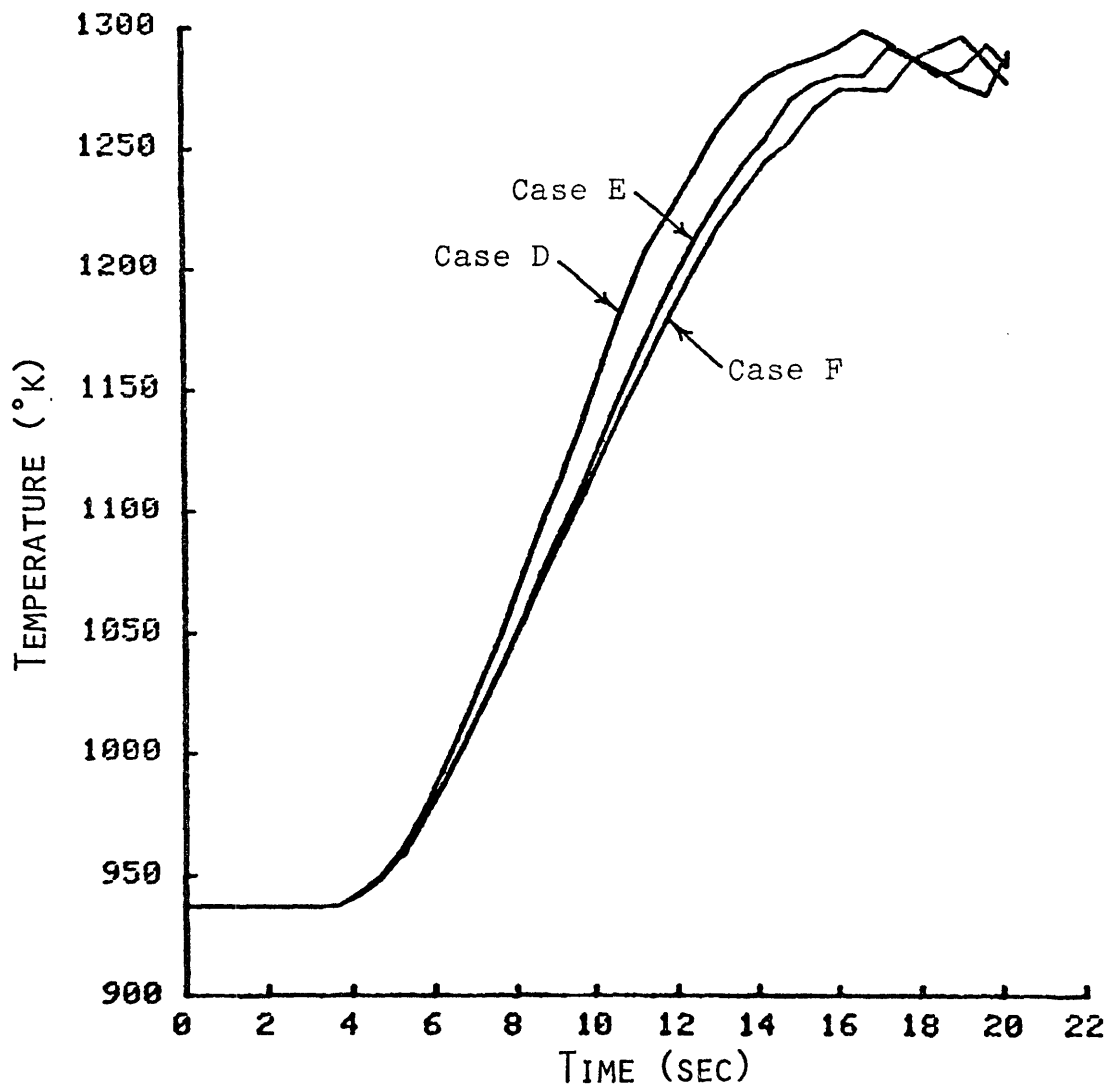
Figure 7.10 217 Pin Bundle - Temperature History
at z=30 inches
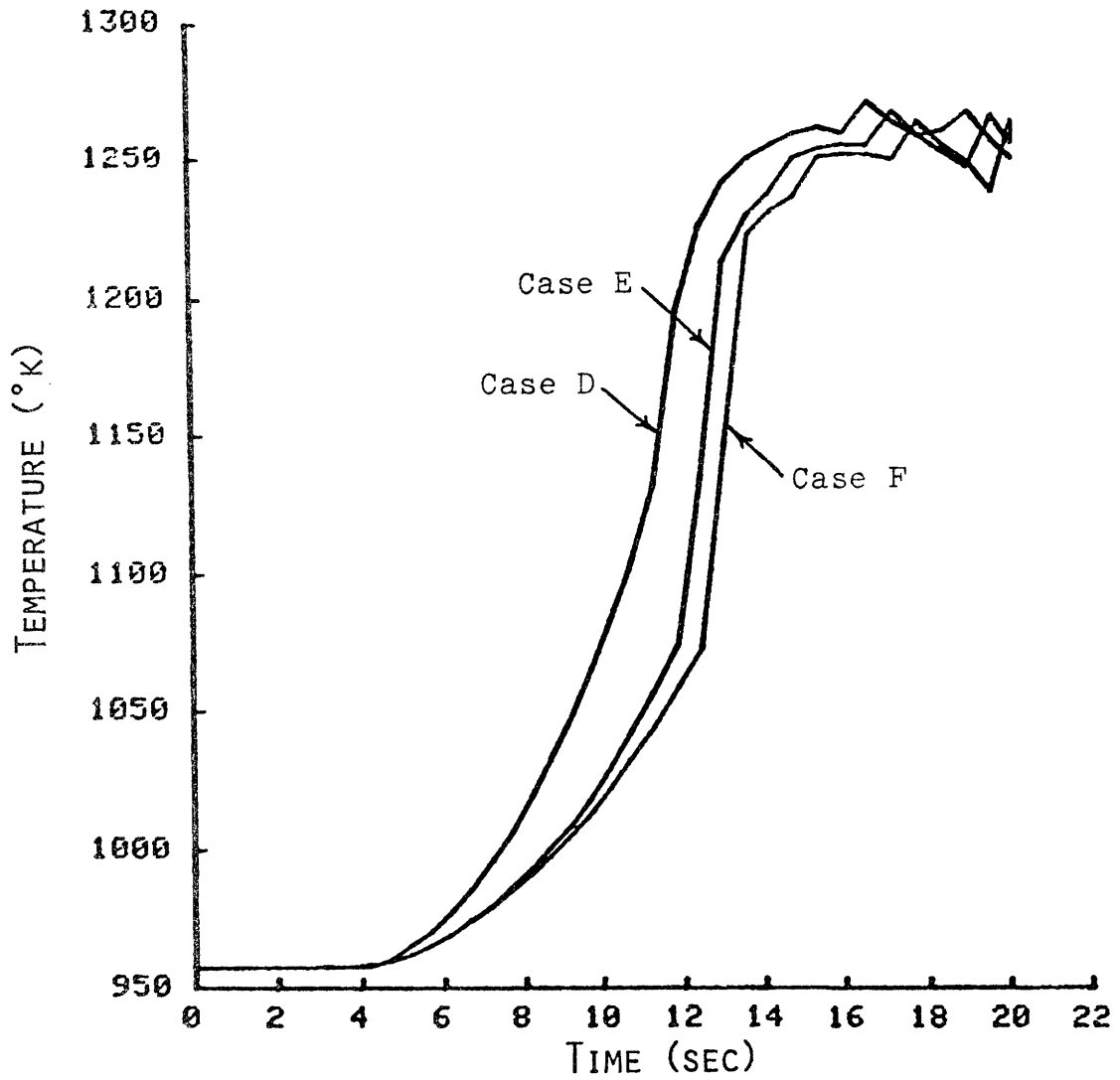
Figure 7.11   217 Pin Bundle – Temperature History
at z=54 inches

Table 7.2

Boiling Inception Times for 217 Pin Bundle Simulations

| | Assumptions | | Boiling Inception |
Case	Radial Heat Losses	Gas Plenum	Time
D	No	No	11.1 sec
E	Hex Can Only	No	12.1 sec
F	Hex Can + Insulation	No	12.5 sec

roughly the same as the ratio of the surface/volume ratios of the two bundles = 291.5/87.6 = 3.3. This makes physical sense, because the significance of heat losses should depend on the amount of surface area per unit volume.

From the results of this comparison it can be concluded that radial heat losses to the hex can and surrounding structure during a loss-of-flow transient are not nearly as significant in a 217 pin bundle as in a 19 pin bundle.

CHAPTER 8

Summary and Recommendations

8.1   Models and Correlations

This section will briefly summarize the work described in Chapters two through six, and will make recommendations on how to improve these models and correlations.

The fluid conduction model in Chapter 2 allows for heat flow between adjacent fluid cells due to conduction. It can be used in either an explicit or semi-implicit formulation. When using the explicit formula one must be careful that the time step limitation introduced is no more restrictive than the convective limit. The code currently requires the user to input a conduction Nusselt Number, which is taken as a constant throughout the calculation. It would be beneficial to replace this approximation with a more physical model for the Nusselt Number, in the future.

The structure conduction model in Chapter 3 allows for radial heat losses to the structure surrounding the simulated region. The user specifies the physical layout of the

structure and the boundary conditions on the outside (i.e.
heat transfer coefficient and external temperature), and
the code solves the conduction problem within the structure.
Currently, the conduction routine is bypassed for any
channel in which void is present. Chapter 7 showed that
this can cause unphysical results (see Figure 7.8, where
Case B shows a large temperature rise soon after boiling).
A very small void can enter a channel that is significantly
subcooled, and trigger a cutoff in radial heat losses,
causing an unphysical temperature rise. This anomaly could
be corrected in several ways. First, the cutoff point
could be based on temperature rather than void fraction,
and the structure conduction routine could by bypassed
when $T_{liquid} \geq T_{saturation}$. Conversely, a certain cutoff void
fraction could be specified such that for $\alpha < \alpha_{cutoff}$,
structure conduction would still be employed. I would
recommend the former, because once the bulk temperature
reaches saturation the cell will void very quickly.

The fuel rod conduction model in Chapter 4 permits the
user to "construct" his own fuel rod by specifying the
number of axial regions desired, and the number of radial
zones in each region. As of this writing, the boron nitride
fuel pin simulator described in Chapter 7 was the only

option available, but work is presently being completed on a model appropriate for LMFBR fuel rods.

The interfacial exchange coefficients described in Chapter 5 are an improvement over what was previously in the code, but more work needs to be done on this topic. The interfacial momentum exchange coefficient was developed for axial flow in a single tube, and its applicability to both axial and transverse flow in a triangular rod bundle is questionable at best. The interfacial mass exchange coefficient needs more testing, too. This is especially important, because of the sensitivity of the code to the value of gamma. Some of the numerical problems that have been encountered in boiling could have been caused by an inappropriate value for gamma.

The axial friction factor correlations in Chapter 6 were the best available at the time of their implementation, but since then the correlation of Hawley and Chiu has been refined (see Reference [15]) and improved. Because it is a consistent correlation that goes smoothly from laminar to turbulent flow, rather than the hybrid correlation presently in the code, it is recommended that it be incorporated in the future. The

two phase axial friction factors do present a problem, though. It was mentioned in Chapter 7 that the THERMIT simulations over-predicted the pressure drop in two phase flow. This may have been caused in part by inadequate values for the liquid friction factor. On the other hand, the inlet velocity specified as a boundary condition may have been inappropriate.

The transverse friction factor correlation is also highly suspect in the two phase region, especially at high void fractions. This is because in simplifying the equations it was assumed that the total mass flux, G, was equal to the liquid mass flux, G_ℓ. This assumption breaks down at high void fractions. It is my opinion that an entirely new correlation should be employed, at least for pure vapor flow (if nothing else).

8.2   General

THERMIT for sodium has performed extremely well in the single phase region, especially for the single channel runs presented in Chapter 7. It was also mentioned in Chapter 7 that some inconsistencies were present in two phase flow. It is possible that these were caused by one of the models, but that is unlikely, because they all perform well in the

single phase region. Only the interfacial exchange
coefficients could cause the problems, unless they are
of a numerical nature, which is quite possible.

Several problems occur soon after boiling. First
of all, the pressure drop becomes quite large (the
pressure drop in Cases A - F in Chapter 7 went from 0.2
bars in single phase to $\sim$2.0 bars during boiling).
Secondly, the vapor velocities begin to oscillate.
This leads to an oscillating time step size, which drops
by a factor of 100 or more. Often times the flow reverses
at some axial level in the channel. At this point the code
invariably fails, usually on negative pressures or void
fractions.

It is possible that the key to this problem lies
in the determination of the reason for the oscillation in
the vapor velocities. The vapor velocities are determined
mainly by the momentum exchange between the vapor and
liquid, which is dependent on the momentum exchange due
to shear, K, and the momentum exchange due to mass
transfer, Γ. Because of the finite difference technique
employed in the code, both of these parameters are
calculated explicitly. This could be the problem, because
in a situation as explosive as sodium voiding the maximum
degree of implicitness is required.

In conclusion, some things remain to be done before the sodium version of THERMIT becomes fully operational. Most of the inadequacies of the present version result from the fact that very little work has been done on two fluid, three dimensional modeling of sodium boiling. As more information becomes available and the models in THERMIT are refined accordingly, THERMIT will prove to be a useful tool for LMFBR accident analysis.

REFERENCES

[1]   Reed, W.H., Stewart, H.B., "THERMIT, A Computer Pro-
      gram for Three-dimensional Thermalhydraulic Analysis
      of LWR Cores," (An EPRI/MIT report to be published)

[2]   Meyer, J.E., "Some Physical and Numerical Considera-
      tions for the SSC-S Code," NUREG/CR-0451, BNL-NUREG-
      50913, Brookhaven National Laboratory, (1978)

[3]   El-Wakil, M.M., Nuclear Heat Transport, International
      Textbook Company, Scranton, Pa., (1971)

[4]   Dwyer, O.E., "On the Transfer of Heat to Fluids Flow-
      ing Through Pipes, Annulii, and Parallel Plates,"
      Nucl. Sci. Eng., 17, 336 (1963)

[5]   Arpaci, Vedat S., Conduction Heat Transfer, Addison-
      Wesley, Massachusetts, (1966)

[6]   Ribando, R.J., et al., "Sodium Boiling in a Full-
      length 19-Pin Simulated Fuel Assembly (THORS Bundle
      6A)," ORNL/TM-6553, (1979)

[7]   Nigmatulin, R.I., "Equations of Hydrodynamics and
      Compression Shock in Two-Velocity and Two-Tempera-
      ture Continuum with Phase Transformations," Fluid
      Dynamics, Vol. 2, No. 5 (1968)

[8]   Rivard, W.C., Torrey, M.D., "Numerical Calculation
      of Flashing from Long Pipes Using a Two-field Model,"
      LA-6104-MS, Los Alamos Scientific Laboratory, (1975)

[9]   Autruffe, M.A., "Theoretical Study of Thermohydraulic
      Phenomena for LMFBR Accident Analysis," M.S. Thesis,
      Department of Nuclear Engineering, MIT, (1978)

[10] Kaiser,A., Peppler, W., Voross, L., "Untersuchungen
      der Stromungsform, des Druckabfalls und des Kritis-
      chen Warmeflusses einer Zweiphasenstromung mit Natri-
      um," KFK 2085, Karlsruhe, (1975)

[11] Kottowski, H.M., et al., "Steady State Liquid Metal
      Boiling Pressure Drop Characteristics," in Proc. of
      the Inter. Meeting on Fast Reactor Safety and Rela-
      ted Physics, Chicago, CONF-761001, (1976)

[12] Markley, R.A., Engel, F.C., "LMFBR Blanket Assembly Heat Transfer and Hydraulic Test Data Evaluation," Westinghouse Electric Corp. Advanced Reactors Division, US/DOE Contract No. EY-76-C-02-3045-004

[13] Novendstern, E.H., "Turbulent Flow Pressure Drop Model for Fuel Rod Assemblies Utilizing a Helical Wire-wrap Spacer System," Nuclear Engineering and Design, 22, (1972)

[14] Chiu, C., Todreas, N.E., and Rohsenow, W.M., "Turbulent Flow Split Model and Supporting Experiments for Wire-wrapped Core Assemblies," Submitted to Nuclear Technology for review, February, (1979)

[15] Hawley, J., "Hydraulic Studies of Liquid Metal Fast Breeder Reactor Subassemblies," M.S. Thesis, Department of Nuclear Engineering, MIT, (1980)

[16] Gunter, A.Y., and Shaw, W.A., "A General Correlation of Friction Factors for Various Types of Surfaces in Crossflow," ASME Transactions, 67, (1945)

[17] Ishihara, K., Palen, J.W., Taborek, J., "Critical Review of Correlations for Predicting Two-phase Flow Pressure Drop Across Tube Banks," ASME Paper 77-WA/HT-23 (1977)

[18] Hinkle, W.D. Ed., "Development of Computer Code Models for Analysis of Subassembly Voiding in an LMFBR," Interim Report of the MIT Sodium Boiling Project Covering Work Through September 30, 1979, Energy Laboratory Report No. MIT-EL-80-005 (1980)

[19] Tang, Y.S., Coffield, R.D., Markley, R.A., Thermal Analysis of Liquid Metal Fast Breeder Reactors, American Nuclear Society, (1978)

Appendix A:

T H E R M I T for Sodium — Input Description

Part I Overall Problem Description

The following cards are read via list-directed input (v-format). Fields are separated by one or more blanks or by commas. A nullfield can be specified by the occurrence of consecutive commas. Basically a constant (entered as a field) is assigned to the corresponding list element as if the constant were the right side of an assignment statement whose left side was the list element.

For additional details on the use of list-directed input, the user is referred to the Multics Fortran manual.

Group no.	Format	Contents
1	v	ntc
		ntc = Number of title cards (Note: if ntc=0, the job is ended; if ntc=-1, the job is a continuation of a previous calculation, performed in the same process; if ntc=-2, the job is a restart from a previously created dump file.)
2	10A8	Title cards (these are the only cards in fixed format).

Group No.	Format	Contents

3   V   nc, nz, nr, nitmax, iitmax, iflash, itb, ibb, iwft, narf, nx, nrzs, iht, iss, itam, idump, ntabls, itbt, ibbt, ipowt, ihtpr, ishpr, istrpr.

nc   = Number of cells in X-Y plane.

nz   = Number of axial cells.

nr   = Number of rows of cells in X-Y plane.

nitmax = Maximum number of Newton iterations.

           (Note: if nitmax < 0 the code will automatically reduce the timestep if it fails to meet the convergence criteria after performing abs(nitmax) iterations.)

iitmax = Maximum number of inner iterations.

iflash = Phase change indicator: (0/1) (normal/suppressed).

itb   = Top boundary condition indicator: (0/1) (pressure/velocity).

ibb   = Bottom boundary condition indicator: (0/1) (pressure/velocity).

iwft   = Indicator for transverse wall friction: (0/1) (no friction/Gunter-Shaw correlation).

narf   = Number of axial regions in the fuel.

nx   = Number of fluid channels touching the exterior region (i.e. number affected by radial heat loss).

nrzs   = Number of radial zones in the structure.

iht   = Heat transfer indicator (2 digits, the first one indicating structure, the second, fuel. 0 = no heat transfer, 1 = heat transfer with all properties constant, 2 = full calculation (for structure), or constant gap properties (for fuel), 3 = full calculation (for fuel)).

Group No.	Format	Contents

iss = Heat transfer calculation type: (0/1) (transient/steady state).

itam = Transverse flow indicator: (0/1) (no transverse flow/transverse flow).

idump = Dump file request indicator: (0/1) (no/yes).

ntabls = Number of transient tables.

itbt = Transient table indicator for top boundary condition.
(<=0 multiplier is 1.0 at all times,
>0 multiplier is from table.)

ibbt = Transient table indicator for bottom boundary condition
(<=0 multiplier is 1.0 at all times,
>0 multiplier is from table.)

ipowt = Transient table indicator for power.
(<0 normal exponential is used,
=0 multiplier is 1.0 at all times,
>0 multiplier is from table)

ihtpr = Indicator for fuel heat transfer printout: (0/1) (no/yes).

ishpr = Indicator for short print contents:
(4 digits, each 1 or 0, requesting or not, printout for p, alpha, tl, tv).

istrpr = Indicator for structure heat transfer printout: (0/1) (no/yes).

4   v   epsn, epsi, grav, hdt, pdr, velx, vely, tdelay, cpumax, rnuss, hout, tout, radf, hdr.

epsn = Newton iteration convergence criterion.

epsi = Inner iteration convergence criterion.

grav = Gravitational constant (normally -9.81m/s*s).

Group
No.   Format   Contents

hdt   = Hydraulic diameter in transverse
           direction (m).

pdr   = Pitch/diameter ratio.

velx   = Velocity multiplier for x-transverse
           friction.

vely   = Velocity multiplier for y-transverse
           friction.

tdelay   = Delay time for all transient tables (s).

cpumax   = Maximum number of cpu seconds allowed
           for calculation.

rnuss   = Nusselt number for liquid conduction.
           (<0   explicit solution used,
            =0   liquid conduction bypassed,
            >0   partially implicit method used)

hout   = Heat transfer coefficient between the
           outside wall of the structure and the
           environment (W/m*m*deg.K).

tout   = Constant temperature of the environment
           (deg.K).

radf   = Outer radius of the fuel rod (m).

hdr   = Wire wrap helical pitch to diameter ratio

           (Note: if wire wrap is not present,
           input a large value for this
           parameter. Do not enter zero.)

     The following data is required only when the fuel heat
transfer calculation is requested (i.e. units digit of iht not
equal to 0).

5   v   q0, t0, omg, ftd, fpuo2, hgap, fpress, cpr, expr,
                 grgh, pgas, (gmix(k),k=1,4), burn.

          q0   = Initial total power (w).

                  (Note: if q0<0.0, q0 is set equal to
                  current power.)

Group
No. Format   Contents

           t0   = Delay time (s).

           omg   = Inverse reactor period (1/s).

           ftd   = Fraction of theoretical density
                        of fuel.

           fpuo2   = Fraction of PuO_2 in fuel.

           hgap   = Gap heat transfer coefficient
                        (W/m*m*deg.K).

           fpress   = Fuel pressure on clad for gap
                        conductance model (Pa=N/m*m).

           cpr   = Coefficient for above pressure.

           expr   = Exponent for above pressure.

           grgh   = Gap roughness (m).

           pgas   = Gap gas pressure (pa).

           gmix(1)   = Helium fraction in gap gas.

           gmix(2)   = Argon fraction in gap gas.

           gmix(3)   = Krypton fraction in gap gas.

           gmix(4)   = Xenon fraction in gap gas.

           burn   = Fuel average burnup (Mwd/mtU).

Part II   Detailed Input Data

The following cards are read via NPS free-format input
processor. Fields are separated by blanks. Entry (or
group of entries) repetition is allowed; for example
n(a b m(c d e) f) where: a,b,c,d,e,f are entries
(integer or real) and n,m are integers representing the
number of repetitions; note that no blanks must appear
between a left parenthesis and the integer preceding it.

Up to ten levels of nesting are permitted.

The end of a group is marked by a $-sign.

Group No.		Contents
1	ncr(nr)	= Number of cells in each row.
2	indent(nr)	= Indentation for each row.

The following four arrays are required only when the fuel heat transfer calculation is requested (i.e. units digit of iht not equal to 0).

3	ifcar(narf)	= Index number of first cell in each axial region of fuel.
4	nrzf(narf)	= Number of radial zones in each axial region of fuel.
5	nrmzf(nrzfmx,narf)	= Number of radial meshes per zone in the fuel (nrzfmx=the maximum value in nrzf).
6	mnrzf(nrzfmx,narf)	= Material in each radial zone of the fuel: (1/2/3/4/5/6)(fuel/gap/type 316 stainless steel/type 304 stainless steel/ liquid sodium/degraded marimet insulation used in THORS experiments).

The following three arrays are required only when the structure heat transfer calculation is requested (i.e. tens digit of iht not equal to 0).

7	inx(nx)	= Index number of each fluid channel touching the exterior.
8	mnrzs(nrzs)	= Material in each radial zone of the structure (see mnrzf for options available.
9	nrmzs(nrzs)	= Number of radial meshes per zone in the structure.

-

Group
No.   Contents

The following thirteen arrays are always required.

10 arx(nz,nc)   = Mesh cell areas in the X-direction(m**2).

11 ary(nz,nc)   = Mesh cell areas in the Y-direction(m**2).

12 arz(nz+1,nc) = Mesh cell areas in the Z-direction(m**2).

13 vol(nz,nc)   = Mesh cell volumes (m**3).

14 hedz(nc)   = Heated equivalent diameter z-direction(m).

15 wedz(nc)   = Wetted equivalent diameter z-direction(m).

16 dx(nc)   = Mesh spacing in the X-direction (m).

17 dy(nc)   = Mesh spacing in the Y-direction (m).

18 dz(nz+2)   = Mesh spacing in the Z-direction (m).

19 p(nz+2,nc)   = Initial pressures (Pa).

20 alp(nz+2,nc) = Initial vapor volume fractions.

21 tv(nz+2,nc)   = Initial vapor temperature (deg.K).

                    (Note: initial liquid temperature set
                    equal to tv.)

22 vvz(nz+1,nc) = Initial vapor axial velocity (m/s).

                    (Note: initial liquid velocity set
                    equal to vvz.)

The following six arrays are required only when the
fuel heat transfer calculation is requested (i.e. units
digit of iht not equal to 0).

23 twf(nz,nc)   = Fuel wall surface temperature (deg.K).

24 qz(nz)   = Axial power shape.

25 qt(narf,nc)   = Transverse power shape.

26 qr(nfmlmx,narf) = Fuel pin radial power shape (nfmlmx=
                    maximum number of cells (nodes-1) in
                    the fuel).

Group No.	Contents
27 rn(narf,nc)	= Number of fuel rods in each channel, at each axial region.
28 drzf(nrzfmx,narf)	= Thickness of each radial zone in the fuel (m).

The following three arrays are required only when the structure heat transfer calculation is requested (i.e. tens digit of iht not equal to 0).

Group No.	Contents
29 pcx(nx)	= Perimeter in contact with structure, for each exterior channel (m).
30 drzs(nrzs)	= Thickness of each radial zone in the structure (m).
31 tws(nz)	= Initial wall temperature of the structure (deg.K).

The following data is required only when transient tables are used (i.e. ntabls not equal to 0).

For each table enter first the number of entries in the table (in v-format), then enter the time/multiplier pairs in NIPS-format (as described above). The time points must be in ascending order.

Group No.	Contents
nentry	= Number of entries in table 1.
32 time(nentry) multiplier(nentry)	= Time/multiplier pairs for table 1.
nentry	= Number of entries in table 2.
33 time(nentry) multiplier(nentry)	= Time/multiplier pairs for table 2.
• • •	
nentry	= Number of entries in table ntabls.
34+ time(nentry) multiplier(nentry)	= Time/multiplier pairs for table ntabls.

Note that the tables are not saved in the dump file.
If needed they have to be provided every time a full
restart is performed.

Part III Time Cards (see Part I for v-format description)

Format	Contents

v   tend, dtmin, dtmax, dtsp, dtlp, clm, iredmx.

tend   = End of time zone (s).

dtmin   = Minimum time step (s).

dtmax   = Maximum time step (s).

dtsp   = Short print time interavl (s).

dtlp   = Long print time interval (s).

clm   = Convective limit multiplier.

iredmx = Maximum number of time step reductions.

> (Note: as many time cards as needed may
> be input; if dtmin>=dtmax, then this
> will be the time step used throughout
> the current time zone; if tend=0.0, the
> case is ended; if tend<0.0, then the
> restart option is requested.)

Part IV Restart Option

The following items (previously defined except for natc) are
read via "restart" namelist when the restart option is invoked:

```
nitmax,litmax,epsn  ,epsi  ,iflash,itb  ,ibb   ,
hdt    ,pdr  ,grav ,iht   ,iss  ,q0   ,t0    ,
omg    ,iwft ,idump ,itbt  ,ibbt  ,ipowt ,tdelay,
itam   ,natc ,ntabls,cpumax,rnuss ,ihtpr ,ishpr ,
istrpr,hout  ,tout
```

       natc = Number of additional title cards

The input should look like:

           $restart f1,f2,f3,...,fn,$end

where each fI is a field consisting of:

           all blanks, or
           name = constant, or
           name = list of constants.

The order of input is immaterial; as many cards as needed

may be used; the $end signifying the end of the namelist input

should appear only on the last card.

For additional details on the use of namelist input, the

user is referred to a standard Fortran manual.

The following comments apply only to a full restart (i.e.

ntc=-2):

cpumax is not stored in the dump file, so it must always

be supplied for a full restart;

       if natc is not equal to 0, enter additional title cards

(format 10A8);

       note that if not supplied at restart itbt, ibbt, ipowt

and ntabls are assumed equal to 0;

4)   if ntabls is not equal to 0, then transient table data must be supplied as described in Part II.

    After the restart information (and when applicable, additional title cards and transient tables) the time cards are supplied.

*   *   *

As of 1 May 1980

Appendix B: INPUT FILES FOR THERMIT TEST CASES

This appendix contains the input files for the THERMIT

runs described in this thesis. The first several lines in

each input file contain the title, integer parameters, and

real parameters, in that order. The lines with the dollar

signs are arrays. Appendix A describes the input parameters.

For more details see Reference [1].

B.1 4 Channel Steady State Conduction Test Case

```
2
4 Channel Steady State Conduction Test Case (Explicit)
Four channels, sixteen axial cells, no structure conduction.
4 16 2 3 50 0 0 1 1 1 4 0 1 1 0 1 0 0 0 1 1010 0
1.0e-9 1.0e-10 -9.81 3.20e-3 1.243 2.76 5.78 0.
2000.0 -7.0 0.0 0.0 2.921e-3 52.174
0.635e+5 1.00e6 0.  1.  0. 0.207e5
0. 0. 0. 0. 1.0e7 1.0 0. 0. 0. 0.
2 2                                            $ncr
0 0                                            $indent
1                                              $ifcar
3                                              $nrzf
2 1 1                                          $nrmzf
3(0)                                           $mnrzf
2(16(0.0) 16(2.24e-3))                         $arx
32(0.)    32(1.90e-3)                          $ary
68(9.63e-5)                                    $arz
64(2.94e-5)                                    $vol
4(4.42e-3)                                     $hedz
4(2.97e-3)                                     $wedz
4(18.71e-3)                                    $dx
4(16.21e-3)                                    $dy
18(0.3048)                                     $dz
4(2.20e5 2.16e5 2.11e5 2.07e5 2.02e5 1.98e5 1.93e5
1.89e5 1.84e5 1.80e5 1.75e5 1.71e5 1.66e5 1.62e5
1.57e5 1.53e5 1.48e5 1.44e5)       $p
72(0.)                                         $alp
72(661.)                                       $tv
68(1.016)                                      $vvz
4(0. 3(661.) 12(0.))                           $twf
0. 0.702 1.0 0.702 12(0.)                      $qz
1. 0. 0. 1.                                    $qt
2(1.0)    2(0.)                                $qr
4(4.75)                                        $rn
1.5875e-3 9.525e-4 3.81e-4                     $drzf
10. 1.e-8 1. 0.5 1.0 0.9 16
0.,,,,,,,
0
```

B.2 9 Channel Transient Conduction Test Case (Explicit)

```
1
9 Channel Transient Conduction Test Case (Explicit)
9 3 3 3 50 0 0 1 1 1 8 0 0 1 0 1 0 0 0 0 0 1010 0
1.0e-9 1.0e-10 -9.8066 1.0 1.5 1.5 1.5 1.0e+3
2000. -7.0 0.0 0.0 1.0 1.0e+6
3(3)                                             $ncr
3(1)                                             $indent
3(3(0.0) 6(0.01))                                $arx
9(0.0) 18(0.01)                                  $ary
36(0.01)                                         $arz
27(1.0e-3)                                       $vol
9(0.1)                                           $hedz
9(0.1)                                           $wedz
9(0.1)                                           $dx
9(0.1)                                           $dy
5(0.1)                                           $dz
45(1.013e+5)                                     $p
45(0.0)                                          $alp
2(5(900.) 5(800.)) 5(700.) 2(5(800.) 5(900.))    $tv
36(0.0)                                          $vvz
100.0 1.0e-1 5.0 5.0 10.0 0.9 15
0.0,,,,,,,
0
```

B.3   9 Channel Transient Conduction Test Case (Semi-implicit)

```
1
9 Channel Transient Conduction Test Case (Semi-implicit)
9 3 3 3 50 0 0 1 1 1 8 0 0 1 0 1 0 0 0 0 0 1010 0
1.0e-9 1.0e-10 -9.8066 1.0 1.5 1.5 1.5 1.0e+3
2000. 7.0 0.0 0.0 1.0 1.0e+6
3(3)                                          $ncr
3(1)                                          $indent
3(3(0.0) 6(0.01))                             $arx
9(0.0) 18(0.01)                               $ary
36(0.01)                                      $arz
27(1.0e-3)                                    $vol
9(0.1)                                        $hedz
9(0.1)                                        $wedz
9(0.1)                                        $dx
9(0.1)                                        $dy
5(0.1)                                        $dz
45(1.013e+5)                                  $p
45(0.0)                                       $alp
2(5(900.) 5(800.)) 5(700.) 2(5(800.) 5(900.)) $tv
36(0.0)                                        $vvz
100.0 1.0e-1 5.0 5.0 50.0 0.9 15
0.0,,,,,,,
0
```

B.4 THORS Bundle 6A Simulation, Case A (No Heat Losses, No Plenum)

```
2
THORS Bundle 6A (19 pin), Test 71H, Run 101
   Steady State, No Heat Losses, No Plenum
1 14 1 10 50 0 0 1 0 1 1 0 1 1 0 1 0 0 0 0 1 0 0
1.e-9 1.e-10 -9.8066 3.20e-3 1.2435 2.76 5.78 1000.0
2000.0 0.0 0.0 811.0 2.921e-3 52.174
1.27e5 80.0 0.0 1.0 0.0 2.07e4
0.0 0.0 0.0 0.0 1.0e7 1.0 0.0 0.0 0.0 0.0
1                                    $ncr
1                                    $indent
1                                    $ifcar
4                                    $nrzf
3 1 2 1                              $nrmzf
1 0 0 0                              $mnrzf
14(0.0)                              $arx
14(0.0)                              $ary
15(3.852e-4)                         $arz
1.176e-4 9(3.914e-5) 4(1.176e-4)     $vol
4.42e-3                              $hedz
2.97e-3                              $wedz
3.6432e-2                            $dx
3.2429e-2                            $dy
2(.3048) 9(.1016) 5(.3048)           $dz
1.78e+5 1.75e+5 1.73e+5 1.72e+5 1.71e+5 1.70e+5
1.68e+5 1.67e+5 1.66e+5 1.65e+5 1.63e+5 1.60e+5
1.56e+5 1.52e+5 1.48e+5 1.44e+5      $p
16(0.0)                              $alp
16(661.0)                            $tv
15(1.016)                            $vvz
0.0 9(661.0) 4(0.0)                  $twf
0.0 .466 .686 .856 .963 1.0 .963
   .856 .686 .466 4(0.0)             $qz
1.0                                  $qt
3(0.0) 1.0 3(0.0)                    $qr
19.0                                 $rn
1.2573e-3 3.302e-4 9.525e-4 3.81e-4  $drzf
10.0 1.0e-6 1.0 2.0 2.0 .9 16
0.0,,,,,,,
0
```

B.4 (Continued)   Restart Files for Cases A to F

```
-2
$restart
iss=0
nitmax=-50
ntabls=2
itbt=1
ibbt=2
cpumax=4000.0
tdelay=11.0
natc=1
$end
     loss of flow transient, first 7 seconds
9
0.0 1.0  .75 .993  1.5 .979  2.25 .966  3.0 .945
3.75 .938  5.25 .934  6.75 .93  10.5 .92 $table1
8
0.0 1.0  .385 .9376  1.535 .7187  2.69 .437
3.845 .344  5.381 .30  6.915 .30  10.0 .313 $table2
18.0 1.0e-6 0.1 0.5 0.5 0.9 16
0.0,,,,,,,
0
```

```
-2
$restart
epsn=1.d-6
epsi=1.d-7
nitmax=-50
iitmax=110
ntabls=2
itbt=1
ibbt=2
cpumax=4000.0
natc=1
$end
   loss of flow transient, bottom of flow ramp, velocity condition
4
6.75 0.93  10.5 0.92  16.5 0.905  27.0 0.90 $table1
9
6.915 0.30  10.0 0.313  10.75 0.29  12.0 0.25  14.5 0.13
17.0 0.10  19.5 0.14  24.5 0.14  27.0 0.12 $table2
28.0 1.0e-6 0.1 0.2 0.2 0.9 16
0.0,,,,,,,
0
```

B.5 THORS Bundle 6A Simulation, Case B (Heat Losses to Sodium-soaked Insulation, No Plenum)

```
2
THORS Bundle 6A (19 pin), Test 71H, Run 101
   Steady State, Heat Loss to Sodium-soaked Insulation, No Plenum
1 14 1 10 50 0 0 1 0 1 1 5 21  1 0 1 0 0 0 0 1 0 1
1.e-9 1.e-10 -9.8066 3.20e-3 1.2435 2.76 5.78 1000.0
2000.0 0.0 0.0 811.0 2.921e-3 52.174
1.27e5 80.0 0.0 1.0 0.0 2.07e4
0.0 0.0 0.0 0.0 1.0e7 1.0 0.0 0.0 0.0 0.0
1                                          $ncr
1                                          $indent
1                                          $ifcar
4                                          $nrzf
3 1 2 1                                    $nrmzf
1 0 0 0                                    $mnrzf
1                                          $inx
3 6 4 5 4                                  $mnrzs
1 4 1 1 1                                  $nrmzs
14(0.0)                                    $arx
14(0.0)                                    $ary
15(3.852e-4)                               $arz
1.176e-4 9(3.914e-5) 4(1.176e-4)           $vol
4.42e-3                                    $hedz
2.97e-3                                    $wedz
3.6432e-2                                  $dx
3.2429e-2                                  $dy
2(.3048) 9(.1016) 5(.3048)                 $dz
1.78e+5 1.75e+5 1.73e+5 1.72e+5 1.71e+5 1.70e+5
1.68e+5 1.67e+5 1.66e+5 1.65e+5 1.63e+5 1.60e+5
1.56e+5 1.52e+5 1.48e+5 1.44e+5            $p
16(0.0)                                    $alp
16(661.0)                                  $tv
15(1.016)                                  $vvz
0.0 9(661.0) 4(0.0)                        $twf
0.0 .466 .686 .856 .963 1.0
.963 .856 .686 .466 4(0.0)                 $qz
1.0                                        $qt
3(0.0) 1.0 3(0.0)                          $qr
19.0                                       $rn
1.2573e-3 3.302e-4 9.525e-4 3.81e-4        $drzf
0.11227                                    $pcx
0.00051 0.02058 0.00549 0.00668 0.00602 $drzs
14(661.0)                                  $tws
10.0 1.0e-6 1.0 2.0 2.0 .9 16
0.0,,,,,,,
0
```

B.6 THORS Bundle 6A Simulation, Case C (Heat Losses to Sodium-soaked Insulation, Gas Plenum Conduction)

```
3
THORS Bundle 6A (19 pin), Test 71H, Run 101
   Steady State, Heat Losses to Sodium-soaked Insulation,
   Gas Plenum Represented
1 15 1 10 50 0 0 1 0 3 1 5 21 1 0 1 0 0 0 0 1 0 1
1.e-9 1.e-10 -9.8066 3.20e-3 1.2435 2.76 5.78 1000.0
2000.0 0.0 0.0 811.0 2.921e-3 52.174
1.27e5 80.0 0.0 1.0 0.0 2.07e4
0.0 0.0 0.0 0.0 1.0e7 1.0 0.0 0.0 0.0 0.0
1                                          $ncr
1                                          $indent
1 11 12                                    $ifcar
4 2 2                                      $nrzf
3 1 2 1 6 1 0 0 1 1 0 0                    $nrmzf
1 0 0 0 2 0 0 0 3 0 0 0                    $mnrzf
1                                          $inx
3 6 4 5 4                                  $mnrzs
1 4 1 1 1                                  $nrmzs
15(0.0)                                    $arx
15(0.0)                                    $ary
16(3.852e-4)                               $arz
1.176e-4 9(3.914e-5) 7.35e-5
   4.41e-5 3(1.176e-4)                     $vol
4.42e-3                                    $hedz
2.97e-3                                    $wedz
3.6432e-2                                  $dx
3.2429e-2                                  $dy
2(.3048) 9(.1016) .1905 .1143 4(.3048)     $dz
1.78e+5 1.75e+5 1.73e+5 1.72e+5 1.71e+5 1.70e+5
1.68e+5 1.67e+5 1.66e+5 1.65e+5 1.63e+5 1.61e+5
1.60e+5 1.56e+5 1.52e+5 1.48e+5 1.44e+5 $p
17(0.0)                                    $alp
17(661.0)                                  $tv
16(1.016)                                  $vvz
0.0 14(661.0)                              $twf
0.0 .466 .686 .856 .963 1.0 .963
   .856 .686 .466 5(0.0)                   $qz
3(1.0)                                     $qt
3(0.0) 1.0 17(0.0)                         $qr
3(19.0)                                    $rn
1.2573e-3 3.302e-4 9.525e-4 3.81e-4
   2(2.54e-3 3.81e-4 2(0.0))               $drzf
0.11227                                    $pcx
0.00051 0.02056 0.00549 0.00668 0.00602 $drzs
15(661.0)                                  $tws
10.0 1.0e-6 1.0 2.0 2.0 .9 16
0.0,,,,,,,
0
```

B.7   217 Pin Bundle Simulation, Case D (No Heat Losses, No Plenum)

```
2
217 Pin Bundle - Comparison With THORS Bundle 6A (19 Pin)
  Steady State, No Heat Losses, No Plenum
1 14 1 10 50 0 0 1 0 1 1 0 1 1 0 1 0 0 0 0 1 0 1
1.e-9 1.e-10 -9.8066 3.20e-3 1.2435 2.76 5.78 1000.0
2000.0 0.0 0.0 811.0 2.921e-3 52.174
1.39e+6 80.0 0.0 1.0 0.0 2.07e+4
0.0 0.0 0.0 0.0 1.0e7 1.0 0.0 0.0 0.0 0.0
1                                        $ncr
1                                        $indent
1                                        $ifcar
4                                        $nrzf
3 1 2 1                                  $nrmzf
1 0 0 0                                  $mnrzf
14(0.0)                                  $arx
14(0.0)                                  $ary
15(4.270e-3)                             $arz
1.301e-3 9(4.338e-4) 4(1.301e-3)         $vol
4.289e-3                                 $hedz
3.207e-3                                 $wedz
0.1246                                   $dx
0.1079                                   $dy
2(.3048) 9(.1016) 5(.3048)               $dz
1.78e+5 1.75e+5 1.73e+5 1.72e+5 1.71e+5 1.70e+5
1.68e+5 1.67e+5 1.66e+5 1.65e+5 1.63e+5 1.60e+5
1.56e+5 1.52e+5 1.48e+5 1.44e+5          $p
16(0.0)                                  $alp
16(661.0)                                $tv
15(1.016)                                $vvz
0.0 9(661.0) 4(0.0)                      $twf
0.0 .466 .686 .856 .963 1.0
.963 .856 .686 .466 4(0.0)               $qz
1.0                                      $qt
3(0.0) 1.0 3(0.0)                        $qr
217.0                                    $rn
1.2573e-3 3.302e-4 9.525e-4 3.81e-4      $drzf
10.0 1.0e-6 1.0 5.0 5.0 .9 16
0.0,,,,,,,
0
```

B.8 217 Pin Bundle Simulation, Case E (Heat Losses to Hex Can, No Plenum)

```
2
217 Pin Bundle - Comparison With THORS Bundle 6A (19 Pin)
  Steady State, Heat Loss to Can Only, No Plenum
1 14 1 10 50 0 0 1 0 1 1 1 21 1 0 1 0 0 0 0 1 0 1
1.e-9 1.e-10 -9.8066 3.20e-3 1.2435 2.76 5.78 1000.0
2000.0 0.0 0.0 811.0 2.921e-3 52.174
1.39e+6 80.0 0.0 1.0 0.0 2.07e+4
0.0 0.0 0.0 0.0 1.0e7 1.0 0.0 0.0 0.0 0.0
1                                        $ncr
1                                        $indent
1                                        $ifcar
4                                        $nrzf
3 1 2 1                                  $nrmzf
1 0 0 0                                  $mnrzf
1                                        $inx
3                                        $mnrzs
1                                        $nrmzs
14(0.0)                                  $arx
14(0.0)                                  $ary
15(4.270e-3)                             $arz
1.301e-3 9(4.338e-4) 4(1.301e-3)         $vol
4.289e-3                                 $hedz
3.207e-3                                 $wedz
0.1246                                   $dx
0.1079                                   $dy
2(.3048) 9(.1016) 5(.3048)              $dz
1.78e+5 1.75e+5 1.73e+5 1.72e+5 1.71e+5 1.70e+5
1.68e+5 1.67e+5 1.66e+5 1.65e+5 1.63e+5 1.60e+5
1.56e+5 1.52e+5 1.48e+5 1.44e+5          $p
16(0.0)                                  $alp
16(661.0)                                $tv
15(1.016)                                $vvz
0.0 9(661.0) 4(0.0)                      $twf
0.0 .466 .686 .856 .963 1.0
.963 .856 .686 .466 4(0.0)               $qz
1.0                                      $qt
3(0.0) 1.0 3(0.0)                        $qr
217.0                                    $rn
1.2573e-3 3.302e-4 9.525e-4 3.81e-4      $drzf
0.3739                                   $pcx
0.003                                    $drzs
14(661.0)                                $tws
10.0 1.0e-6 1.0 5.0 5.0 .9 16
0.0,,,,,,,
0
```

B.9   217 Pin Bundle Simulation, Case F (Heat Losses to Hex Can + Insulation, No Plenum)

```
2
217 Pin Bundle - Comparison With THORS Bundle 6A (19 Pin)
   Steady State, Heat Loss to Sodium-soaked Insulation, No Plenum
1 14 1 10 50  0  0 1 0  1 1 2 21 1 0 1 0 0 0 0 1 0 1
1.e-9 1.e-10 -9.8066 3.20e-3 1.2435 2.76 5.78 1000.0
2000.0 0.0 0.0 811.0 2.921e-3 52.174
1.39e+6 80.0 0.0 1.0 0.0 2.07e+4
0.0 0.0 0.0 0.0 1.0e7 1.0 0.0 0.0 0.0 0.0
1                                          $ncr
1                                          $indent
1                                          $ifcar
4                                          $nrzf
3 1 2 1                                    $nrmzf
1 0 0 0                                    $mnrzf
1                                          $inx
3 6                                        $mnrzs
1 4                                        $nrmzs
14(0.0)                                    $arx
14(0.0)                                    $ary
15(4.270e-3)                               $arz
1.301e-3 9(4.338e-4) 4(1.301e-3)           $vol
4.289e-3                                   $hedz
3.207e-3                                   $wedz
0.1246                                     $dx
0.1079                                     $dy
2(.3048) 9(.1016) 5(.3048)                 $dz
1.78e+5 1.75e+5 1.73e+5 1.72e+5 1.71e+5 1.70e+5
1.68e+5 1.67e+5 1.66e+5 1.65e+5 1.63e+5 1.60e+5
1.56e+5 1.52e+5 1.48e+5 1.44e+5            $p
16(0.0)                                    $alp
16(661.0)                                  $tv
15(1.016)                                  $vvz
0.0 9(661.0) 4(0.0)                        $twf
0.0 .466 .686 .856 .963 1.0
.963 .856 .686 .466 4(0.0)                 $qz
1.0                                        $qt
3(0.0) 1.0 3(0.0)                          $qr
217.0                                      $rn
1.2573e-3 3.302e-4 9.525e-4 3.81e-4        $drzf
0.3739                                     $pcx
0.003 0.02058                              $drzs
14(661.0)                                  $tws
10.0 1.0e-6 1.0 5.0 5.0 .9 16
0.0,,,,,,,
0
```